

Supporting information

Hierarchical mesoporous NanoMUV-2 for the selective delivery of macromolecular drugs

Isabel Abánades Lázaro,^{*a} María Vicent Morales^a, Guillermo Mínguez Espallargas^a and Mónica Giménez-Marqués.^{*a}

^a Instituto de Ciencia Molecular (ICMol), Universitat de València, Catedrático José Beltrán Martínez No 2, 46980 Paterna, Valencia, Spain.

Table of contents

Supporting information.....	1
S1. General Experimental Remarks.....	2
S2. Synthesis.....	4
S3. Characterisation of NanoMUV-2.....	6
S4. Characterisation of Cal@MUV-2.....	17
S5. Cellular internalization of Cal@MUV-2.....	23
S6. PTX loading into MUV-2.....	27
S7. PTX loading to other MOFs.....	30
S8. Cytotoxicity of PTX@NanoMUV-2 and free PTX.....	34
S9 Characterisation of functionalised MUV-2.....	37
S10. Cytotoxicity of functionalised MUV-2.....	54
S11. Characterisation of calcein-loaded surface-functionalised MUV-2.....	57
S12. Cellular internalization of functionalized MOFs.....	68
S13. Charaterisation of Paclitaxel-loaded surface-functionalised MUV-2.....	77
S14. Cytotoxicity Paclitaxel-functionalised samples.....	83
S15. References.....	83

S1. General Experimental Remarks

S1.1 Equipment

Powder X-Ray Diffraction (PXRD): PXRD patterns using 0.7 mm borosilicate capillaries that were aligned on an Empyrean PANalytical powder diffractometer, using Cu Ka radiation ($\lambda = 1.54056 \text{ \AA}$) with a PIXcel detector, operating at 40 mA and 45 kV. Profiles were collected for 4 minutes in the $3^\circ < 2\theta < 40^\circ$ range with a step size of 0.017° . (University of Valencia)

Thermogravimetric Analysis (TGA): was carried out with a Mettler Toledo TGA/SDTA 851 apparatus between 25 and 800 °C under ambient conditions ($10 \text{ }^\circ\text{C}\cdot\text{min}^{-1}$ scan rate and an airflow of $9 \text{ mL}\cdot\text{min}^{-1}$). (University of Valencia)

Nuclear Magnetic Resonance Spectroscopy (NMR): NMR spectra were recorded on a Bruker AVIII 300 MHz spectrometer and referenced to residual solvent peaks. (University of Valencia)

Dynamic Light Scattering: Colloidal analysis was performed by Dynamic Light Scattering (DLS) with a Zetasizer Ultra potential analyser equipped with Non-Invasive Backscatter optics (NIBS) and a 50 mW laser at 633 nm. (University of Valencia).

Scanning Electron Microscopy (SEM): particle morphologies, dimensions and mapping were studied with a Hitachi S-4800 scanning electron microscope at an accelerating voltage of 20 kV. (University of Valencia). Particle size analysis were performed measuring at least 50 different particles. The energy-dispersive X-Ray analysis (EDX) of different elements was studied using a SCIOS 2 field emission scanning electron microscope with a focused ion beam at an accelerating voltage of 20 kV. (University of Valencia)

Fourier Transform Infrared Spectroscopy: IR spectra of solids were collected using a Shimadzu Fourier Transform Infrared Spectrometer, FTIR-8400S, fitted with a Diamond ATR unit. (University of Valencia)

N₂ adsorption isotherms were performed in a Tristar II Plus Micromeritics sorptometer, at 77 K and 273 K, respectively. Activation was set at 150 °C, under vacuum, for 24 hours. (University of Valencia)

Flow Assisted cell sorting: Fluorescence-activated cell sorting (FACS) experiments were performed in a Verse cytometer equipped with three lasers. (University of Valencia)

Confocal microscopy: Confocal images were acquired using an FV1000 confocal laser microscope mounted on a motorised inverted IX81 which includes the following lenses: 10x, 20x, 40x (oil), 60x (oil), 60x (water). This equipment's excitation lines are 405nm, 488nm, 515nm, 559nm, 594nm y 635nm. Moreover, the equipment has an incubation system, which makes it the appropriate equipment for live-cell work. (University of Valencia)

S1.2. *In vitro* Protocols

S1.2a. Cell Culture. HeLa cervical cancer cell line and HEK293 human embryonic kidney cells were maintained at 37 °C with 5% CO₂ in high rich glucose (4500 mg·L⁻¹) Dulbecco's modified Eagle's Medium (DMEM) with phenol red supplemented with 10% (v/v) Fetal Bovine Serum (FBS), 2 mM L-glutamine, 100 units·mL⁻¹ penicillin and 100 µg·mL⁻¹ streptomycin. This was named complete DMEM (cDMEM). The cells were passaged two times a week (at 75-80% of confluence) at a density of 2.8 x 10⁴ cell·cm⁻²

S1.2b. MTS Assay. To measure cell proliferation of HeLa, MCF-7 and HEK293 the (MTS, Promega, UK) reduction assay, based on the cleavage of 3-(4,5-dimethylthiazol-2-yl)-5-(3-carboxymethoxyphenyl)-2-(4-sulfophenyl)-2H-tetrazolium salt was used. The day before the experiment, cells were seeded into a 96 well plate at a density of 10 x 10³ cells per well (100 µL). Prior to the treatments, cells were washed with PBS twice. MOFs were suspended in cDMEM by sonication at different concentrations, added to the cells and incubated – with 5 replicates for each MOF concentration and 8 replicates for media without cells and for untreated cells – for 24 h or 72 h at 37 °C with 5% CO₂. To measure the toxicity, the cells were washed three times with phosphate buffered saline (PBS), the media was replaced with 100 µL of fresh culture media containing 20 µL of MTS/phenazinemethosulfate (in a proportion 20:1) solution, and the plate was incubated for 1 h at 37 °C with 5% CO₂. The plates were read at 490 nm by UV/vis spectrophotometry.

S1.2.c. Cell internalization studies

Fluorescence-assisted cell sorting (FACS): The endocytosis of calcein-loaded MOFs was measured by fluorescence-assisted cell sorting (FACS). In all the FACS experiments, cells were seeded in a Cellstar 24-well plate at a density of 5 x 10⁴ cells/well and incubated for 48 h at 37 °C with 5% CO₂ in complete medium. After 48 h of cell growth, the cells were washed with PBS and incubated with a solution of the MOF nanoparticles in question in media for 30 min, 1.3h or 2h. Then, the media of each well was aspirated and the wells were washed extensively (PBS x 3) to remove non-internalised nanoMOF or incubation conditions. The cells were then harvested by adding 0.1 mL of trypsin and incubated for 5 min at 37 °C with 5% CO₂. The cells were recovered by centrifugation (5 min at 1200 rpm) and re-suspended in 400 µL of cDMEM without phenol red. Finally, the samples were measured in a Verse analyser cytometer.

Confocal Microscopy: Cells were seeded in an imaging 8-well plate at a density of 5 x 10⁵ cell·mL⁻¹ and incubated for 24 h at 37 °C with 5% CO₂ in cDMEM. Then, the media was aspirated, the cells washed twice with PBS 10x and incubated with dispersions of the Cal@MOFs or free calcein in cDMEM for 2 hours. At the end of the incubation period, the 8-well plate was aspirated, and washed twice with fresh PBS, followed by incubation with 4% PFA in PBS 10X for 15 minutes. Then, the fixing solution was aspirated and the cells were washed twice with PBS. Finally, a 1:20 DAPI solution in PBS was added and the cells were measured in an FV1000 confocal microscope. For the colocalisation studies, prior to the addition of fixing solution, the cells were incubated with a 60 nM concentration of lysotracker in PBS 10X, which was followed by two washes with fresh PBS. For the live cells experiments the cells were measured with the confocal microscope at 37 °C after this step, whereas for the fixed cells, the 4% PFA protocol was followed.

S1.3 Methodology for degradation and drug release in PBS 10X.

The degradation and calcein release experiments were performed upon dispersion (sonication *ca.* 1 minute) of *ca.* 6 mg of sample in 10 mL of PBS 10X and left stirring in an incubator. After a certain time, the dispersion was centrifuged and 100 μ L of the supernatant was collected and measured upon a calibration curve with a 1:2 dilution. The percentage of H₄TTFTB and calcein released was calculated based on the maximum absorbance of the supernatant

S2. Synthesis

All reagents unless otherwise stated were obtained from commercial sources and were used without further purification.

Synthesis of NanoMUV-2: In separate vials, 60 mg of ligand¹ (0.088 mmol) and 90 mg of Fe₃O(CH₃COO)₆]ClO₄·3H₂O² (0.133 mmol) were dissolved in 9 mL of DMF. Both solutions were mixed in a 15 mL pyrex jar, in which 1.8 mL of acetic acid was placed. The jar was placed in the oven and heated to 105 °C. After 60 hours, the temperature was cooled down to room temperature. Then, the solid was collected by centrifugation (15 min, 5000 rpm) and washed (sonication centrifugation cycles) with fresh DMF (x3) and with EtOH (x2). The solid was further activated by shaking a fresh EtOH dispersion in an incubator for 5 days, followed by centrifugation and two further washes with EtOH. The solid was dried at room temperature for 24 hours and under vacuum for 2 hours. The resultant MUV-2 MOF has the molecular formula [Fe₃O(OH₂)₂(OH₂)]₂[TTFTB]₃,¹ which during this supporting information will be simplified as (Fe₃O)₂(L)₃.

Synthesis of Cal@NanoMUV-2: 20 mg of Soxhlet activated NanoMUV-2 were dispersed by sonication (15 minutes) in 10 mL of a calcein solution (2mg·mL⁻¹) in EtOH and stirred at room temperature for 24 hours. The solid was collected by centrifugation (5000 rpm, 15 min), and submitted to dispersion centrifugation cycles with fresh ethanol until the supernatant solution remained colorless (7 times).

Synthesis of PTX@NanoMUV-2: 20 mg of Soxhlet-activated NanoMUV-2 were dispersed by sonication (15 minutes) in 20 mL of a PTX solution (1 mg·mL⁻¹) in EtOH and stirred at room temperature for 48 hours. The solid was collected by centrifugation (5000 rpm, 15 min), and submitted to dispersion centrifugation cycles with fresh ethanol (2 mL X 2 times). Note that the same PTX loading procedure was performed for UiO-66 and MIL-100 in parallel.

Synthesis of NanoMUV-2-Oct: 20 mg of NanoMUV-2 were dispersed by sonication (15 minutes) in 10 mL of a Br-Octanoic acid solution (5 mg·mL⁻¹) in EtOH with 0.1 mL of TEA and stirred at room temperature for 24 hours. The solid was collected by centrifugation (5000 rpm, 15 min), and submitted to dispersion centrifugation cycles with fresh ethanol (x5). MUV-2-Oct was dried under vacuum for 24 hours before characterization. Note that a similar procedure on a lower scale was performed for Cal@NanoMUV-2 and PTX@NanoMUV-2.

Synthesis of NanoMUV-2-FA: 20 mg of NanoMUV-2 were dispersed by sonication (15 minutes) in 10 mL of FA solution (2mg·mL⁻¹) in water and stirred at room temperature for 24 hours. The solid was collected by centrifugation (5000 rpm, 15 min), and submitted to dispersion centrifugation cycles with fresh ethanol (x5). MUV-2-FA was dried under vacuum for 24 hours before characterization. Note that a similar procedure on a lower scale was performed for Cal@NanoMUV-2 and PTX@NanoMUV-2.

Synthesis of UiO-66: 1,4-Benzenedicarboxylic acid (448 mg, 2.7 mmol) was dissolved in 30 mL of DMF. In a separate vial, the metal precursor, zirconium chloride (629 mg, 2.7 mmol) was dissolved in 30 mL of DMF. Both solutions were sonicated until complete dissolution and mixed. Subsequently, acetic acid (4.2 mL, 7% v/v) was added.³ The solution was heated to 120 °C for 24 h yielding UiO-66 nanoparticles, which were collected by centrifugation (4500 rpm, 15 min), and subsequently washed by dispersion centrifugation cycles with DMF (x2) and ethanol (x3).

Synthesis of MIL-100: 1,3,5-Benzenetricarboxylic acid (369 mg, 2.28 mmol) and Iron(III) chloride hexahydrate (1.62 g, 4.06 mmol) were dissolved in distilled water (20 mL).⁴ The reaction was heated to 130 °C over 30 s, then maintained at this temperature for 5 min 30 s. The reacting mixture was cooled down to room temperature and centrifuged at 10000 rpm for 25 min. The solid was washed with water (x3 dispersion centrifugation cycles) and dried at 150 °C under vacuum for 24 hours.

S3. Characterisation of NanoMUV-2

S3.1. Powder X-ray diffraction

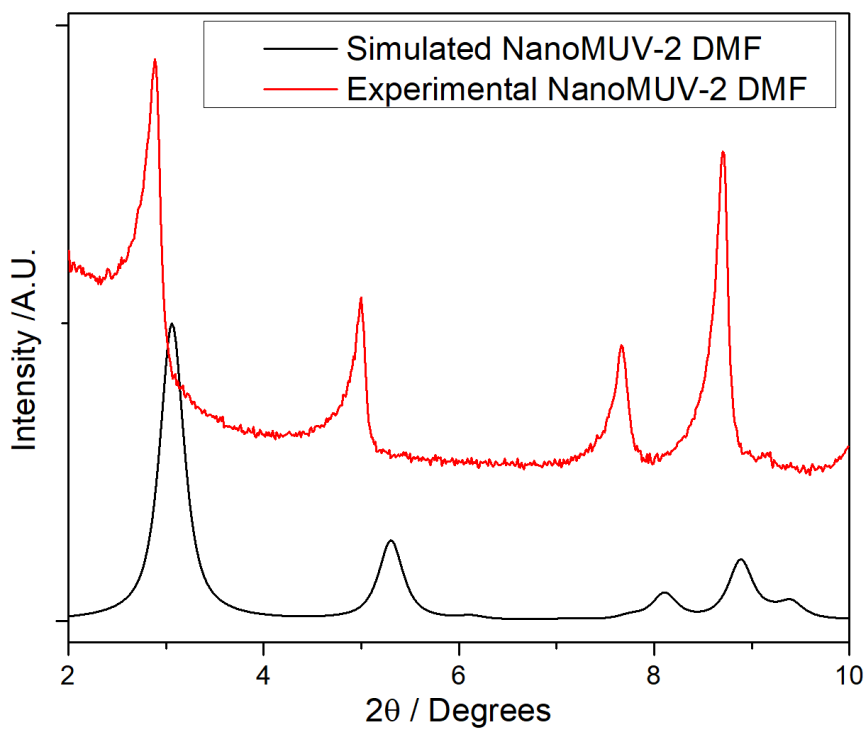


Figure S1: Comparison of experimental and simulated PXRD pattern of NanoMUV-2 as synthesized.

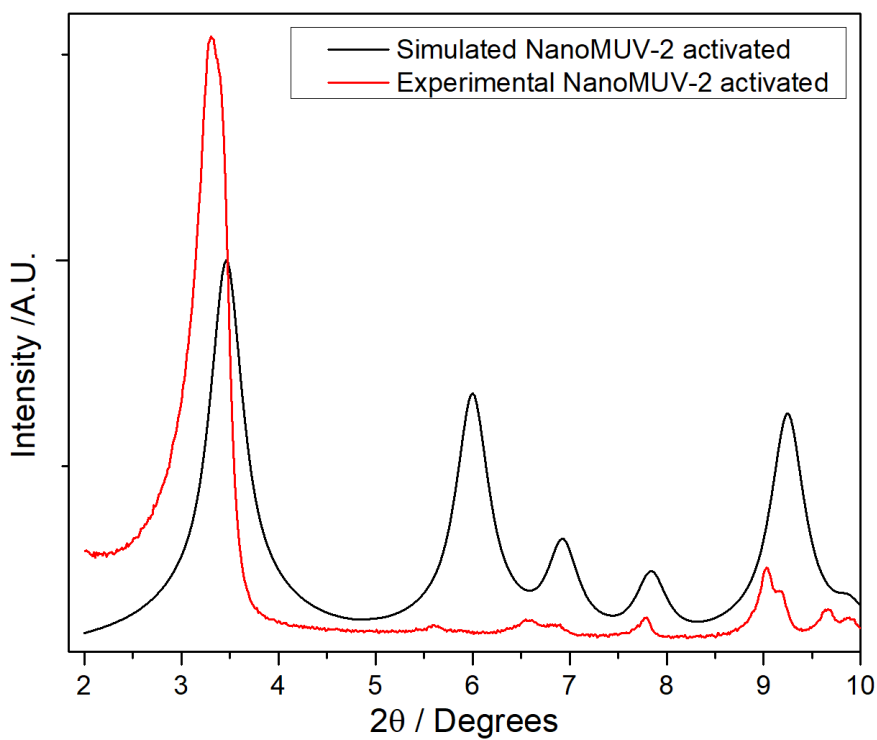


Figure S2: Comparison of experimental and simulated PXRD pattern of activated NanoMUV-2.

S3.2 Scanning Electron Microscopy and energy-dispersive X-ray analysis

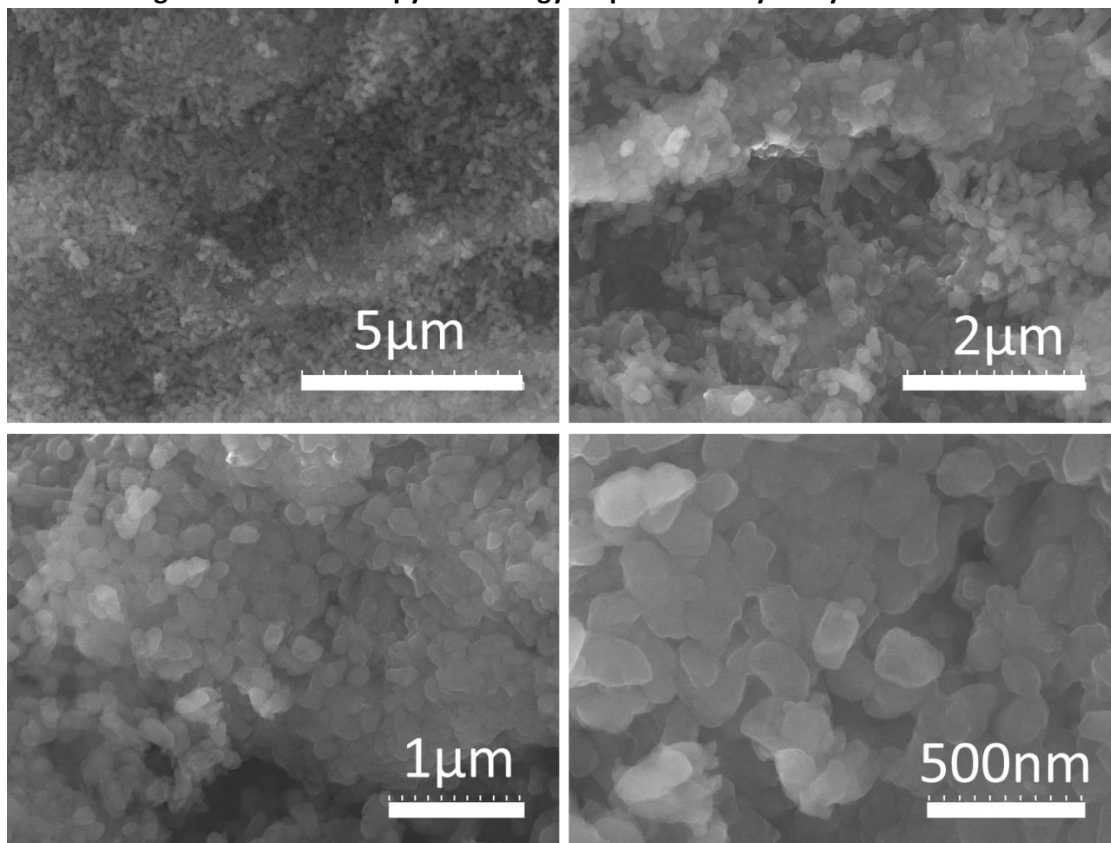


Figure S3: Scanning electron microscope images of NanoMUV-2.

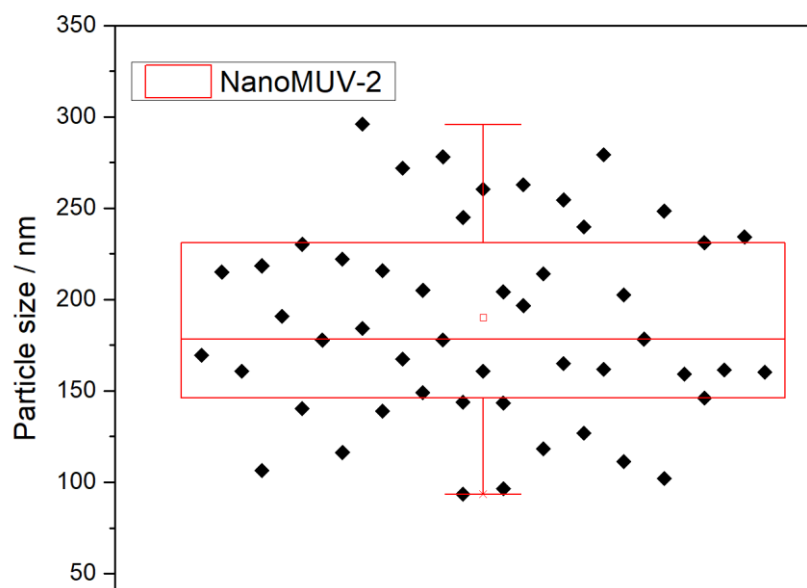


Figure S4: Box chart representation of particle size. Bin size of 10 nm. Average size and standard deviation, 25% and 75% quartiles. Average particle size $ca. 190 \pm 59$ nm.

S3.3 Thermogravimetric analysis

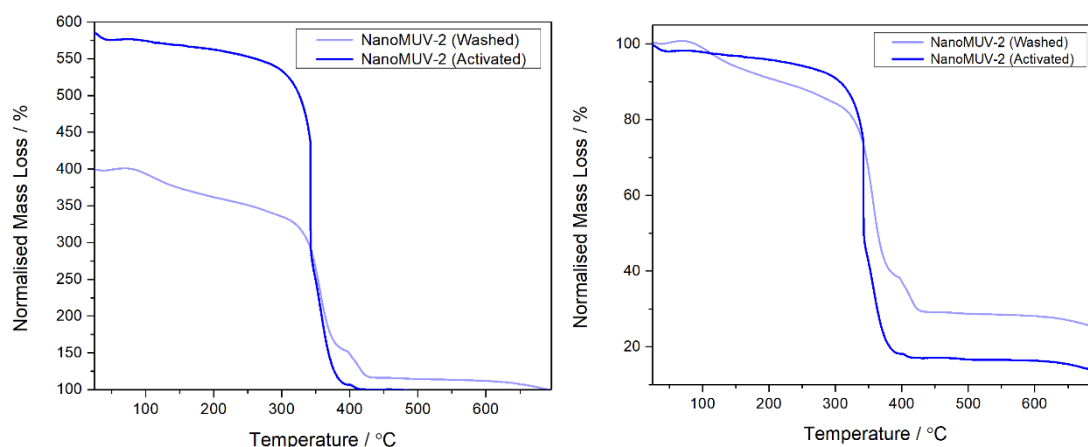


Figure S5: TGA profiles of washed and Soxhlet-activated samples with the end (left) or the start (right) of the decomposition profile normalized to 100%, showing an increase in the inorganic content for the washed sample as a consequence of the inclusion of unreacted metal cluster as previously reported.

$$R_{\text{exp}} = \frac{M_w[\text{MOF}]}{M_w[\text{Residue}]} = \frac{M_w[\text{MOF}]}{M_w[\text{Metal Residue}]} = \frac{M_w[(\text{Fe}_3\text{O})_2(\text{L})_3]}{M_w 3 * [\text{Fe}_2\text{O}_3]}$$

Theoretical MW MOF 2517.4 g·mol⁻¹ leads to a theoretical R of 5.35, whereas the experimental R 5.37 is in agreement with the theoretical molecular formula of the MOF.

S3.4 Fourier-Transmitted Infra-red (FT-IR)

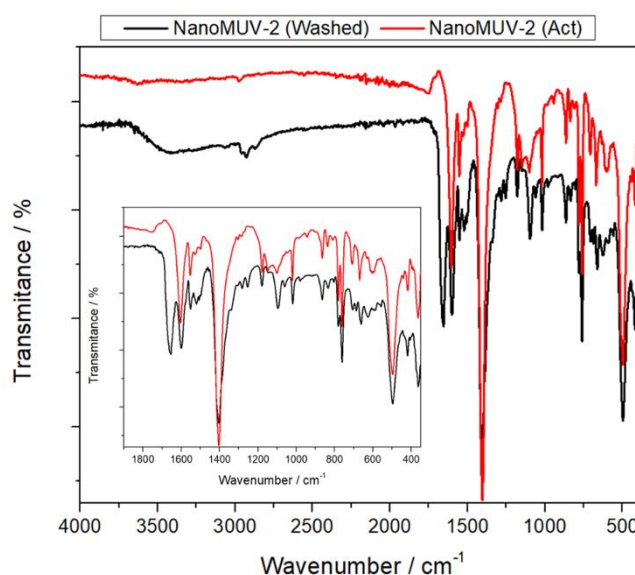


Figure S6: FT-IR spectra of washed and Soxhlet-activated MUV-2, showing the presence of free linker and cluster only in the washed sample.

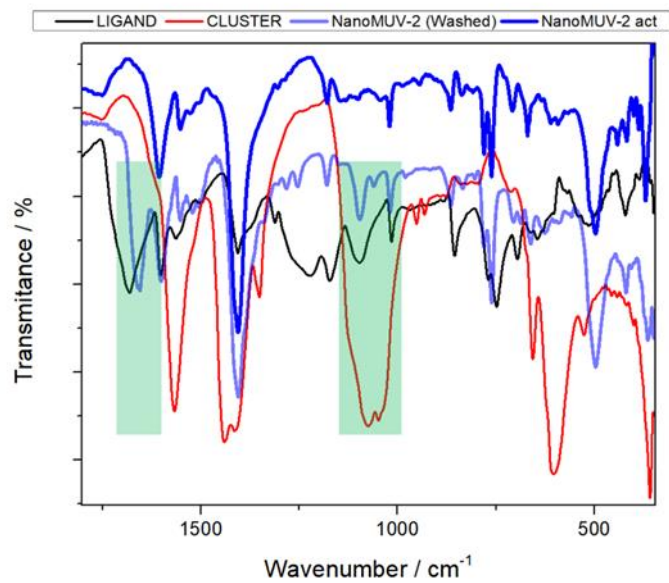


Figure S7: FT-IR spectra of washed and Soxhlet-activated NanoMUV-2 alongside free linker and cluster precursors, showing the presence of free linker and cluster only in the washed sample.

S3.5 N₂ adsorption and desorption isotherms

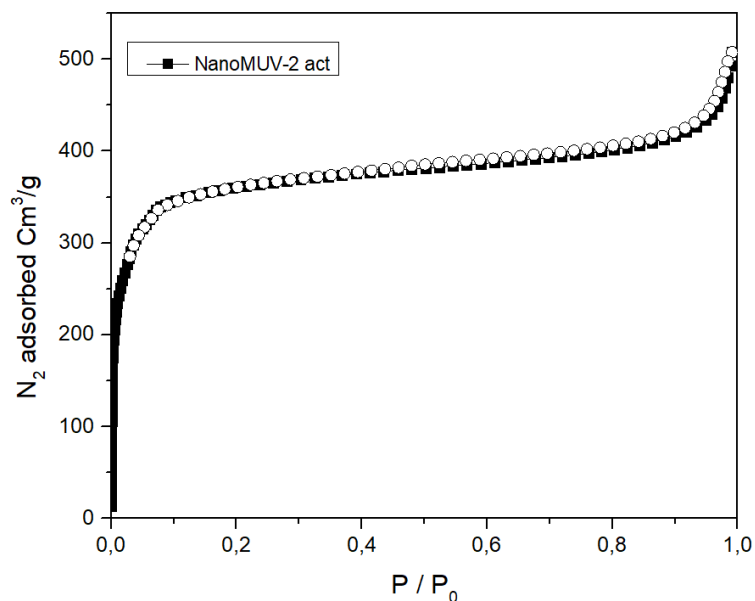


Figure S8: N₂ adsorption and desorption isotherms of Soxhlet-activated NanoMUV-2. The increase in adsorption at high pressures characteristic of small particle size is observed.

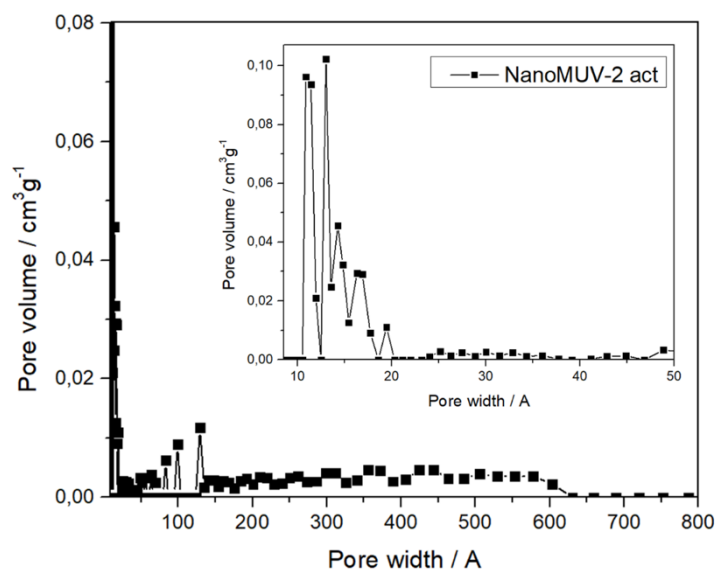


Figure S9: Pore size distribution extracted from N₂ adsorption and desorption isotherms of Soxhlet activated NanoMUV-2.

Table S1: Data extracted from N₂ adsorption and desorption isotherms of Soxhlet activated NanoMUV-2.

S _{BET} Surface area	1404 m ² ·g ⁻¹
Langmuir surface area	1877 m ² ·g ⁻¹
t-plot micropore surface area	1092 m ² ·g ⁻¹
External surface area	313 m ² ·g ⁻¹
Total pore volume (P/P ₀ = 0.9)	0.644 cm ³ ·g ⁻¹
Micropore volume	0.420 cm ³ ·g ⁻¹
Mesopore volume	0.224 cm ³ ·g ⁻¹

S3.6 Dynamic Light Scattering

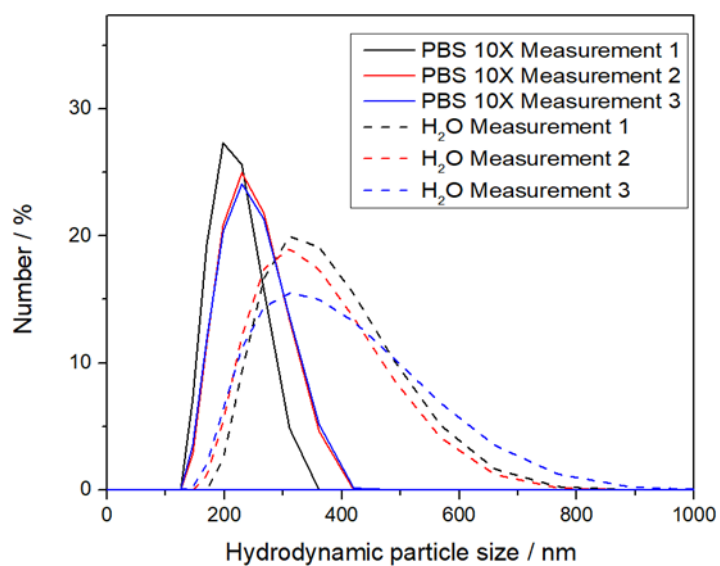


Figure S10: Dynamic light scattering profile showing the number % of particles as a function of their diameter, both in water and PBS 10X. Each measurement was performed with a waiting time of 1 minute, showing slightly bigger particle sizes than SEM but no significant aggregation over time. 0.1 mg·mL⁻¹ dispersion of NanoMUV-2.

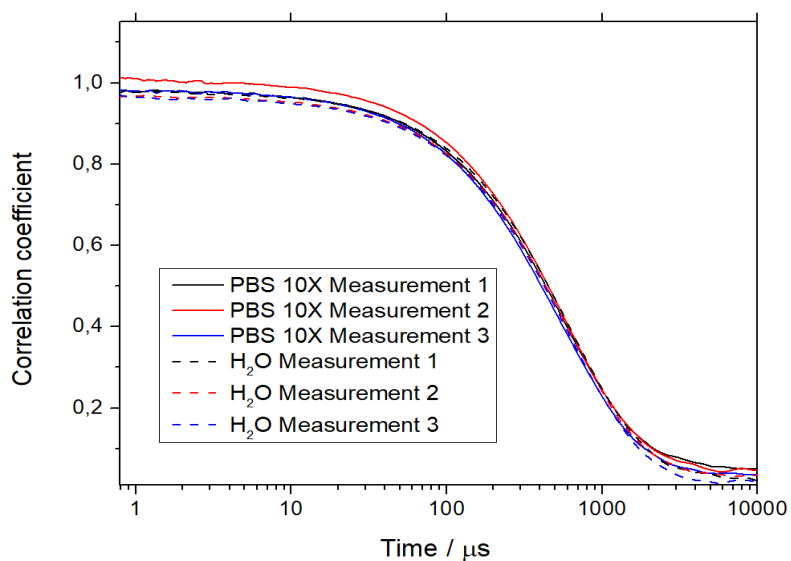


Figure S11: Correlogram of 0.1mg·mL⁻¹ dispersion of NanoMUV-2 in PBS 10X and water, showing no aggregates over the course of time.

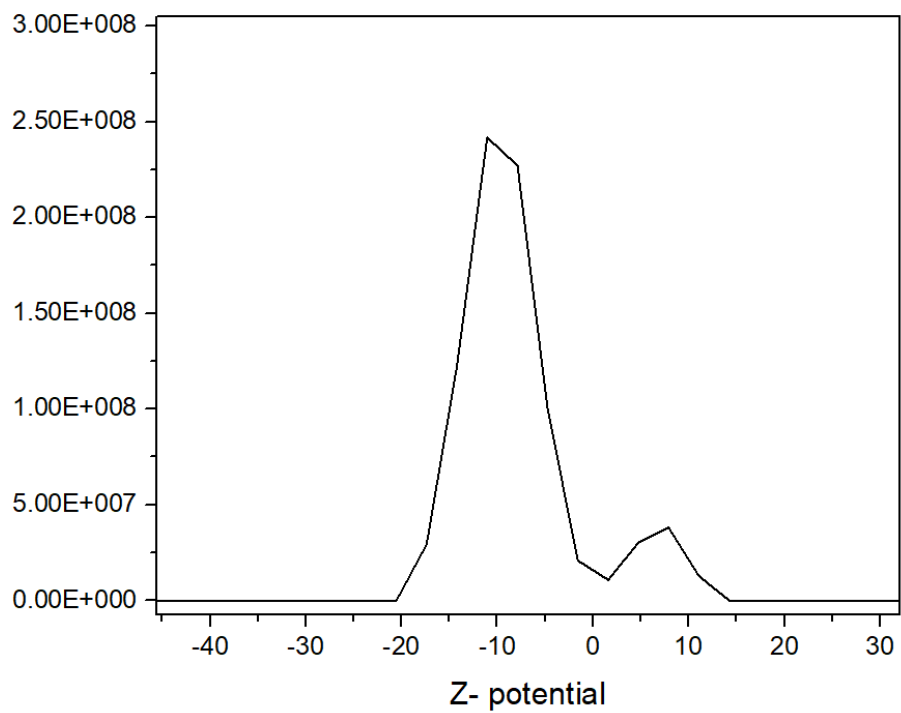


Figure S12: Z-potential analysis of NanoMUV-2 in water.

S3.7 Degradation under simulated physiological conditions

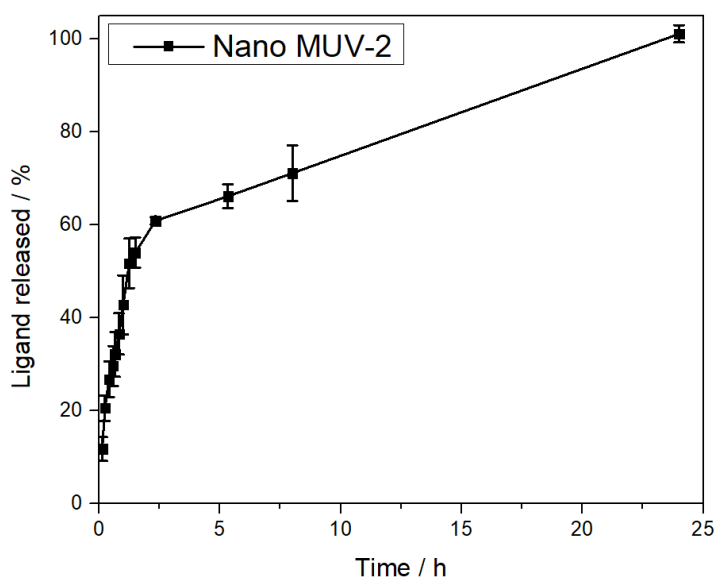


Figure S13: Degradation profile of MUV-2 in PBS 10X based on the linker release for three independent experiments, showing complete degradation with no remaining solid after 24 hours.

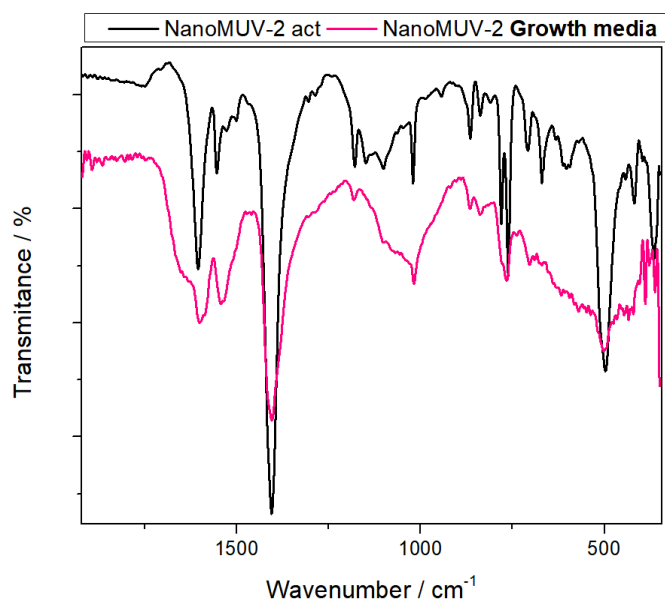


Figure S14: FT-IR profile of NanoMUV-2 activated and after immersion in cell growth media, showing the formation of a protein corona and the signals coming from the MOF.

S3.8 Cell culture studies of NanoMUV-2 and its components

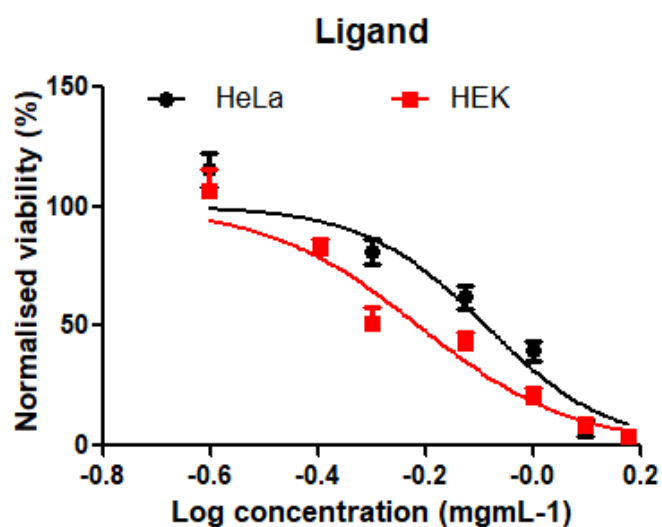


Figure S15: Cell proliferation assays (MTS) carried out on HeLa and HEK cells after 72 h incubation with a solution of TTFNa₄ in growth media, showing similar IC₅₀ values for both cell lines. Each experiment has been performed 4 independent times, each with n=5.

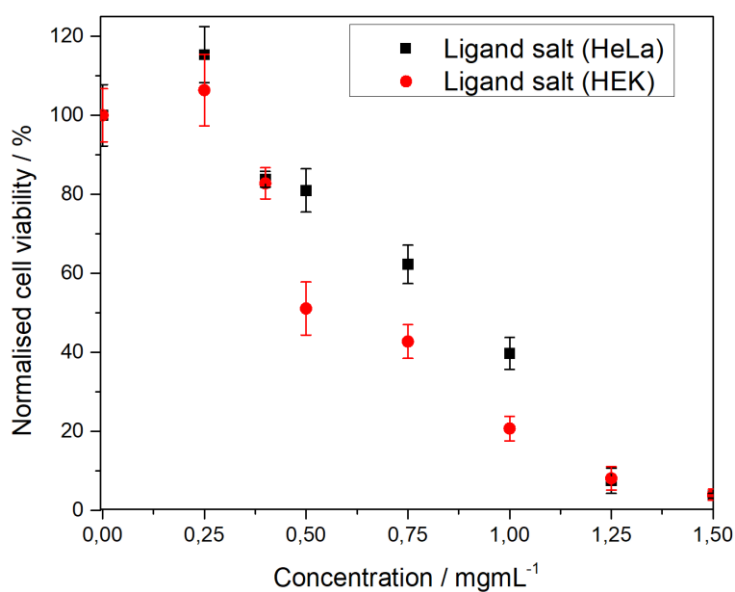


Figure S16: Cell proliferation assays (MTS) carried out on HeLa and HEK cells after 72 h incubation with a solution of TTFNa₄ in growth media, showing similar IC₅₀ values for both cell lines. Each experiment has been performed 4 independent times, each with n=5.

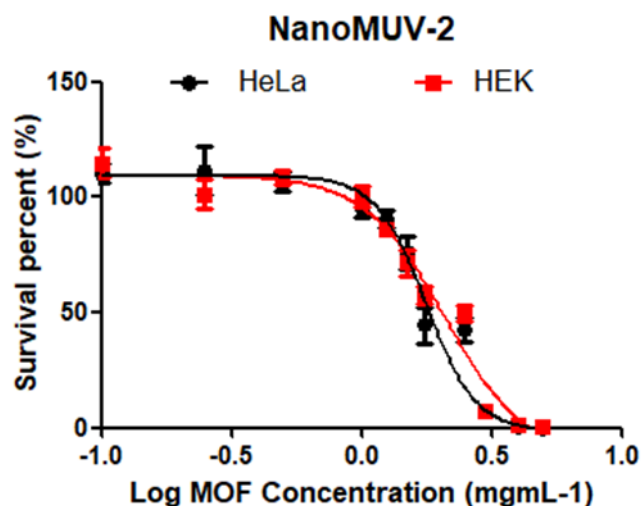


Figure S17: Cell proliferation assays (MTS) carried out on HeLa and HEK cells after 72 h incubation with a solution of TTFNa₄ in growth media, showing similar IC₅₀ values for both cell lines. Each experiment has been performed 3 independent times, each with n=4.

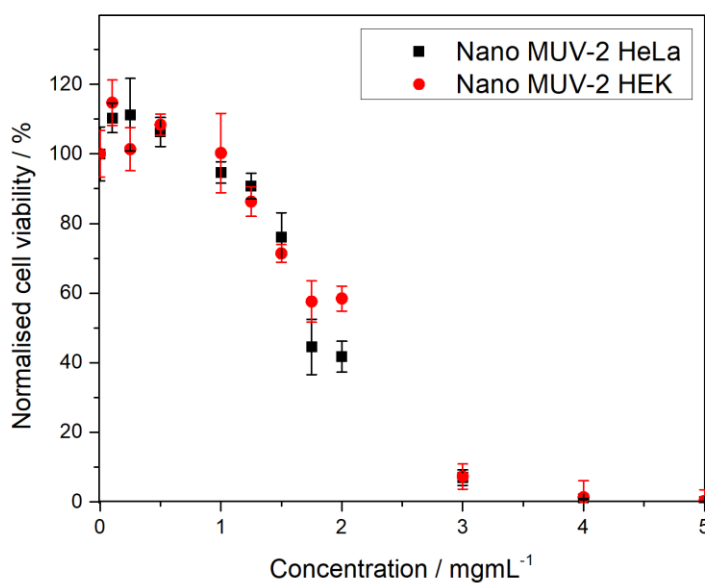


Figure S18: Comparison of cell proliferation assays (MTS) carried out on HeLa and HEK cells after 72 h incubation with a dispersion of NanoMUV-2 in growth media, showing similar IC₅₀ values for both cell lines. Each experiment has been performed 3 independent times, each with n=4.

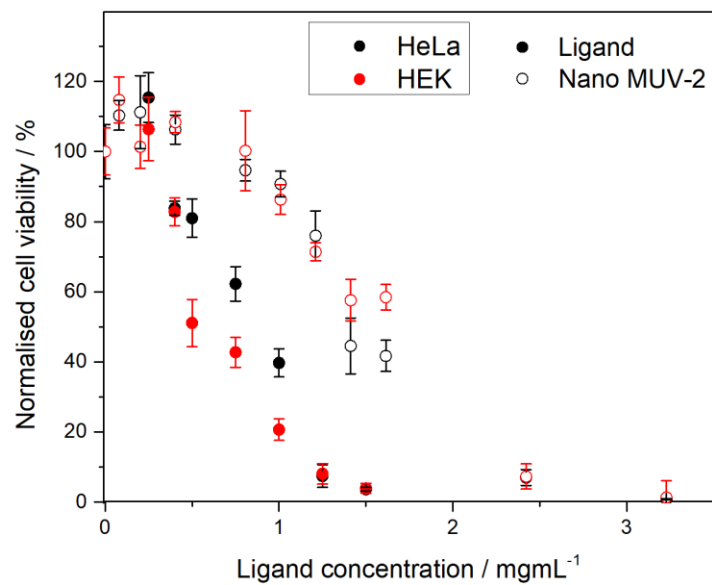


Figure S19: Comparison of cell proliferation assays (MTS) carried out on HeLa and HEK cells after 72 h incubation with a dispersion of NanoMUV-2 and a solution of its ligand salt in growth media, analysed as a function of the concentration of ligand present (ca. 80 w/w% in the MOF).

S4. Characterisation of Cal@MUV-2

Calcein determination was performed upon UV-Vis analysis of the supernatant from calcein loading mixed with the supernatant from the washes. A *ca.* 17.5 w/w % of calcein loading was determined.

S.4.1 PXRD of Cal@NanoMUV-2

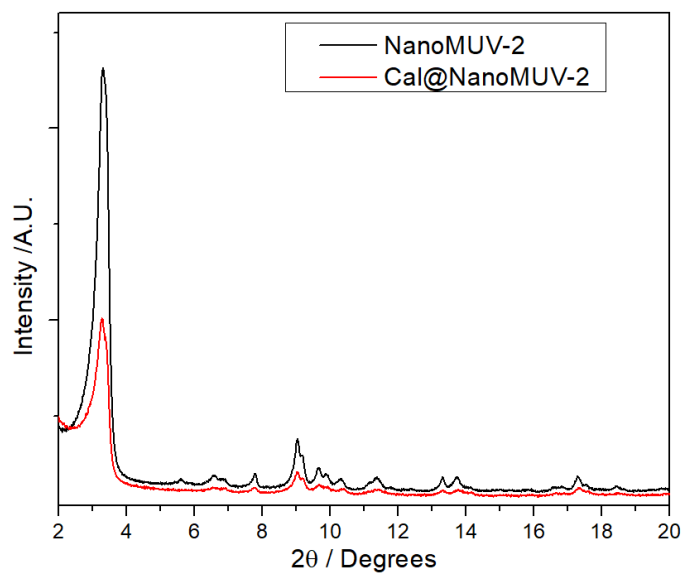


Figure S20: Comparison of experimental PXRD pattern of NanoMUV-2 and Cal@NanoMUV-2, showing retained crystallinity after calcein loading.

S4.2 SEM of Cal@NanoMUV-2

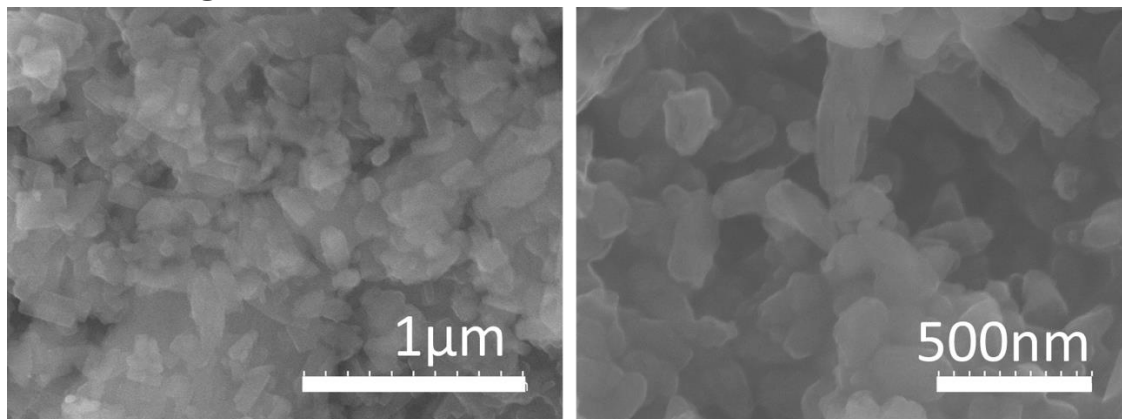


Figure S21: Scanning electron microscope images of Cal@NanoMUV-2, showing maintained morphology.

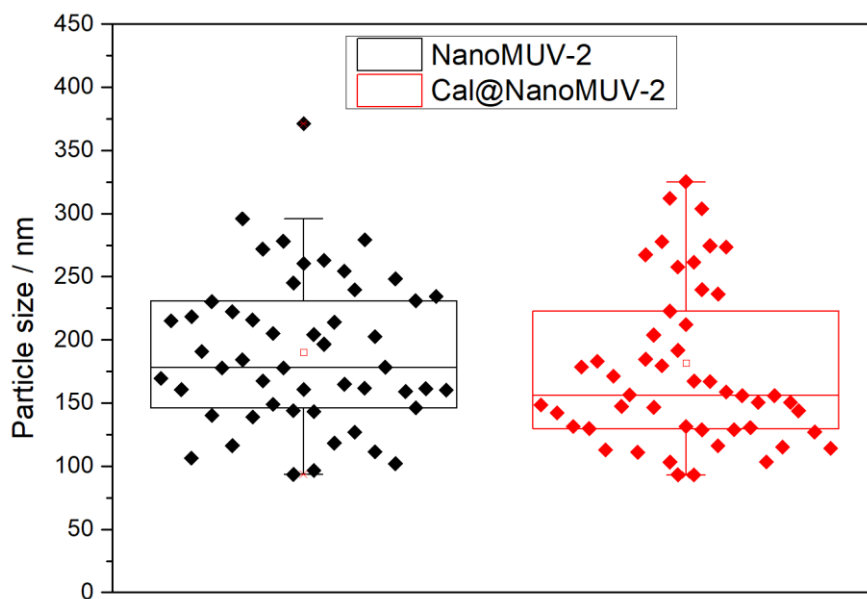


Figure S22: Comparison of particle size analysis of NanoMUV-2 and Cal@NanoMUV-2, showing no statistical difference between the two samples.

S4.3 TGA of Cal@NanoMUV-2

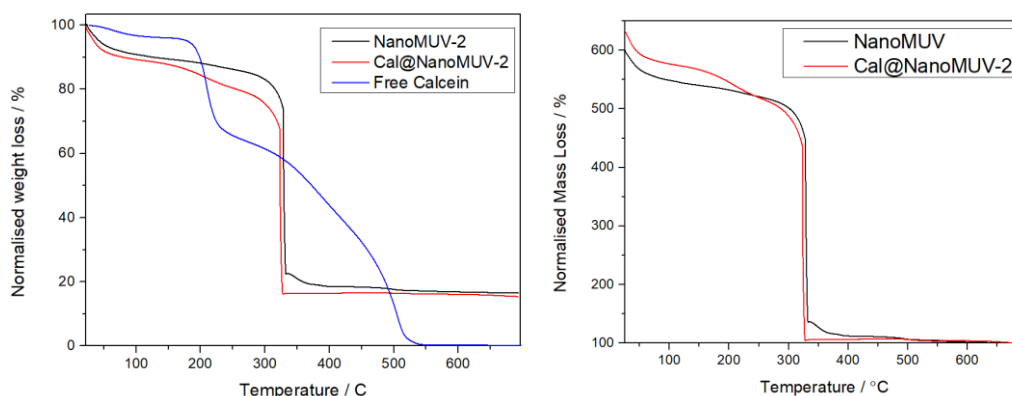


Figure S23: TGA profiles of Cal@NanoMUV-2 with the start (left) or the end (right) of the decomposition profile normalized to 100% compared to NanoMUV-2 and free calcein, showing an increase in the organic content that corresponds to calcein loading.

The amount of Calcein present in the same was calculated using the following methodology, taking into account the number of iron atoms present in the MOF and the residue.⁵

$$R_{\text{exp}} = \frac{M_w[\text{MOF}]}{M_w[\text{Residue}]} = \frac{M_w[\text{MOF}]}{M_w[\text{Metal Residue}]} = \frac{2 \cdot M_w[(\text{Fe}_3\text{O})_2(\text{L})_3] + x \cdot M_w[\text{Calcein}]}{M_w 3[\text{Fe}_2\text{O}_3]}$$

$$x \text{ Calcein} = \frac{R_{\text{exp}} * M_w[\text{Residue}] - M_w[\text{MOF}]}{M_w[\text{Calcein}]} = 0.80$$

Thus,

$$\frac{w}{w} \text{ Calcein} = \frac{0.80 * M_w[\text{Calcein}]}{M_w[(\text{Fe}_3\text{O})_2(\text{L})_3] + 0.80 * M_w[\text{Calcein}]} * 100 = 16.5\%$$

The calculated calcein loading by TGA and TGA are in agreement.

Table S2: mass per cent of Calcein within the samples extracted by different techniques.

UV-Vis	TGA	Average ± SD
17.5	16.5	17 ± 0.5

S4.5 FT-IR of Cal@NanoMUV-2

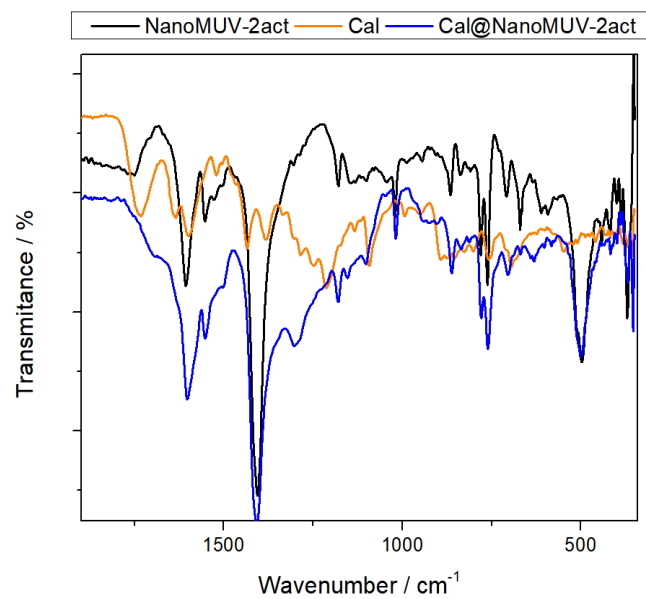


Figure S24: FT-IR of calcein-loaded NanoMUV-2 and pristine NanoMUV-2 compared with free calcein, indicating the attachment of calcein to the metal clusters.

S4.6 N₂ adsorption and desorption isotherms

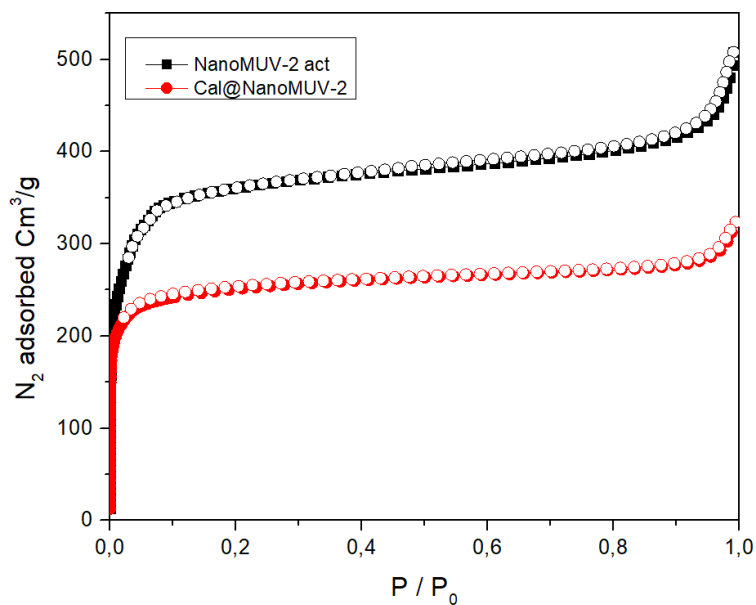


Figure S25: N₂ adsorption and desorption isotherms of Soxhlet-activated Cal@NanoMUV-2.

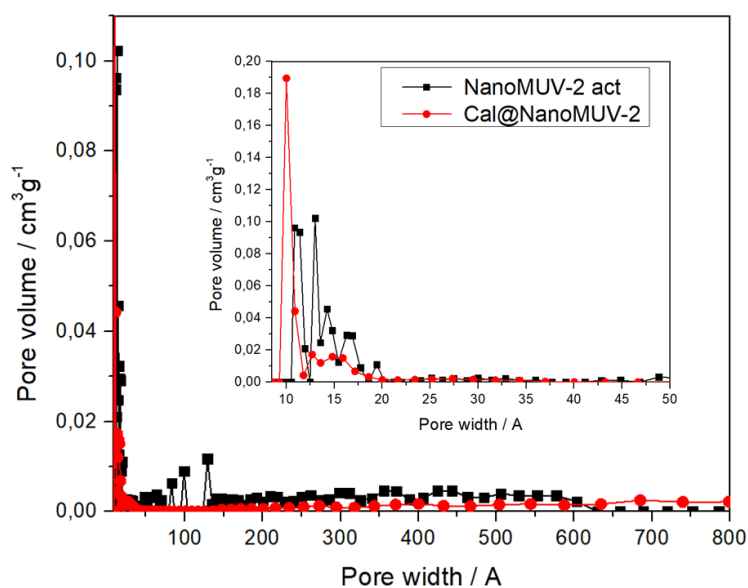


Figure S26: Pore size distribution extracted from N₂ adsorption and desorption isotherms of Cal@NanoMUV-2.

Table S3: Data extracted from N₂ adsorption and desorption isotherms of soxhlet-activated NanoMUV-2 and Cal@NanoMUV-2.

Sample	MUV-2	Cal@NanoMUV-2
S _{BET} Surface area (m ² g ⁻¹)	1404	969
Langmuir surface area (m ² g ⁻¹)	1877	1207
t-plot micropore surface area(m ² g ⁻¹)	1092	781
External surface area (m ² g ⁻¹)	313	188
Total pore volume (P/P0=0.9) (cm ³ g ⁻¹)	0.644	0.429
Micropore volume (cm ³ g ⁻¹)	0.420	0.305
Mesopore volume (cm ³ g ⁻¹)	0.224	0.124

S4.7 Calcein release from Cal@NanoMUV-2

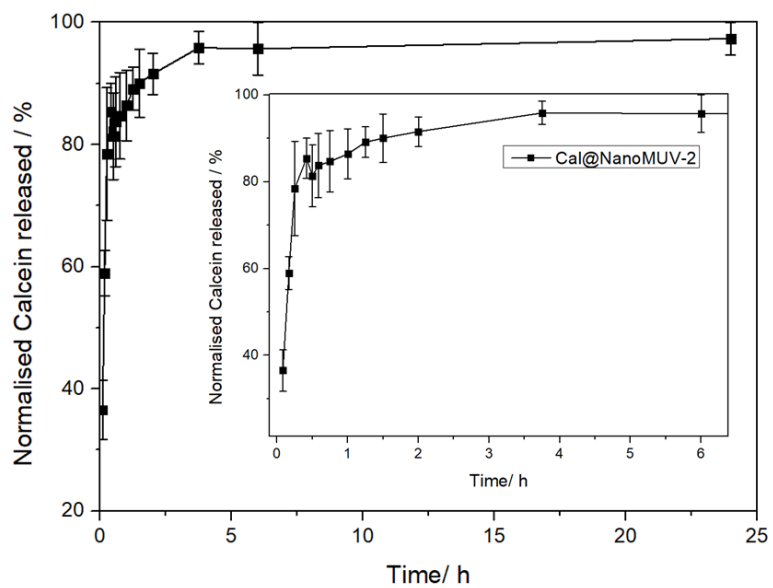


Figure S27: Average of calcein release profiles of MUV-2 in PBS 10X based on the linker release performed three independent times, each of them with n=3.

S5. Cellular internalization of Cal@MUV-2

S5.1 Flow-Assisted cell sorting

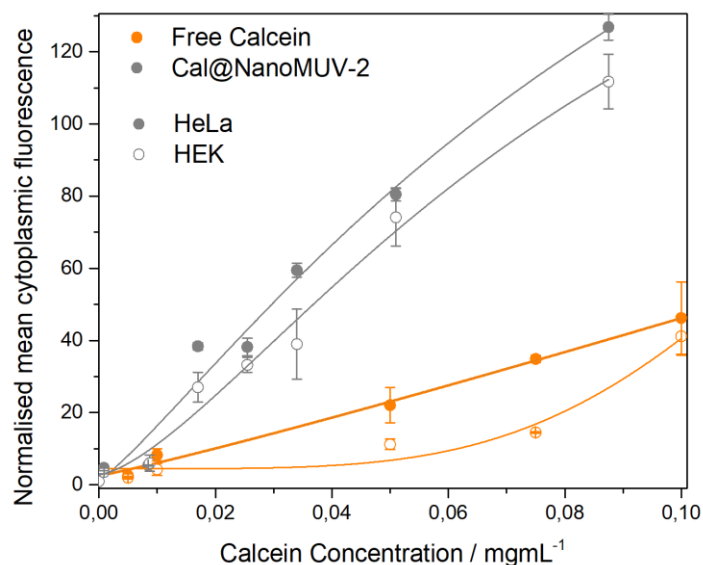


Figure S28: Normalised cytoplasmic fluorescence of HeLa and HEK cells upon incubation with different concentrations of free calcein and Cal@NanoMUV-2. Normalisation was performed toward the cytoplasmic fluorescence of the untreated controls (expressed as a fold increase in fluorescence). Error bars represent the standard deviation of 3 independent experiments.

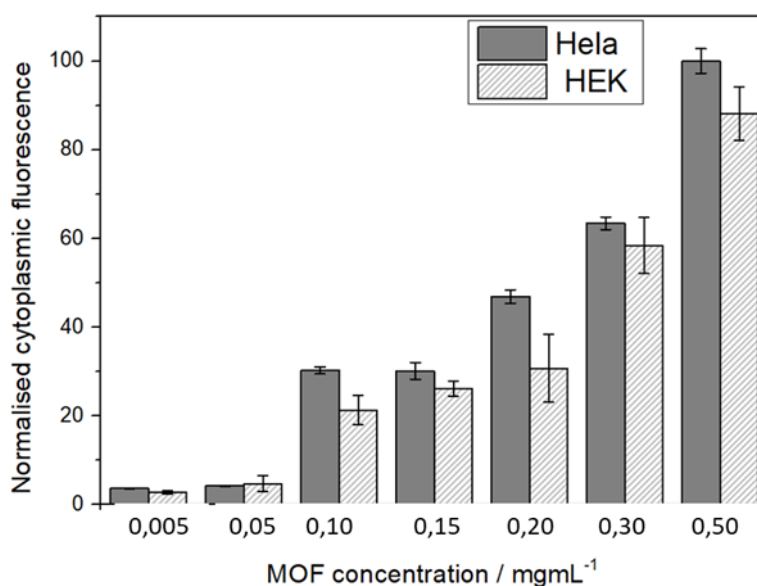


Figure S29: Normalised cytoplasmic fluorescence of HeLa and HEK cells upon incubation with different concentrations of Cal@NanoMUV-2. Normalisation was performed at the highest value (100%) after normalization to the untreated control. Error bars represent the standard deviation of 3 independent experiments.

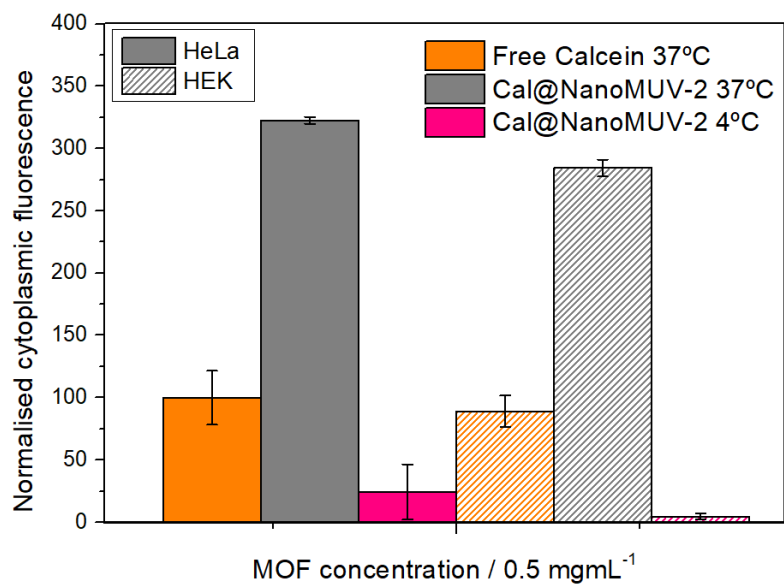


Figure S30: Normalised cytoplasmic fluorescence of HeLa and HEK cells upon incubation with different free calcein and a 0.5 mg·mL⁻¹ concentration of Cal@NanoMUV-2 at 37°C and 4°C. Normalisation (100%) was performed upon calcein at 37 °C, and calcein loading was taken into account for the normalisation. Error bars represent the standard deviation of 3 independent experiments.

S5.2 Confocal microscopy

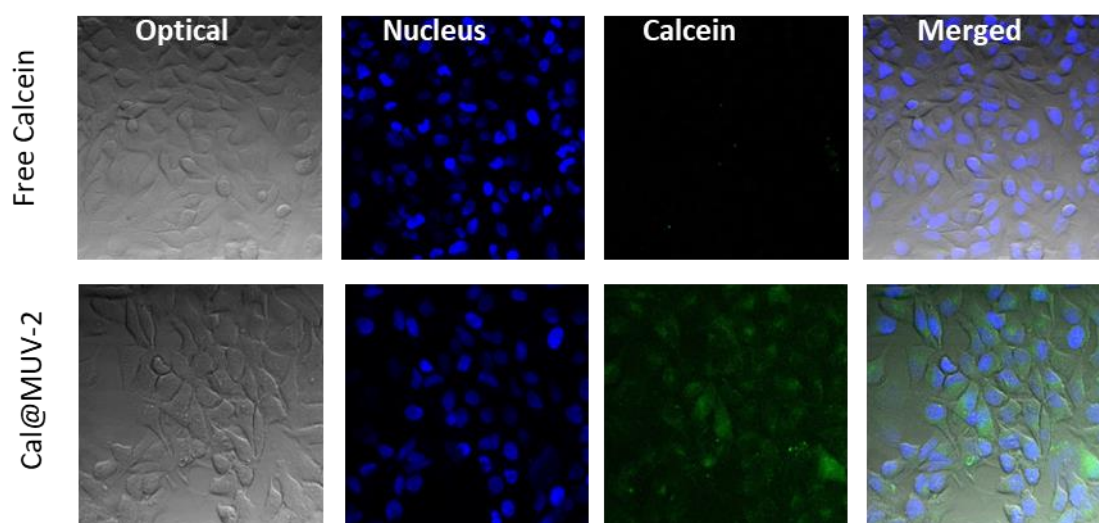


Figure S31: Confocal microscopy images of HeLa cells upon incubation with $0.2 \text{ mg}\cdot\text{mL}^{-1}$ of Cal@NanoMUV-2 and the equivalent free calcein concentration. 20X amplification.

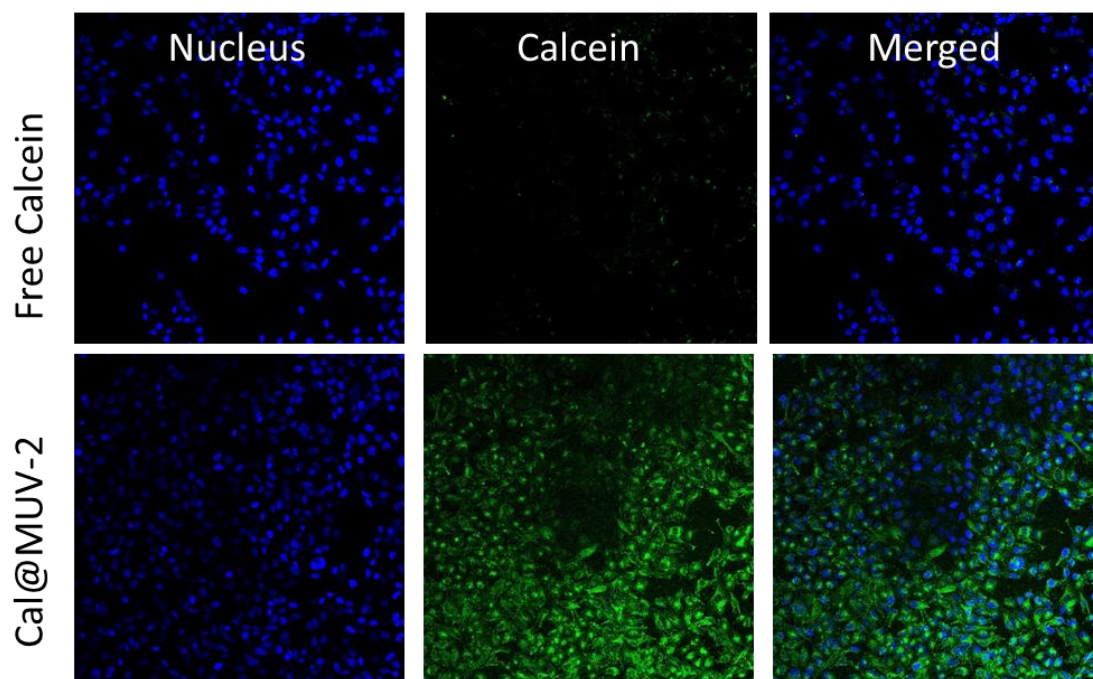


Figure S32: Confocal microscopy images of HeLa cells upon incubation with $0.2 \text{ mg}\cdot\text{mL}^{-1}$ of Cal@NanoMUV-2 and the equivalent free calcein concentration. 20X amplification.

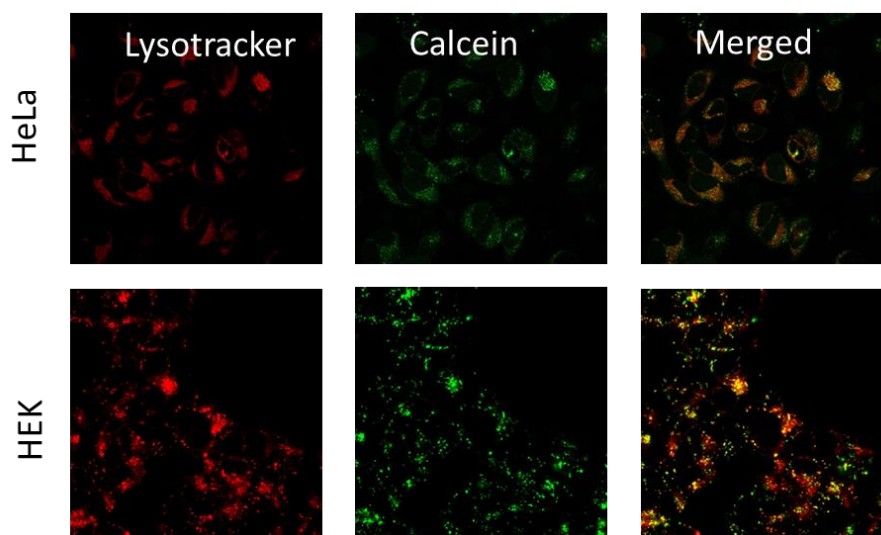


Figure S33: Confocal microscopy images of HeLa and HEK live cells upon incubation with 0.2 mgmL^{-1} of Cal@NanoMUV-2, showing lysosome colocalization.

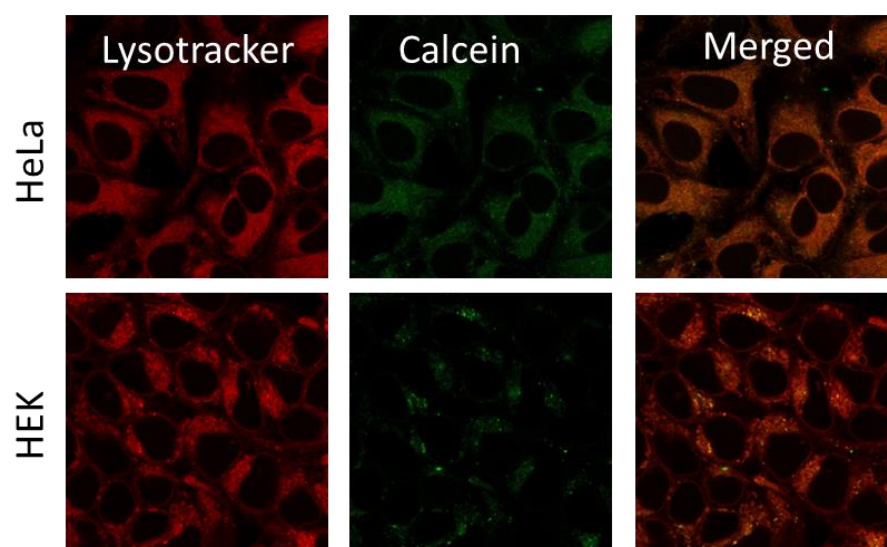


Figure S34: Confocal microscopy images of HeLa and HEK fixed cells upon incubation with 0.05 mgmL^{-1} of Cal@NanoMUV-2, showing lysosome colocalisation.

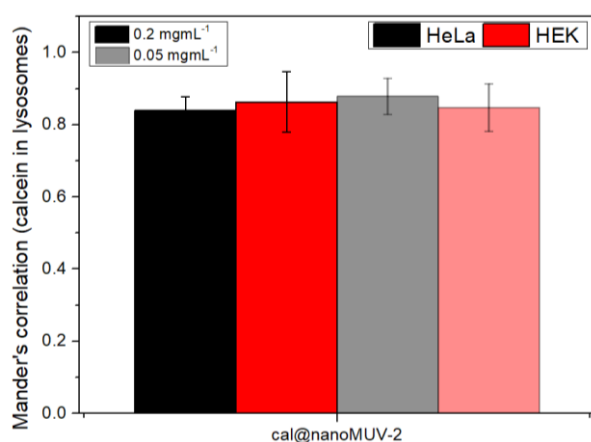


Figure S35: Mander's colocalisation coefficients. The error bars correspond to the standard deviation of 5 different images.

S6. PTX loading into MUV-2

PTX determination was performed upon UV-Vis analysis of the supernatant from PTX loading mixed with the supernatant from the washes. A *ca.* 22 w/w % of PTX loading was determined.

S6.1. PXRD of PTX@NanoMUV-2

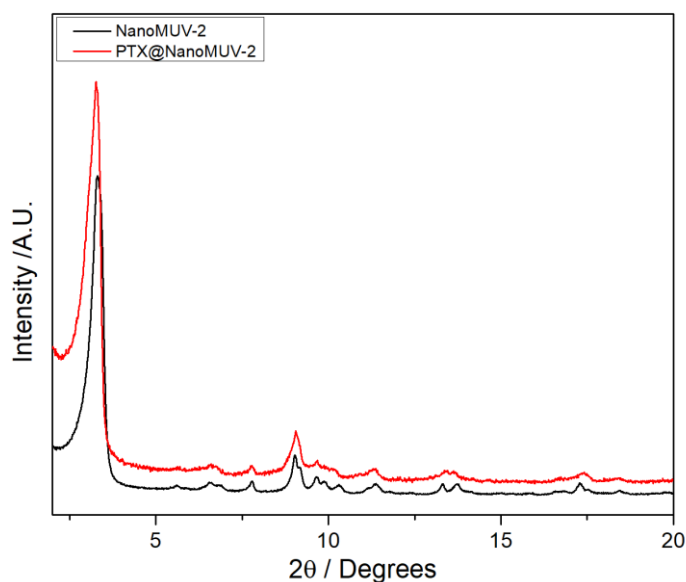


Figure S36: Comparison of PXRD patterns of NanoMUV-2 before and after Paclitaxel loading experiments.

S6.2 SEM PTX@NanoMUV-2

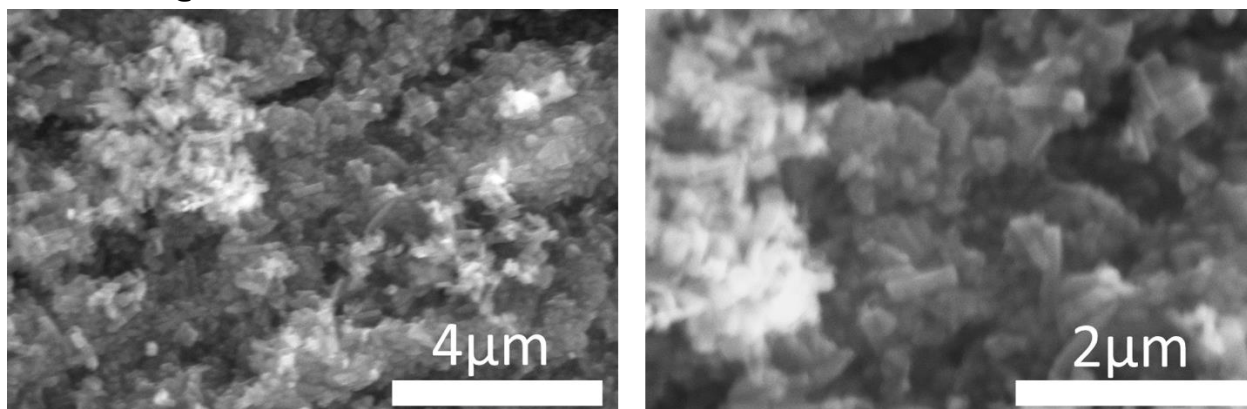


Figure S37: Scanning electron microscope images of PTX@NanoMUV-2.

Table S4: Data extracted from EDX analysis. The EDX profile of PTX@NanoMUV-2, shows a slightly smaller Linker to metal ratio than the theoretical formula, which corresponds to the formula $(\text{Fe}_3\text{O})_2(\text{L})_{2.60}(\text{tax})_x$. This indicates that the PTX loading in EtOH produces missing linker defects in the structure.

S/Fe	L/Fe
1.734	0.434

S6.3 FT-IR of PTX@NanoMUV-2

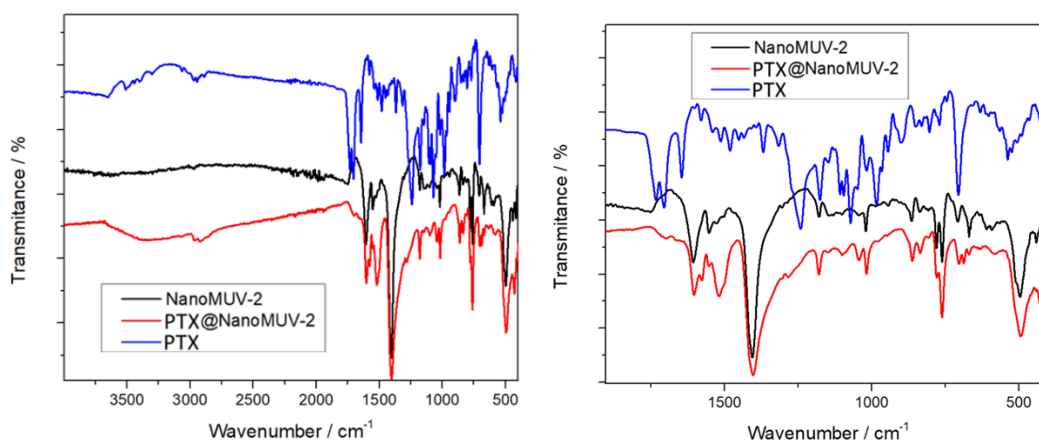


Figure S38: FT-IR profiles of NanoMUV-2, Free Paclitaxel and PTX@NanoMUV-2, showing vibration bands corresponding to PTX loading.

S6.4 TGA of PTX@NanoMUV-2

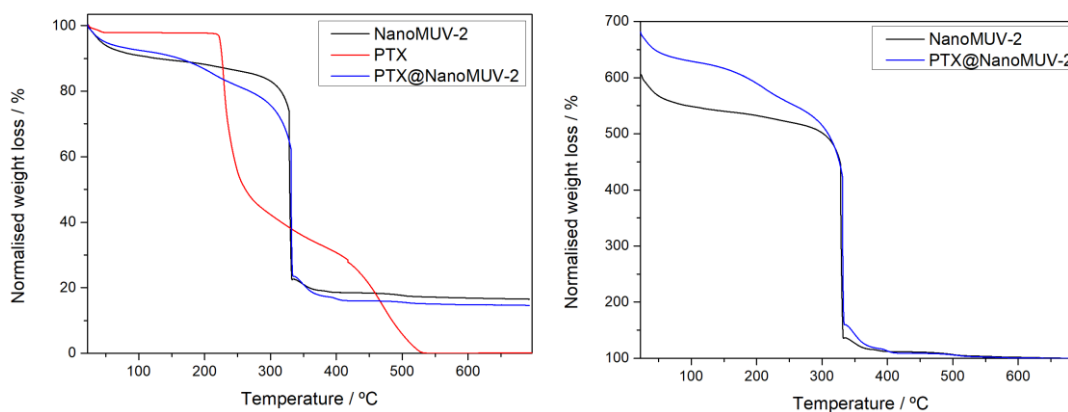


Figure S39: TGA profiles of NanoMUV-2 before and after Paclitaxel loading.

Examination of the profiles taking into account the linker deficiency calculated by EDX (0.434 L per Fe), results in ca. 0.129 molecules of Paclitaxel per iron,⁵ with the theoretical formula $(\text{Fe}_3\text{O})_2(\text{H}_2\text{O})_3(\text{OH})_3(\text{L})_{2.60}(\text{tax})_{0.77}$, which corresponds to ca. 23 w/w%, which is in agreement with the PTX content determined by UV-Vis.

Table S5: mass per cent of PTX within the samples extracted by different techniques.

UV-Vis	TGA	Average \pm SD
22	23	22.5 \pm 0.5

S6.5 N₂ adsorption and desorption of PTX@NanoMUV-2

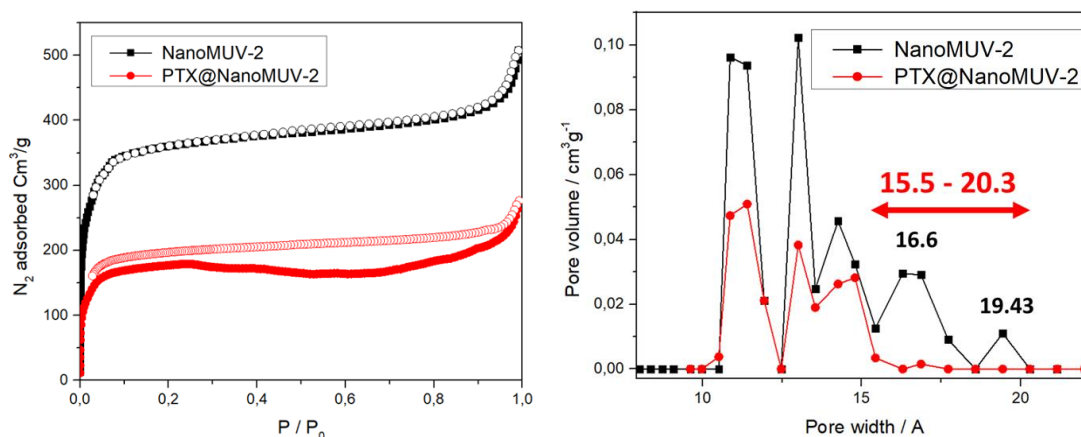


Figure S40: N₂ adsorption and desorption isotherms (left) and pore distribution (right) of Soxhlet-activated NanoMUV-2 and PTX@NanoMUV-2, showing over a 50% decrease in porosity according to BET surface area that indicates Paclitaxel pore loading. Note that a 22.5±0.5 w/w% of Paclitaxel loading was determined.

Table S6: Data extracted from N₂ adsorption and desorption isotherms of Soxhlet-activated NanoMUV-2.

	NanoMUV-2	PTX@NanoMUV-2
SBET Surface area	1404 m ² ·g ⁻¹	662 m ² ·g ⁻¹
Langmuir surface area	1877 m ² ·g ⁻¹	862 m ² ·g ⁻¹
t-plot micropore surface area	1092 m ² ·g ⁻¹	558 m ² ·g ⁻¹
Total pore volume	0.6444 cm ³ ·g ⁻¹	0.315 cm ³ ·g ⁻¹
Micropore volume	0.420 cm ³ ·g ⁻¹	0.223 cm ³ ·g ⁻¹

S7. PTX loading to other MOFs

Following the same procedure of PTX loading into UiO-66 and MIL-100(Fe) and PTX determination, negligible PTX loading was determined by UV-Vis for all the control samples.

S7.1 PXRD of PTX@Loaded samples

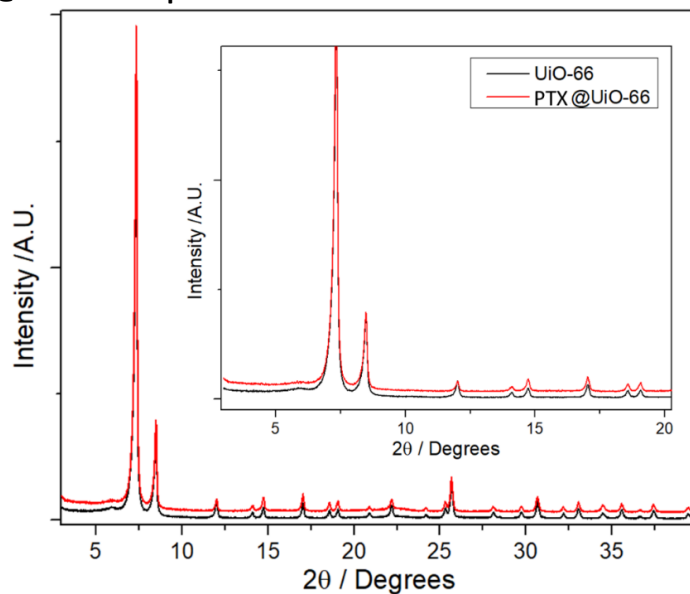


Figure S41: Comparison of PXRD patterns of UiO-66 before and after Paclitaxel loading experiments.

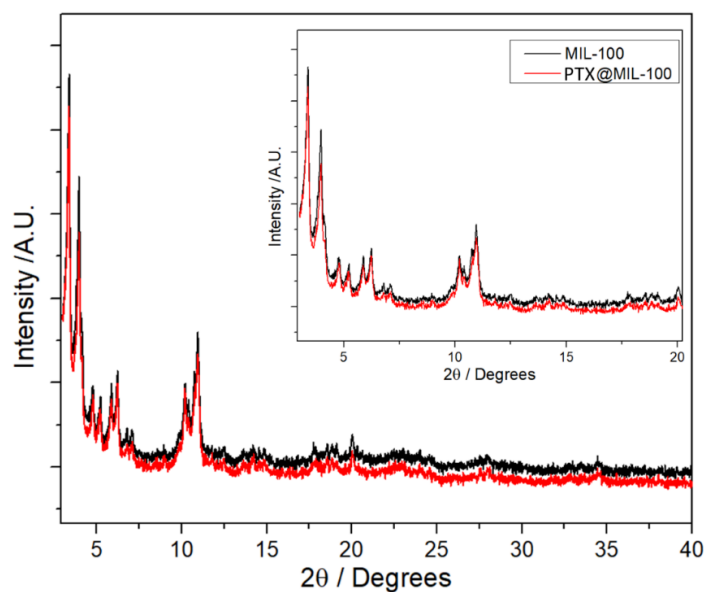


Figure S42: Comparison of PXRD patterns of MIL-100 before and after Paclitaxel loading experiments.

S7.2 SEM PTX@Loaded samples

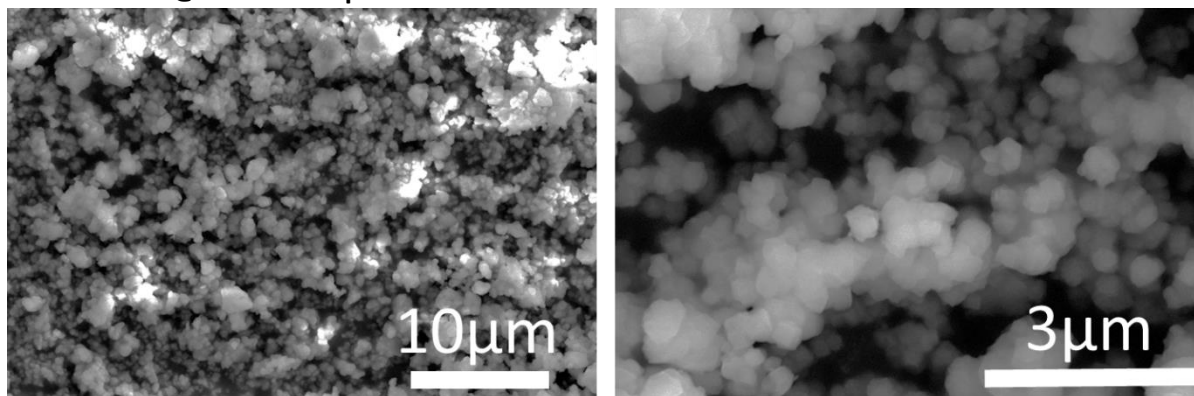


Figure S43: Scanning electron microscope images of PTX@UiO-66.

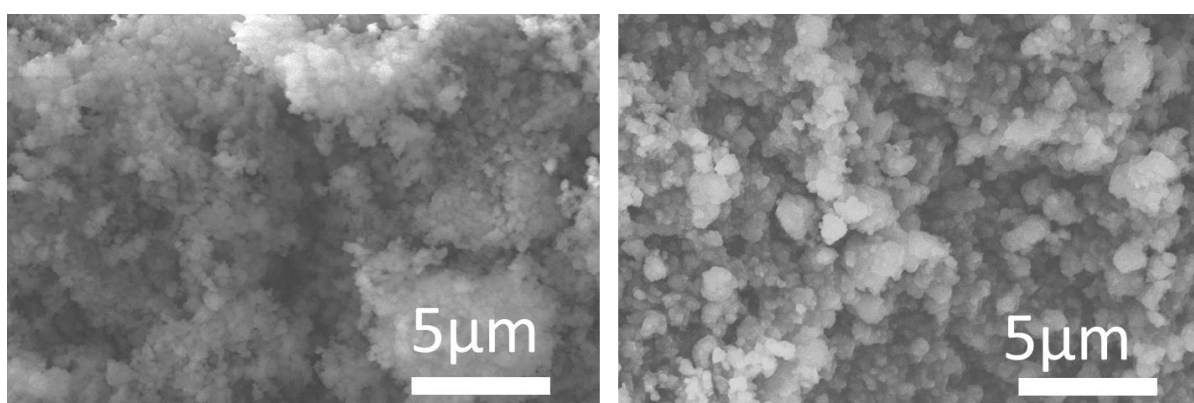


Figure S44: Scanning electron microscope images of PTX@MIL-100.

S7.3 FT-IR of PTX@Loaded samples

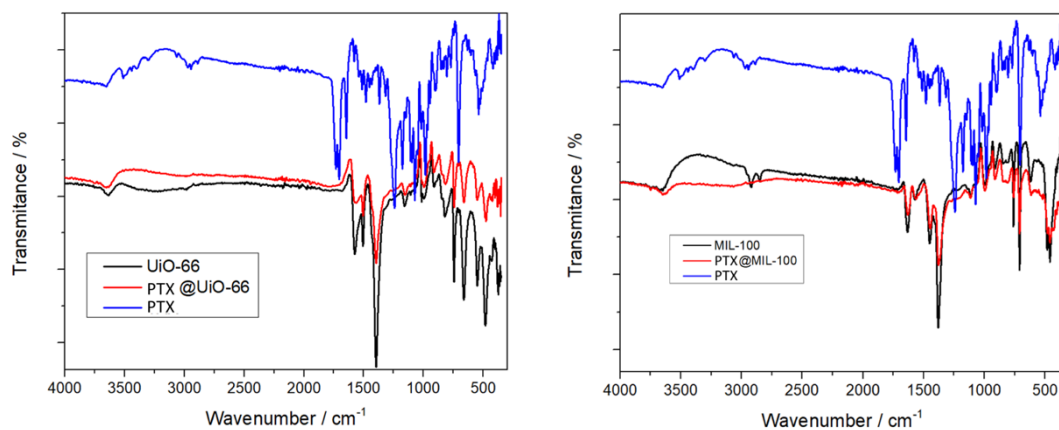


Figure S45: FT-IR profiles of UiO-66 (left) and MIL-100 (right), Free Paclitaxel and PTX@UiO-66, showing no vibration bands corresponding to PTX loading.

S7.4 TGA of PTX@Loaded samples

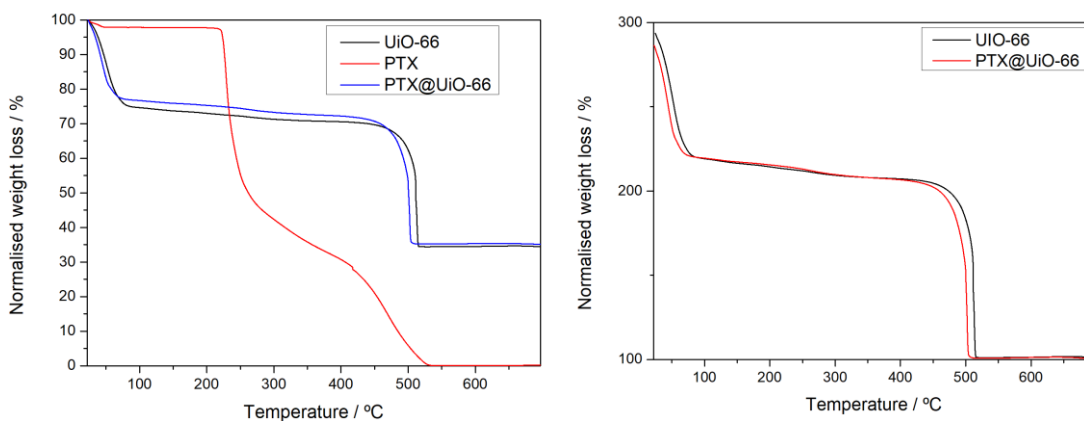


Figure S46: TGA profiles of UiO-66 before and after Paclitaxel loading, indicating the appearance of defects due to minor reduction in the organic content contribution.

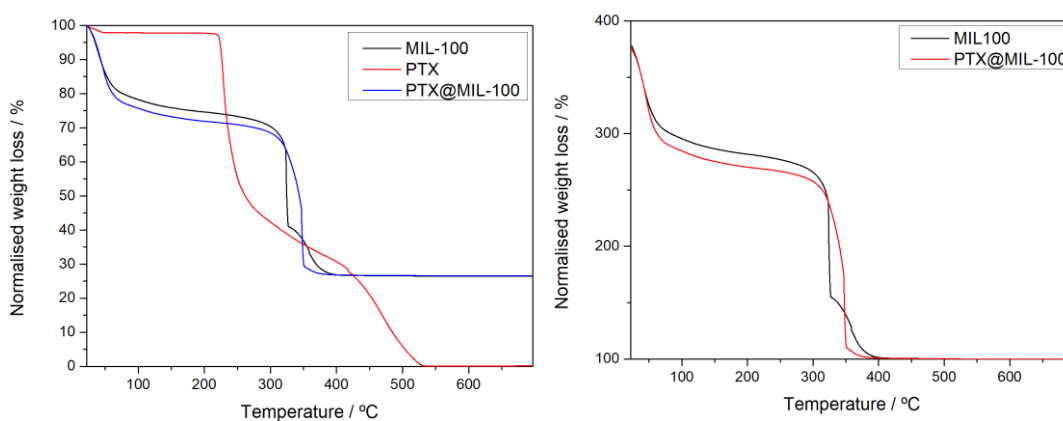


Figure S47: TGA profiles of MIL-100 before and after Paclitaxel loading, indicating the appearance of defects due to minor reduction in the organic content contribution.

S7.5 N₂ adsorption and desorption of PTX@Loaded samples

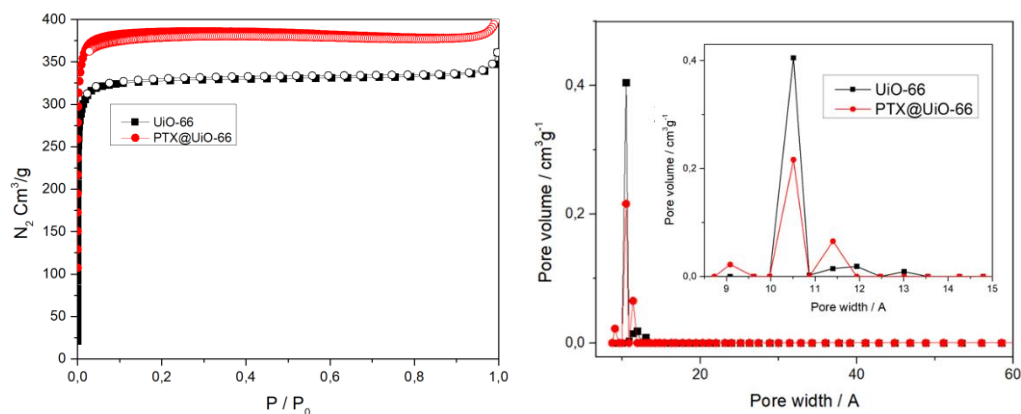


Figure S48: (left) N₂ adsorption and desorption isotherms and (right) pore size distribution of UiO-66 and PTX@UiO-66.

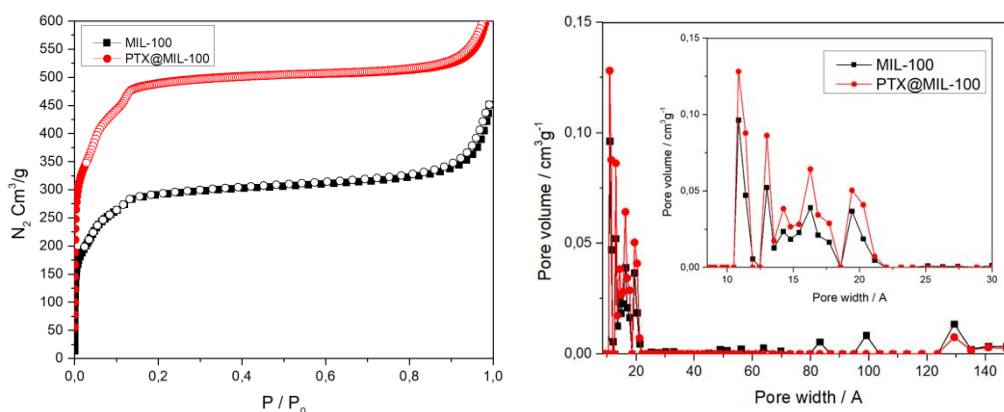


Figure S49: (left) N₂ adsorption and desorption isotherms and (right) pore size distribution of MIL-100 and PTX@MIL-100.

In both cases, the increase in the material's porosity could be due to the creation of defects, as suggested by the thermal decomposition profiles.

Table S7: Data extracted from N₂ adsorption and desorption isotherms.

	UiO-66	PTX@UIO-66	MIL-100	PTX@MIL-100
SBET Surface area / m²·g⁻¹	1347	1572	1018	1653
Langmuir surface area / m²·g⁻¹	1472	1654	1578	2367
t-plot micropore surface area / m²·g⁻¹	1291	1530	713	1011
Total pore volume / cm³·g⁻¹	0.525	0.5885	0.349	0.813
Micropore volume / cm³·g⁻¹	0.482	0.577	0.309	0.467

S8. Cytotoxicity of PTX@NanoMUV-2 and free PTX

S8.1 Cytotoxicity of free Paclitaxel

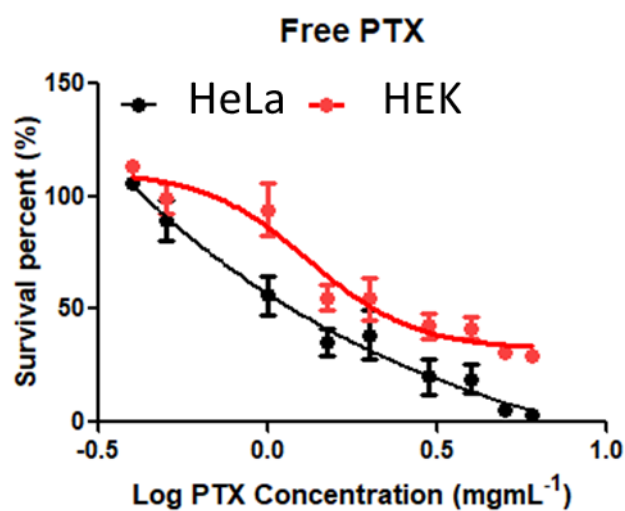


Figure S50: Cell proliferation assays (MTS) carried out on HeLa and HEK cells after 72 h incubation with PTX in growth media. Each experiment has been performed 3 independent times, each with n=4.

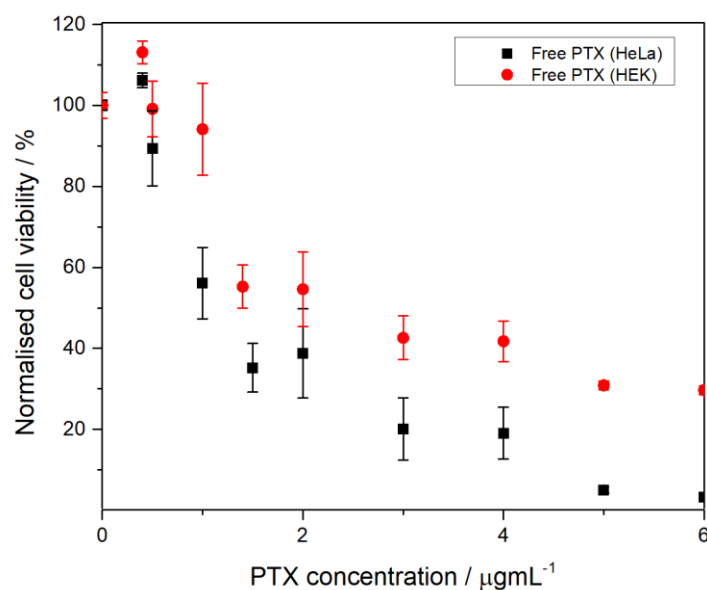


Figure S51: Cell proliferation assays (MTS) carried out on HeLa and HEK cells after 72 h incubation with PTX in growth media. Each experiment has been performed 3 independent times, each with n=4.

S8.2 Cytotoxicity PTX@NanoMUV-2

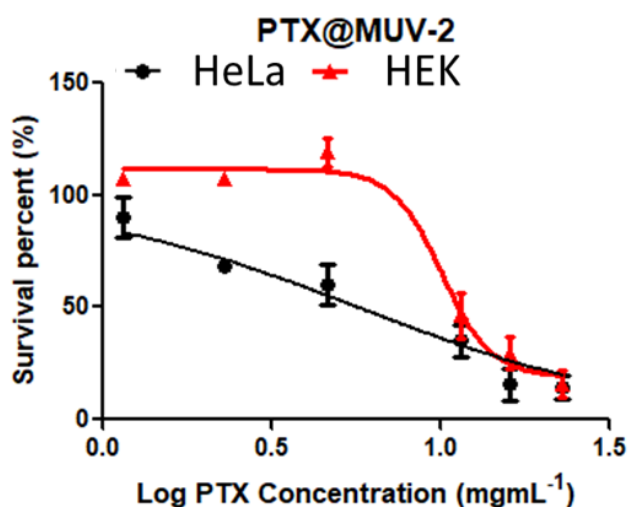


Figure S52: Cell proliferation assays (MTS) carried out on HeLa and HEK cells after 72 h incubation with PTX@NanoMUV-2 in growth media. Each experiment has been performed 3 independent times, each with n=4.

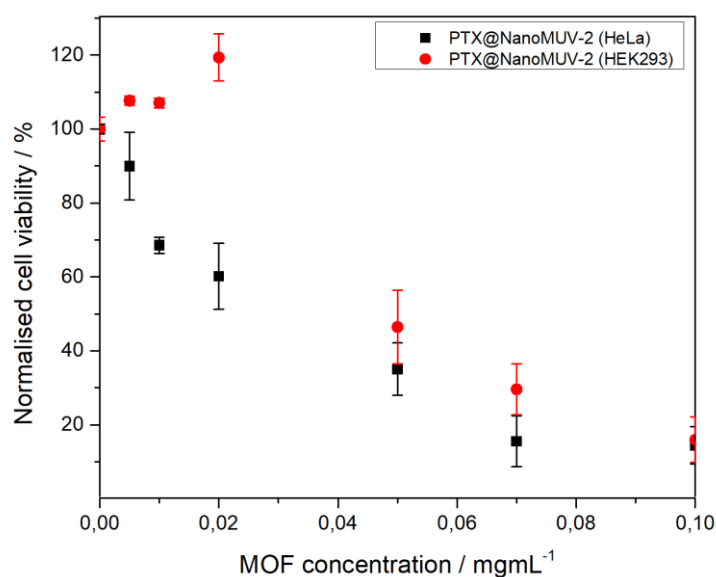


Figure S53: Cell proliferation assays (MTS) carried out on HeLa and HEK cells after 72 h incubation with PTX@NanoMUV-2 in growth media. Each experiment has been performed 3 independent times, each with n=4.

Table S8: IC₅₀ values and selectivity index based on PTX concentration.

Sample	IC ₅₀ HeLa (µgmL ⁻¹)	IC ₅₀ HEK(µgmL ⁻¹)	Selectivity index
Free Paclitaxel	1.048 ± 0.116	1.319 ± 0.158	1.26
PTX@NanoMUV-2	5.73 ± 0.519	10.06 ± 0.905	1.76

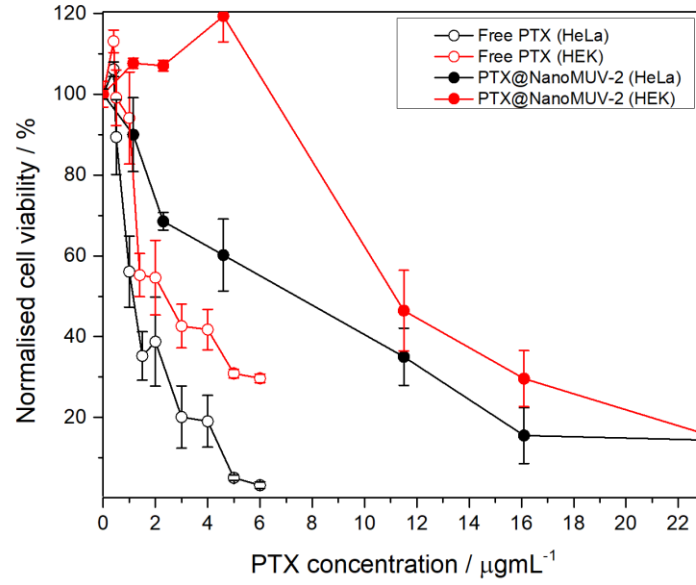


Figure S54: Comparison of cell proliferation assays (MTS) carried out on HeLa and HEK cells after 72 h incubation with free PTX and PTX@NanoMUV-2 in growth media. Each experiment has been performed 3 independent times, each with n=4.

S9 Characterisation of functionalised MUV-2

S9.1 Characterisation of MUV-2-Oct

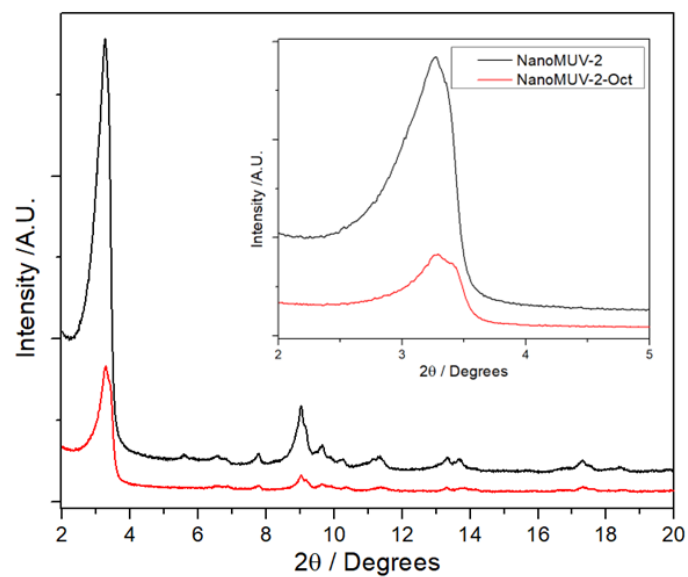


Figure S55: Comparison of experimental PXRD pattern of NanoMUV-2 activated before and after oct-Br surface functionalisation.

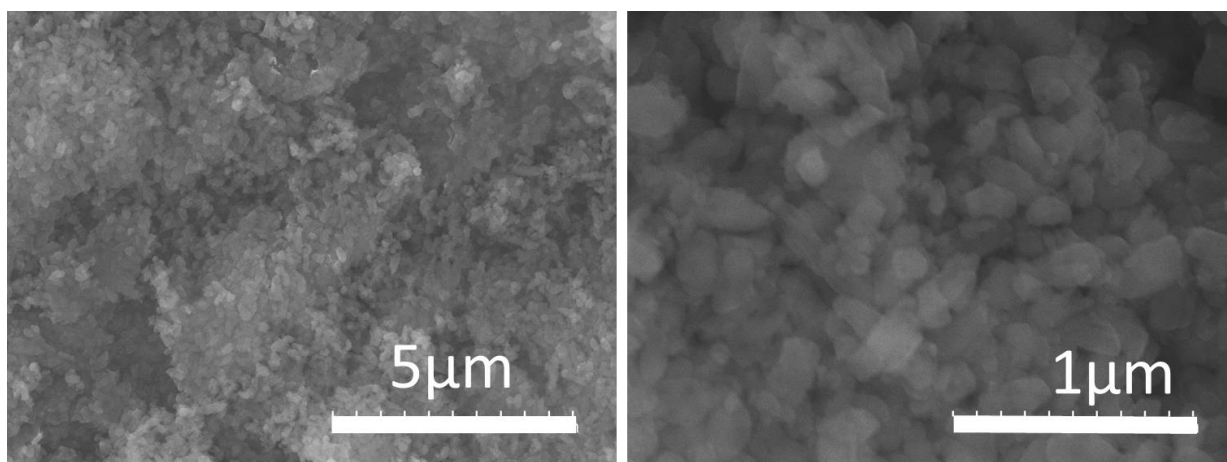


Figure S56: Scanning electron microscope images of NanoMUV-2-Oct.

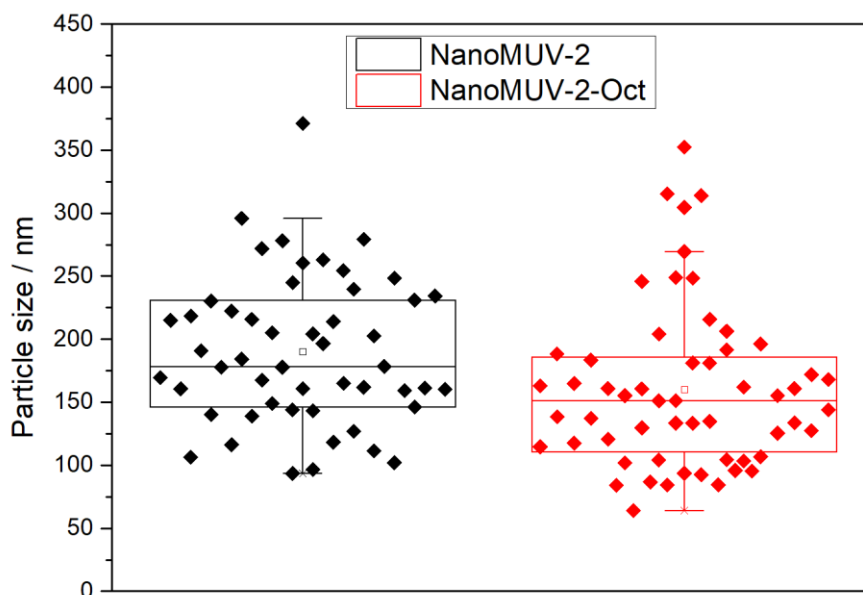


Figure S57: Comparison of particle size analysis of NanoMUV-2-Oct and NanoMUV-2, showing no statistical difference between the two samples.

Table S9: Data extracted from EDX analysis, showing 2.1 S per Fe according to the theoretical molecular formula $(\text{Fe}_3\text{O})_2(\text{L})_3$. The presence of Br in 8-Bromo octanoic acid allows for the calculation of its molecular ratios in comparison to S and Fe, which can be converted into a mass fraction within the estimated structure. ca. 0.53 oct (Br) per S and ca. 0.28 Oct/Fe, lead to the estimated $(\text{Fe}_3\text{O})_2(\text{L})_3(\text{Oct})_{1.68}$ simplified structure, in which Br-Oct correspond to ca. 13 w/w%.

Br-Fe	Br/L	S/Fe	L/Fe
0.28	0.535	2.11	0.53

Table S10: Molar and mass fractions extracted from EDX analysis.

Molar fraction Br Vs Fe	0.220
Mass fraction Oct	0.129

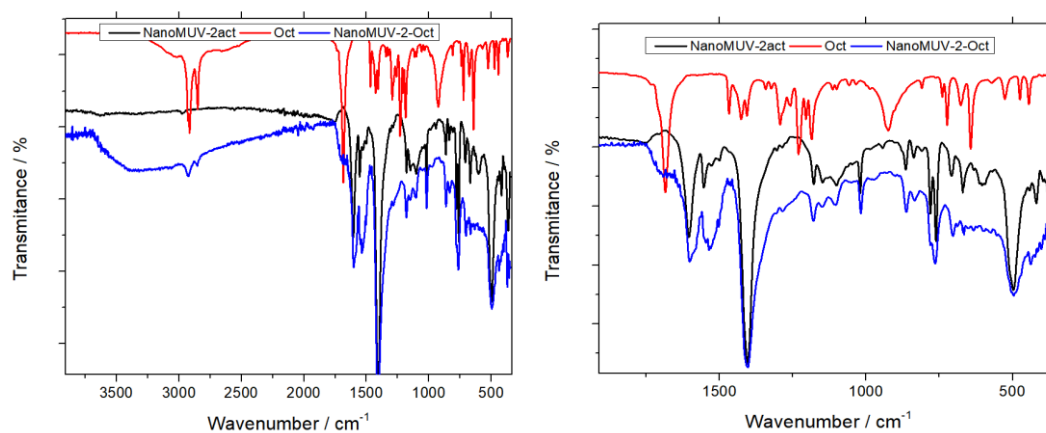


Figure S58: FT-IR profiles of NanoMUV-2, Free oct and NanoMUV-2-Oct, showing vibration bands corresponding to oct functionalisation.

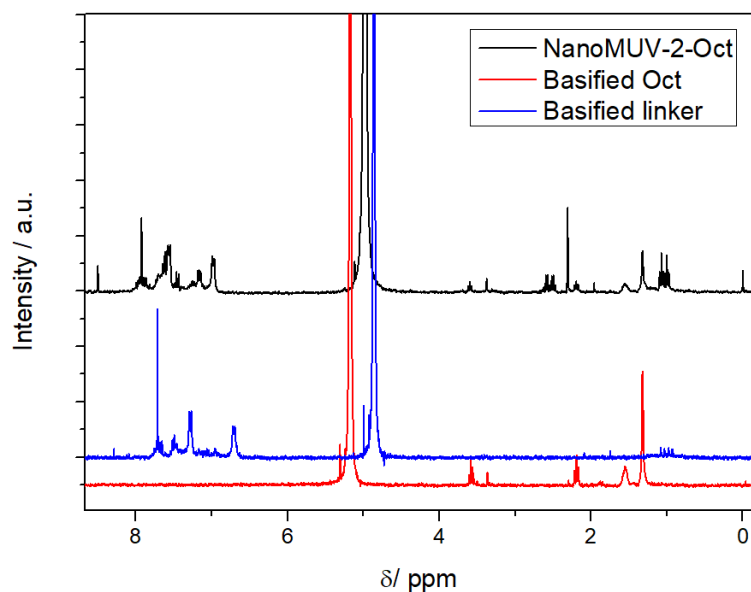


Figure S59: Basified ^1H NMR profile of NanoMUV-2-Oct in D₂O, compared to free Oct and TTF ligand, showing that upon basification several ligand species with different degrees of deprotonation co-exist, together with Oct characteristic signals.

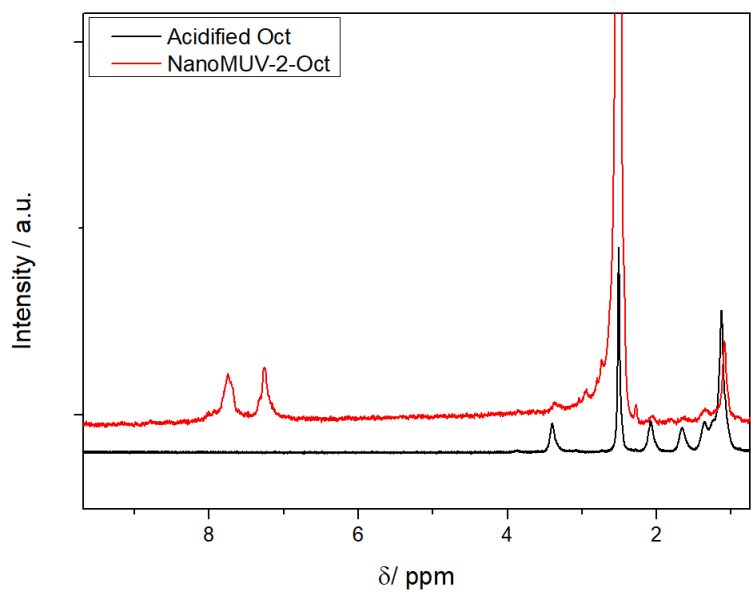


Figure S60: Acid-digested ^1H NMR spectra of NanoMUV-2-Oct compared to acidified Oct in DMSO, showing the characteristic signal of 8-Bromo octanoic. The analysis based on the molar ratio between Oct and ligand signals results in ca. 0.493 Oct per ligand, which is equivalent to a ca. 11.4% w/w for the theoretical formula $(\text{Fe}_3\text{O})_2(\text{L})_3(\text{Oct})_{1.479}$

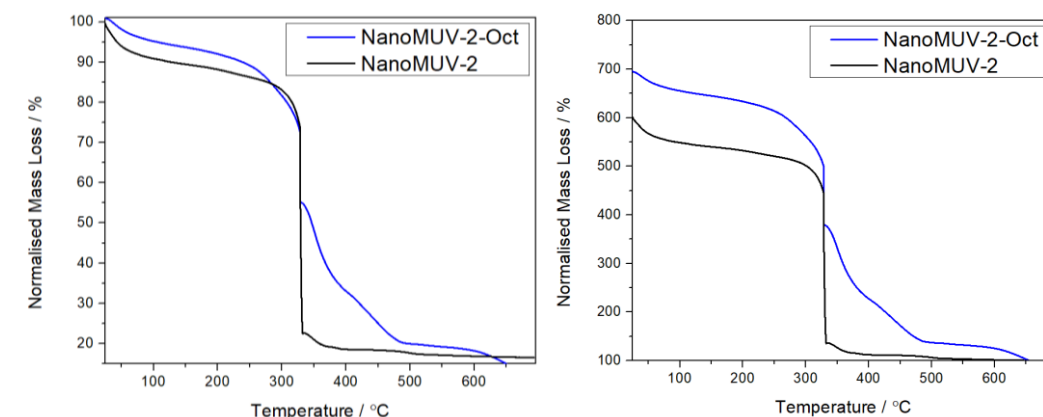


Figure S61: TGA profiles of NanoMUV-2 and NanoMUV-2-Oct with the start (left) and end (right) of the decomposition profile normalized to 100%, showing an increase in the organic content for the surface functionalised sample and a change in the decomposition profile.

The following calculations were performed in order to extract the amount of Oct present in the structure through TGA.⁵

$$R_{\text{exp}} = \frac{M_w[\text{MOF}]}{M_w[\text{Residue}]} = \frac{M_w[\text{MOF}]}{M_w[\text{Metal Residue}]} = \frac{M_w[(\text{Fe}_3\text{O})_2(\text{L})\text{X}(\text{Oct})_x * \text{nmr}]}{M_w 3 * [\text{Fe}_2\text{O}_3]}$$

Assuming that the M_w of the Soxhlet activated NanomUV-2 has not been altered (i.e. surface functionalization with Oct has not replaced linker in the structure) given that no color coming from the linker was observed in the supernatant after surface functionalization, the TGA of NanoMUV-2 (act) has been used to extract its molecular weight using the following formula.

$$R_{\text{exp}} = \frac{M_w[\text{MOF}]}{M_w[\text{Residue}]} = \frac{M_w[\text{MOF}]}{M_w[\text{Metal Residue}]}$$

$$M_w[\text{MOF}] = R_{\text{exp}} * M_w 3 * [\text{Fe}_2\text{O}_3]$$

Then, in the following formula, this molecular weight has been substituted to extract the weight per cent of oct within the structure.

$$R_{\text{exp}} = \frac{M_w[\text{MOF}]}{M_w[\text{Residue}]} = \frac{M_w[\text{MOF}]}{M_w[\text{Metal Residue}]} = \frac{M_w[(\text{Fe}_3\text{O})_2(\text{L})_3(\text{Oct})_x]}{M_w 3 * [\text{Fe}_2\text{O}_3]}$$

$$R_{\text{exp}} = \frac{M_w[\text{NanoMuv2}] + X * M_w[\text{Oct}]}{M_w 3 * [\text{Fe}_2\text{O}_3]}$$

Then,

$$X \text{ Oct} = (R_{\text{exp}} * M_w 3 * [\text{Fe}_2\text{O}_3] - M_w [\text{NanoMUV} - 2]) / M_w [\text{Oct}]$$

This resulted in the following structure simplified $(\text{Fe}_3\text{O})_2(\text{L})_3(\text{Oct})_{1.5}$

Once the structure has been obtained, the weight per cent of Oct in the structure can be calculated as

$$\frac{w}{w} \% Oct = \frac{\text{number of oct in the structure} * M_w[\text{oct}]}{M_w[\text{MOF}]} * 100 = 11\%$$

The w/w% obtained agrees with the weight per cent estimated with the data extracted by EDX analysis and ¹HNMR.

This degree of functionalization is too high to be only located at the outer surface, meaning that at least in part, the pore channels (inner surface) of the MOF have been functionalized).

Table S11: mass per cent of Oct within the samples extracted by different techniques.

EDX	¹ HNMR	TGA	Average ± SD
12.9	11.4	11	11.8 ± 0.8

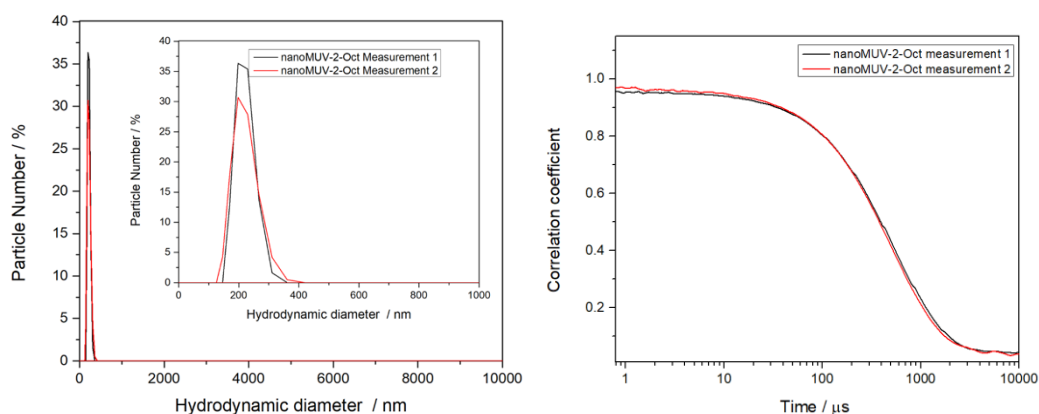


Figure S62: (left) Dynamic light scattering profile showing the number % of particles as a function of their diameter in PBS 10X. Each measurement was performed with a waiting time of 10 minutes, showing slightly bigger particle sizes than SEM but no significant aggregation over time. $0.1 \text{ mg}\cdot\text{mL}^{-1}$ dispersion of NanoMUV-2-Oct. (right) Correlogram of $0.1 \text{ mg}\cdot\text{mL}^{-1}$ dispersion of NanoMUV-2-Oct in PBS 10X, showing no aggregates over the course of time.

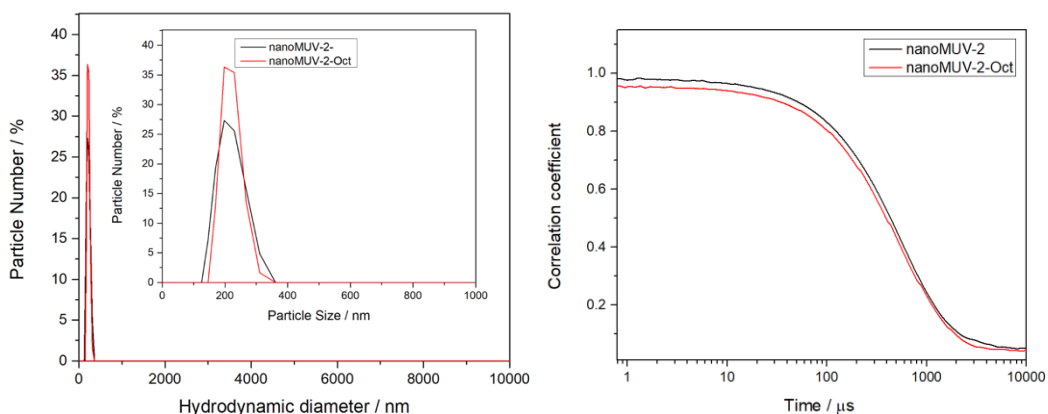


Figure S63: (Left) Comparison of dynamic light scattering profile of NanoMUV-2-Oct and NanoMUV-2 showing the number % of particles as a function of their diameter in PBS 10X. The colloidal stability upon surface functionalisation seems to have improved. (Right) Correlogram of $0.1 \text{ mg}\cdot\text{mL}^{-1}$ dispersion of NanoMUV-2-Oct in PBS 10X, showing no aggregates over the course of time.

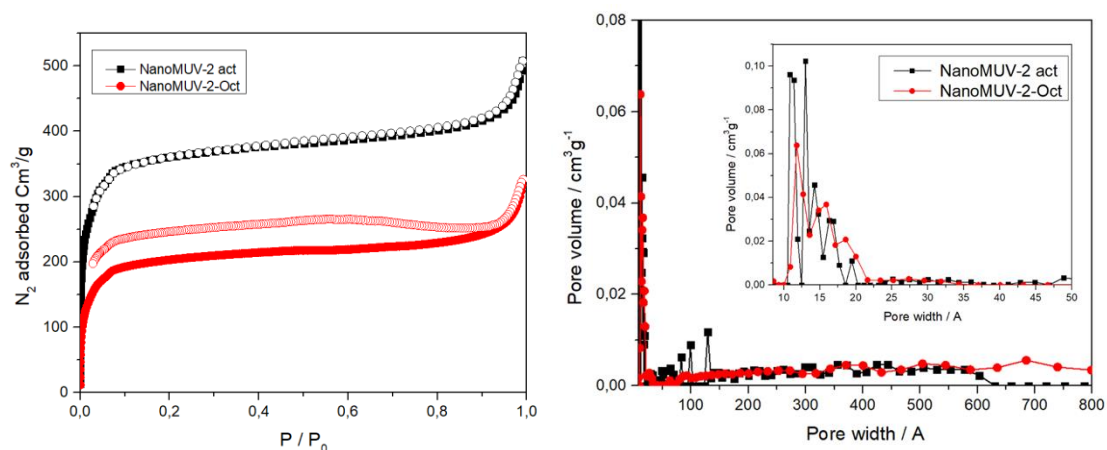


Figure S64: (Left) N_2 adsorption and desorption isotherms NanoMUV-2 and NanoMUV-2-Oct, showing a decrease in adsorption upon surface modification, both as a consequence of the higher molecular weight of the functionalized MOF and the partial pore blockage due to inner surface functionalization. (Right) Pore size distribution extracted from N_2 adsorption isotherm NanoMUV-2 and NanoMUV-2-Oct.

Table S12: Data extracted from N_2 adsorption and desorption isotherms of soxhlet-activated NanoMUV-2. The changes in porosity do not correspond strictly to a *ca.* 13% decrease due to the increased molecular weight, which together with the high degree of functionalization and the reduced size of the mesopores, indicated inner surface functionalization.

	NanoMUV-2	NanoMUV-2-Oct
SBET Surface area / $m^2 \cdot g^{-1}$	1404	773
Langmuir surface area / $m^2 \cdot g^{-1}$	1877	1090
t-plot micropore surface area / $m^2 \cdot g^{-1}$	1092	561
Total pore volume / $cm^3 \cdot g^{-1}$	0.644	0.368
Micropore volume / $cm^3 \cdot g^{-1}$	0.420	0.224

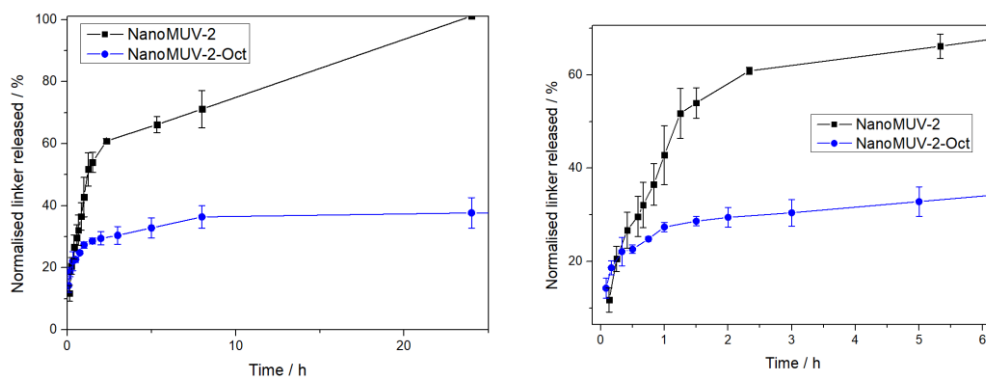


Figure S65: Degradation profile of NanoMUV-2-Oct in PBS 10X compared with NanoMUV-2 (based on 3 experiments), showing incomplete degradation after 24 hours.

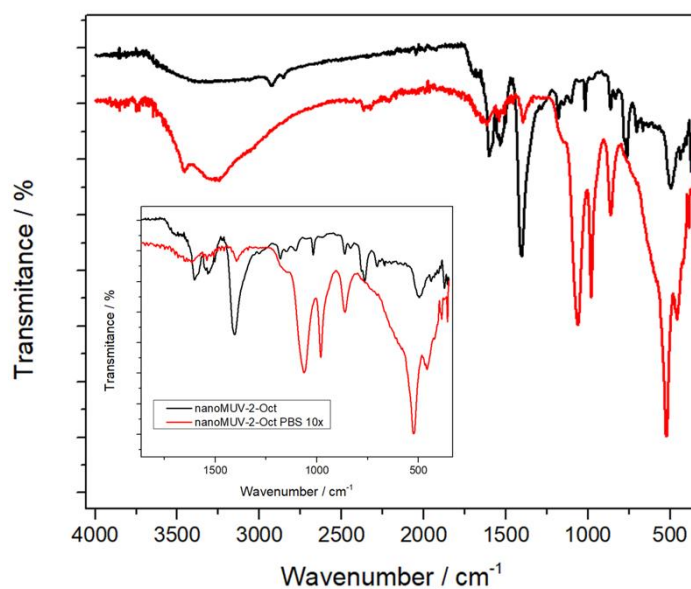


Figure S66: FT-IR profiles of NanoMUV-2-Oct before and after immersion in PBS 10X for 15 minutes. After immersion the sample was centrifuged, the supernatant removed and washed once with EtOH. The samples were dried at room temperature for 3 hours before FT-IR.

S9.2 Characterisation of MUV-2-FA

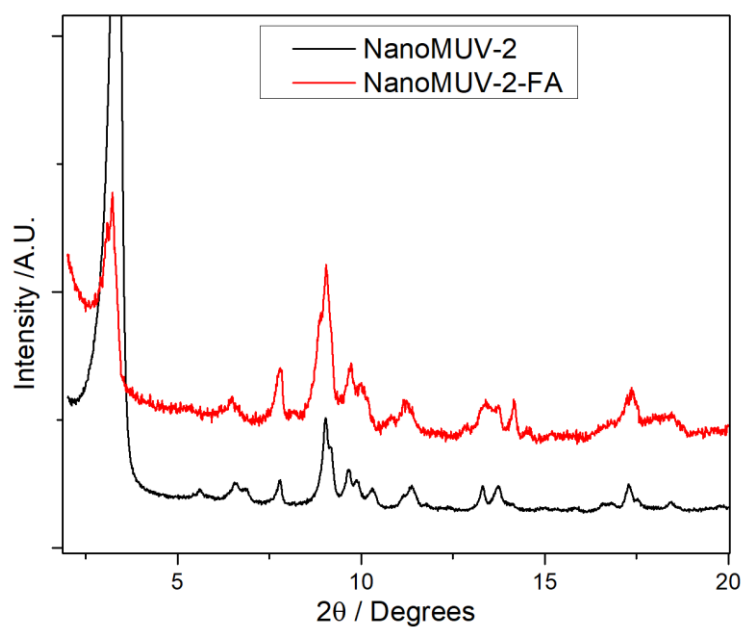


Figure S67: Comparison of PXRD patterns of NanoMUV-2 before and after surface FA functionalisation.

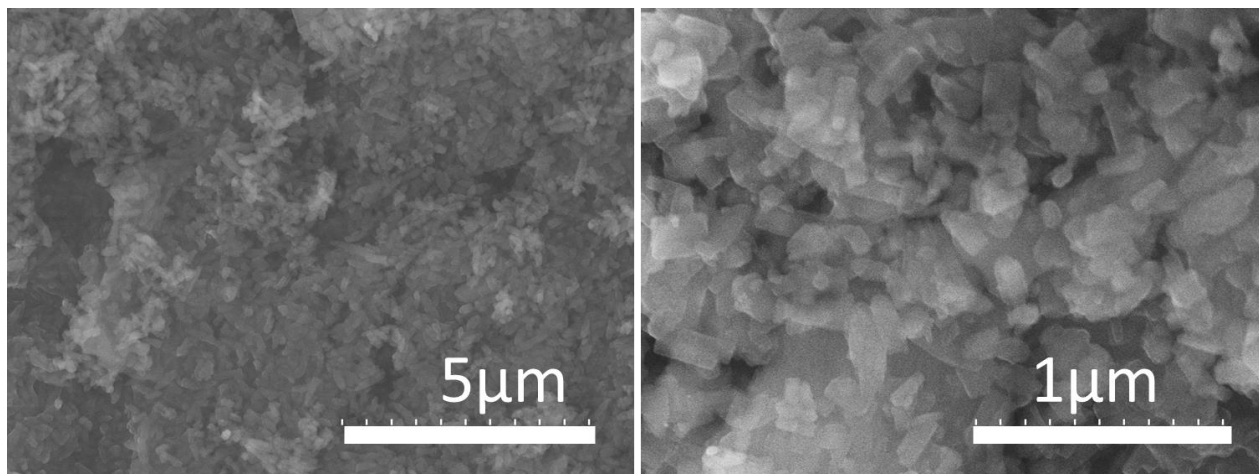


Figure S68: Scanning electron microscope images of NanoMUV-2-FA.

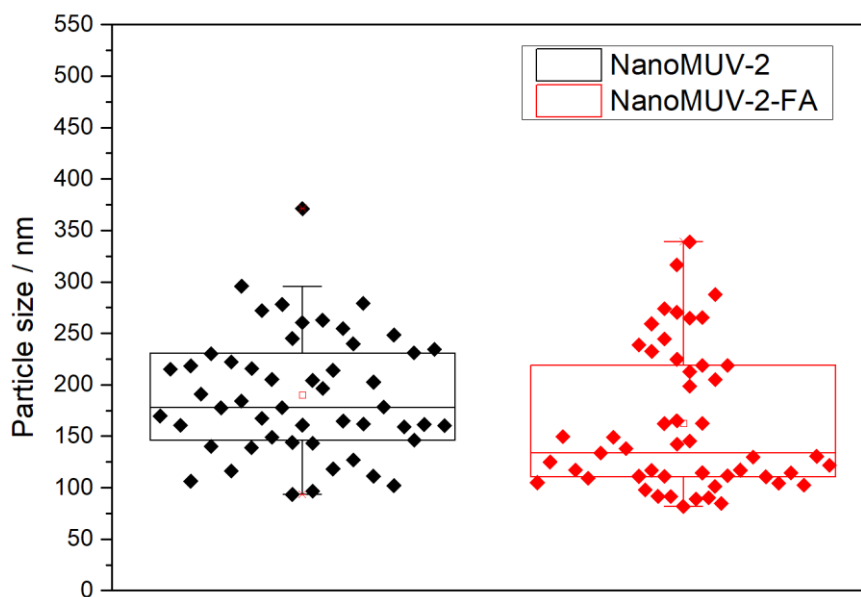


Figure S69: Comparison of particle size analysis of NanoMUV-2-FA and NanoMUV-2, showing no statistical difference between the two samples, showing an average of *ca.* 163 nm and standard deviation of *ca.* 70 nm, with no statistical significance with NanoMUV-2 *ca.* 190 ± 59 nm).

EDX analysis showed 1.611S per Fe, which is significantly lower than the expected (S/Fe 2) for the theoretical molecular formula $(\text{Fe}_3\text{O})_2(\text{L})_3$. The experimental ratio corresponds to a structure with the approximated linker to metal ratio of $(\text{Fe}_3\text{O})_2(\text{L})_{2.41}(\text{FA})_x$

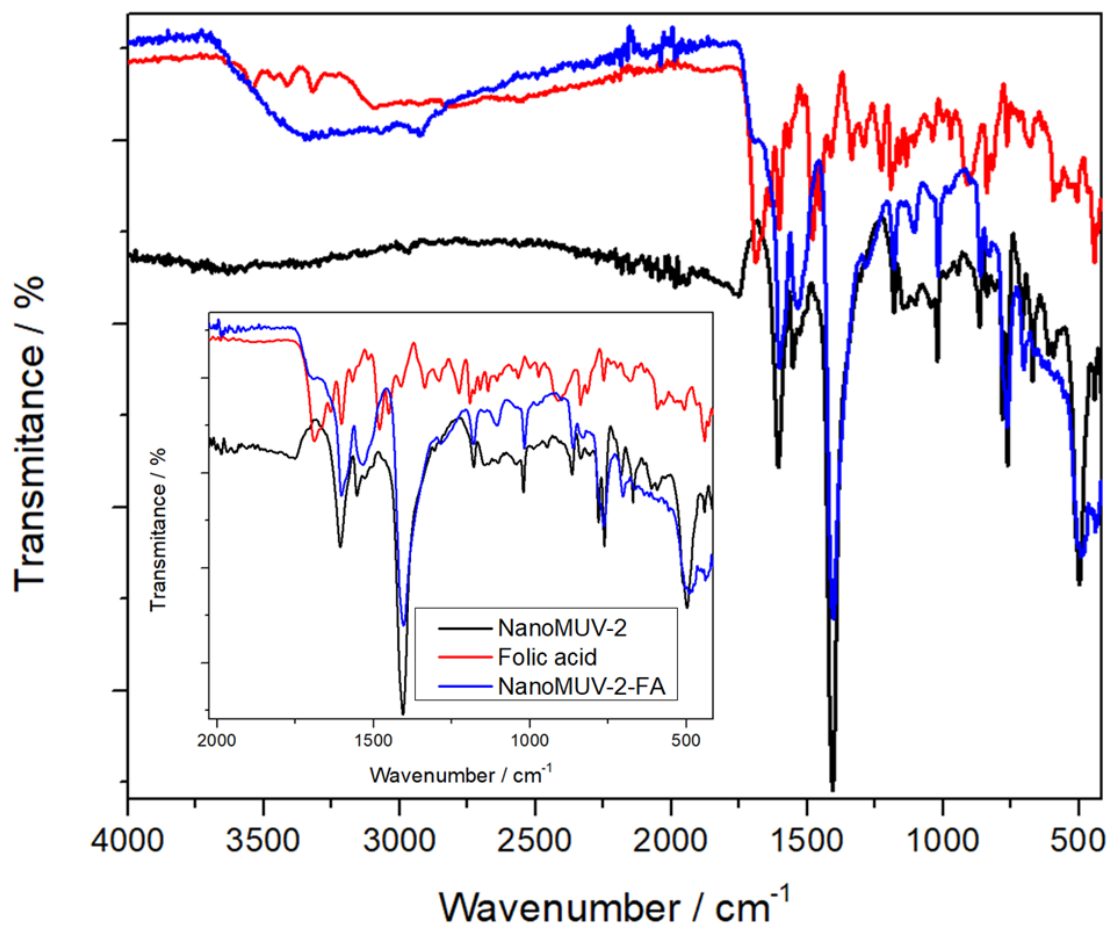


Figure S70: FT-IR profiles of NanoMUV-2-FA, Free folic acid and NanoMUV-2, showing vibration bands corresponding to folic acid functionalisation.

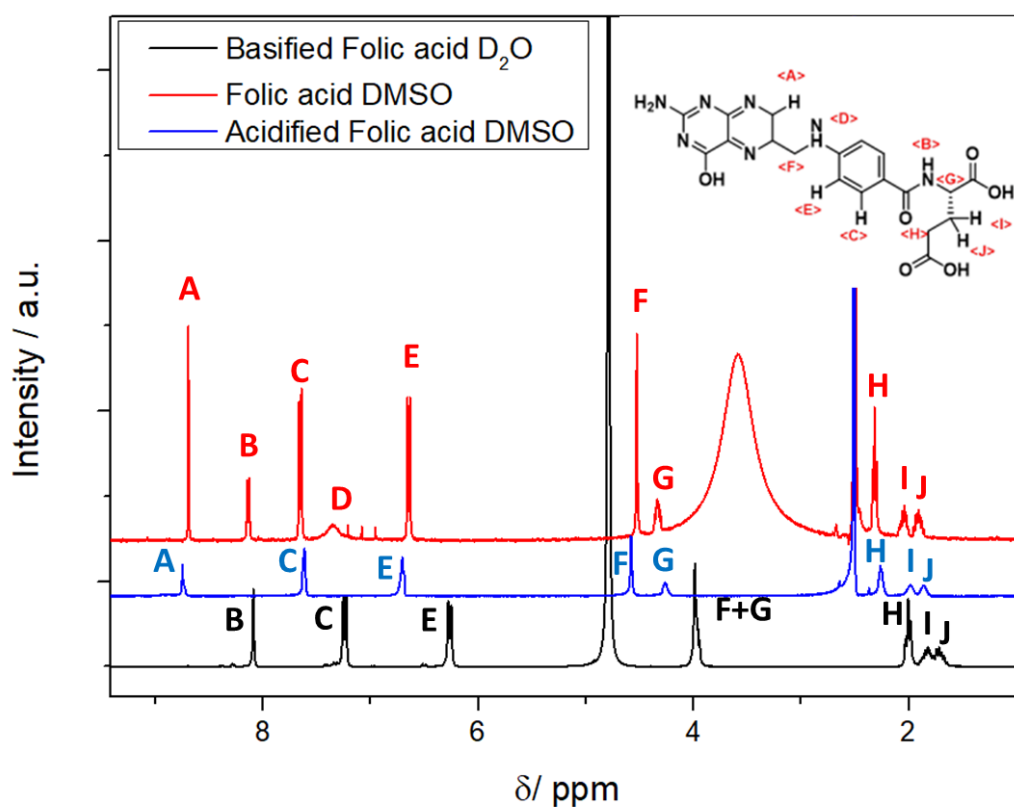


Figure S71: ^1H NMR spectra of folic acid under different conditions, showing the disappearance of certain signals upon acidification of basification, but the prevalence of H, I, and J signals, which were used for estimation of folic acid content in the samples.³

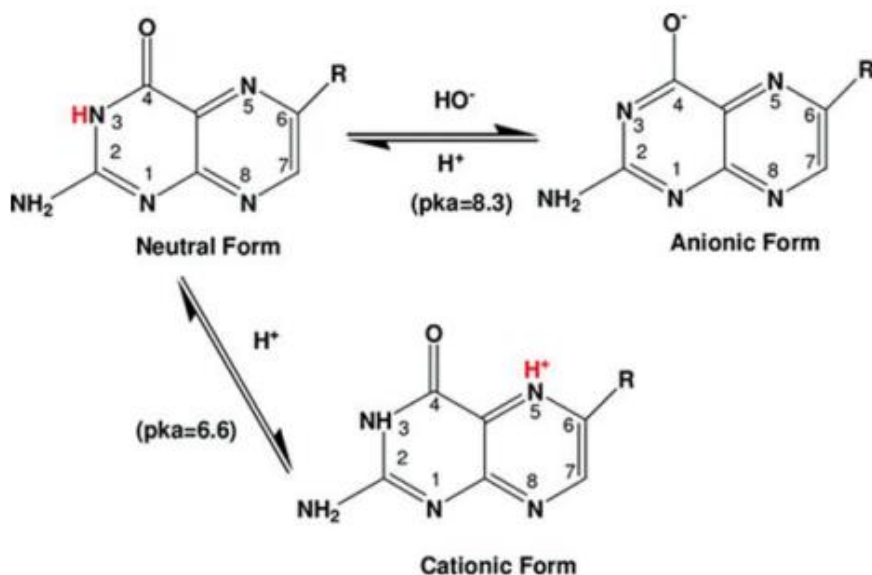


Figure S72: Examples of folic acid conformational changes upon pH changes.³

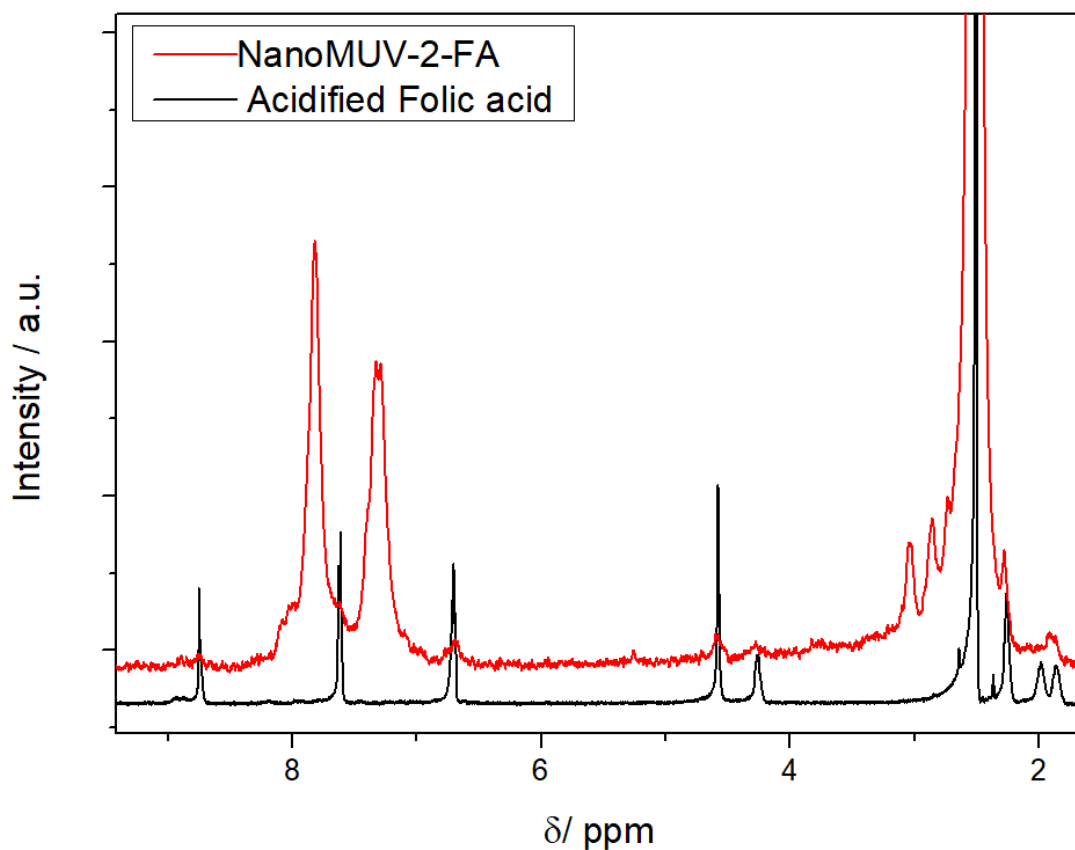


Figure S73: Acid-digested ^1H NMR spectra of NanoMUV-2FA compared to acidified Folic acid in DMSO, showing the characteristic signal of folic acid. The analysis based on the molar ratio between folic acid and ligand signals results in ca. 0.195 Folic acid per ligand (8.9 mol%), which is equivalent to a ca. 9.2% w/w for the theoretical formula $(\text{Fe}_3\text{O})_2(\text{L})_3(\text{FA})_{0.585}$. However, as EDX showed a reduced ligand content, taking the data obtained by EDX into account results in the approximate molecular formula $(\text{Fe}_3\text{O})_2(\text{L})_{2.41}(\text{FA})_{0.47}$, which corresponds to 8.9 w/w %.

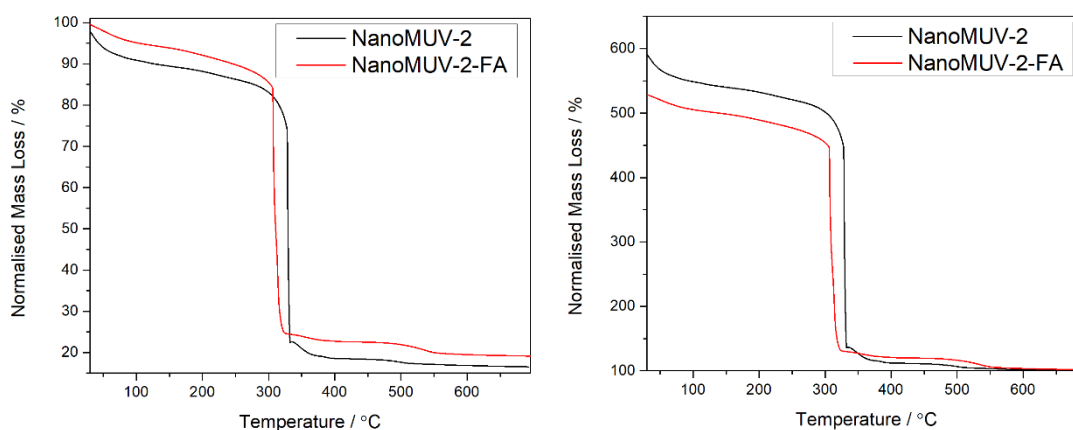


Figure S74: TGA profiles of NanoMUV-2 and NanoMUV-2-FA with the start (left) or the end (right) of the decomposition profile normalized to 100%. This indicates partial displacement of the linker by FA functionalization.

The following calculations were performed to extract the amount of FA present in the structure through TGA.⁵

$$R_{\text{exp}} = \frac{M_w[\text{MOF}]}{M_w[\text{Residue}]} = \frac{M_w[\text{MOF}]}{M_w[\text{Metal Residue}]} = \frac{M_w[(\text{Fe}_3\text{O})_2(\text{L})\text{X}(\text{FA})_x * \text{nmr}]}{M_w 3 * [\text{Fe}_2\text{O}_3]}$$

As TGA and EDX indicate partial displacement of the linker by FA, we have applied the following formula to simultaneously calculate ligand and fa content.

$$X_{\text{ligands}} = \frac{R_{\text{exp}} * M_w 3 * [\text{Fe}_2\text{O}_3] - M_w [(\text{Fe}_3\text{O})_2]}{M_w \text{Ligand} + \text{NMR RATIO} * M_w \text{FA}} = 2.375$$

Then,

$$\text{Folic acid} = \text{Ligand} * \text{nmr} \frac{\text{FA}}{\text{LIGAND}} \text{RATIO} = 0,463$$

This resulted in the following structure $(\text{Fe}_3\text{O})_2(\text{H}_2\text{O})_6(\text{L})_{2.375}(\text{FA})_{0,463}$, which is in great agreement with the composition obtained by EDX and ¹HNMR.

Once the structure has been obtained, the weight per cent of FA in the structure can be calculated as

$$\frac{w}{w} \% \text{FA} = \frac{\text{number of FA in the structure} * M_w[\text{FA}]}{M_w[\text{MOF}]} * 100 = 8,8\%$$

Table S13: mass per cent of FA within the samples extracted by different techniques.

EDX+ ¹ HNMR	TGA	Average ± SD
8.9	8.8	8.9 ± 0.05

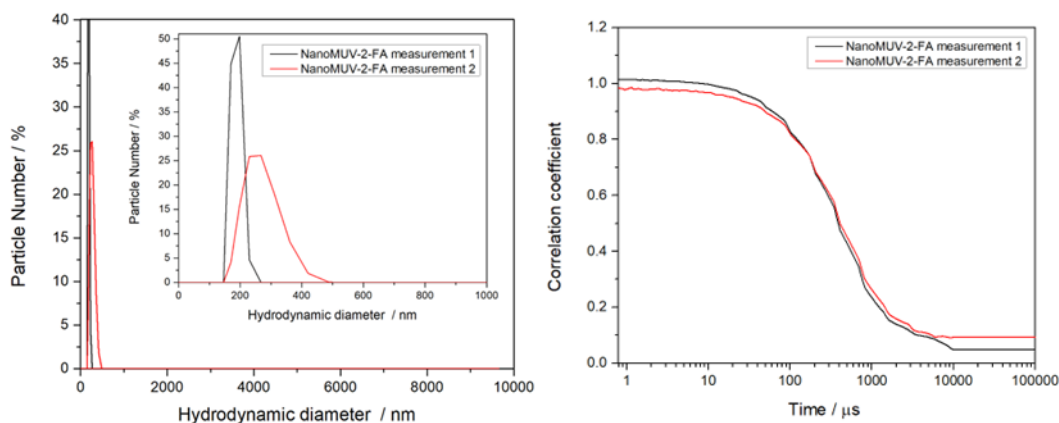


Figure S75: (Left) Dynamic light scattering profile showing the number % of particles as a function of their diameter in PBS 10X. Each measurement was performed with a waiting time of 10 minutes, showing slightly bigger particle sizes than SEM but no significant aggregation over time. $0.1 \text{ mg}\cdot\text{mL}^{-1}$ dispersion of NanoMUV-2-FA. (Right) Correlogram of $0.1 \text{ mg}\cdot\text{mL}^{-1}$ dispersion of NanoMUV-2-FA in PBS 10X, showing no aggregates over time.

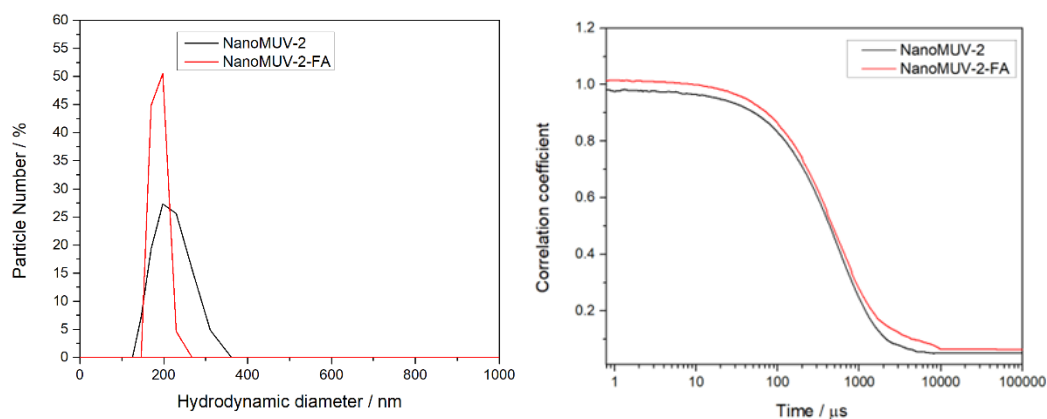


Figure S76: (left) Comparison of DLS profile of NanoMUV-2-FA and NanoMUV-2 showing the number % of particles as a function of their diameter in PBS 10X. The colloidal stability upon surface functionalisation seems to have improved. (Right) Correlogram of $0.1 \text{ mg}\cdot\text{mL}^{-1}$ dispersion of NanoMUV-2-FA in PBS 10X compared to NanoMUV-2, showing no aggregates over time.

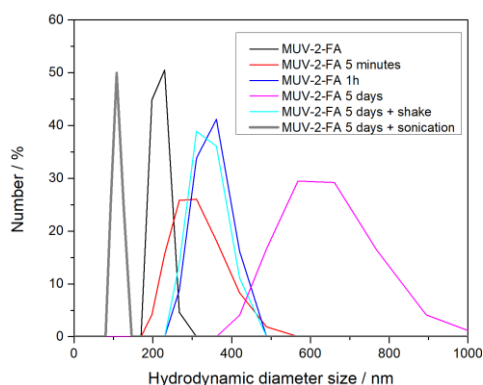


Figure S77: Dynamic light scattering profile showing the number % of particles as a function of their diameter in PBS 10X for different times.

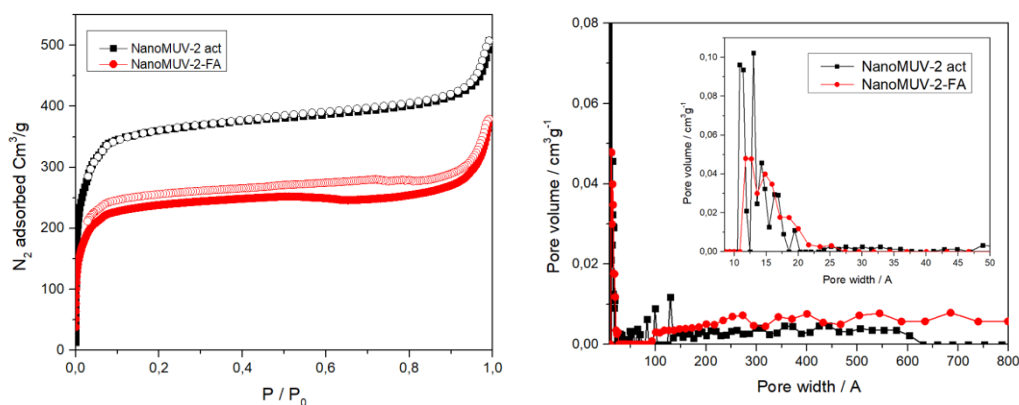


Figure S78: (Left) N_2 adsorption and desorption isotherms NanoMUV-2 and NanoMUV-2-FA, showing a decrease in adsorption upon surface modification, both as a consequence of the higher molecular weight of the functionalized MOF and of the partial pore blockage due to inner surface functionalization. (Right) Pore size distribution extracted from N_2 adsorption isotherm NanoMUV-2 and NanoMUV-2-FA. Large pores correspond to interparticle space. The disappearance of the mesopores may be related with a partial pore blockage.

Table S14: Data extracted from N_2 adsorption and desorption isotherms. Whereas the Mw extracted through TGA for NanoMUV-2(per Fe) is ca. 457 gmol^{-1} , for NanoMUV-2-FA corresponds to 384.4 gmol^{-1} due to the partial ligand displacement previously determined. Thus, the changes in porosity correspond to partial pore blockage and inner surface functionalization.

	NanoMUV-2	NanoMUV-2-FA
SBET Surface area / $\text{m}^2 \cdot \text{g}^{-1}$	1404	861
Langmuir surface area / $\text{m}^2 \cdot \text{g}^{-1}$	1877	1221
t-plot micropore surface area / $\text{m}^2 \cdot \text{g}^{-1}$	1092	656
Total pore volume / $\text{cm}^3 \cdot \text{g}^{-1}$	0.6444	0.417
Micropore volume / $\text{cm}^3 \cdot \text{g}^{-1}$	0.420	0.277

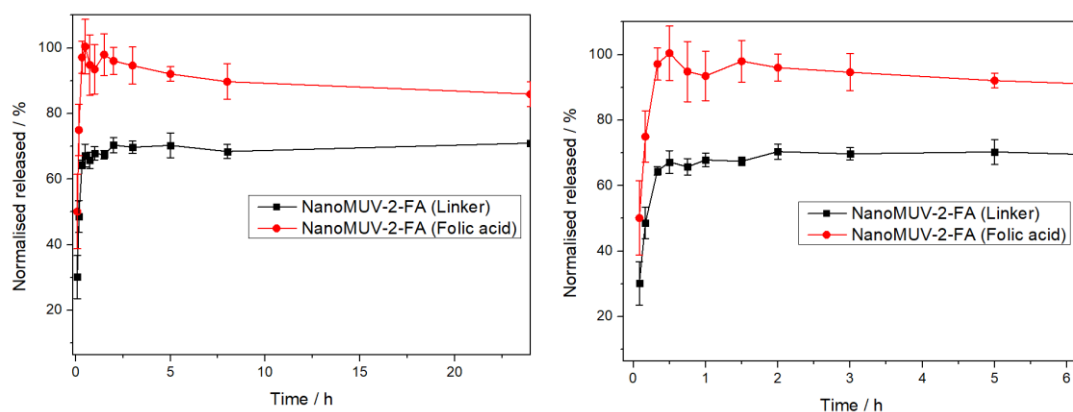


Figure S79: (Left) Degradation kinetics profile of NanoMUV-2-FA in PBS 10X based on the linker and folic acid release (based on 3 experiments). (Right) Amplification of the degradation profile reveals that folic acid is released faster than the constituent linker due to surface functionalization. The profiles show uncomplete degradation after 24 hours.

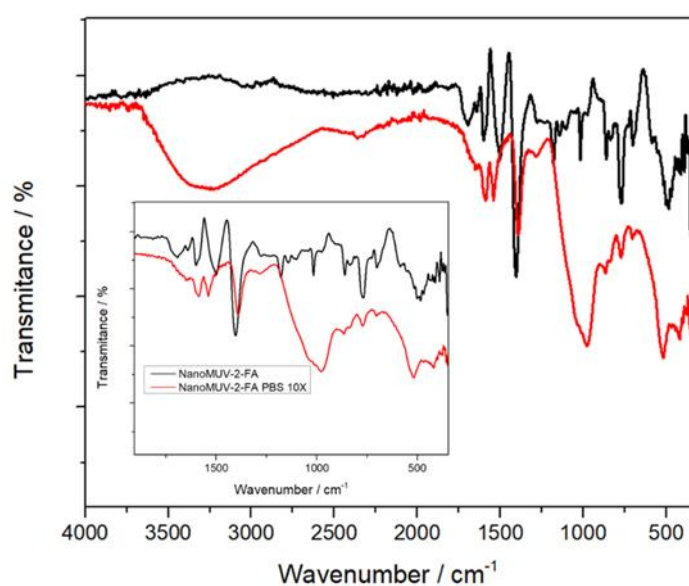


Figure S80: FT-IR profiles of NanoMUV-2-FA before and after immersion in PBS 10X for 15 minutes. After immersion the sample was centrifugated, the supernatant removed and washed once with EtOH. The samples were dried at room temperature for 3 hours before FT-IR.

S10. Cytotoxicity of functionalised MUV-2

S10.1 Cytotoxicity MUV-2-Oct

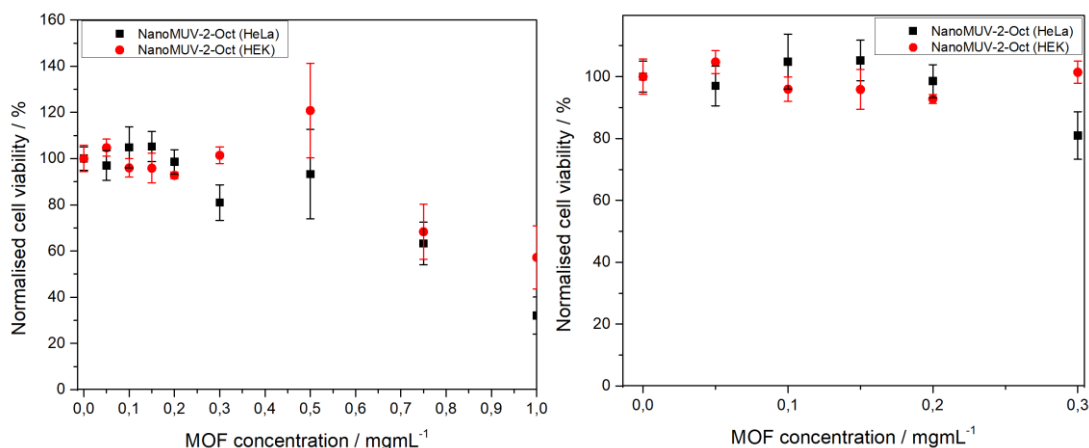


Figure S81: (Left) Cell proliferation assays (MTS) carried out on HeLa and HEK cells after 72 h incubation with NanoMUV-2-Oct in growth media. Each experiment has been performed 3 independent times, each with n=4. (Right) Magnification.

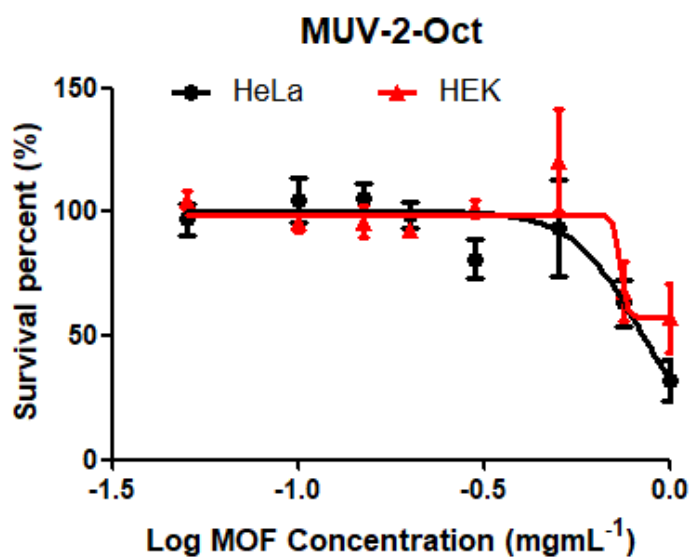


Figure S82: Cell proliferation assays (MTS) carried out on HeLa and HEK cells after 72 h incubation with NanoMUV-2-Oct in growth media. Each experiment has been performed 3 independent times, each with n=4. IC₅₀ for HeLa cells $0.830 \pm 0.237 \text{ mg} \cdot \text{mL}^{-1}$, for HEK it cannot be determined with the available data but is $>0.75 \text{ mg} \cdot \text{mL}^{-1}$

S10.2 Cytotoxicity MUV-2-FA

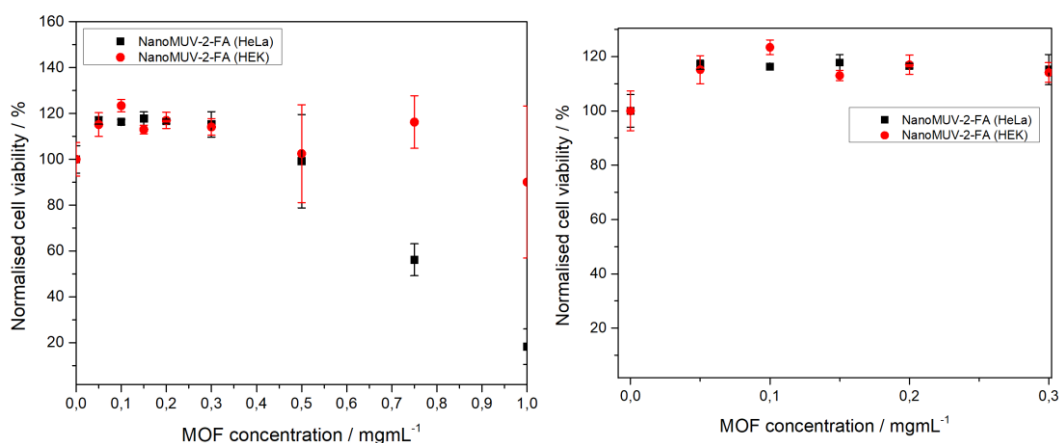


Figure S83: (Left) Cell proliferation assays (MTS) carried out on HeLa and HEK cells after 72 h incubation with NanoMUV-2-FA in growth media. Each experiment has been performed 3 independent times, each with n=4. (Right) Magnification.

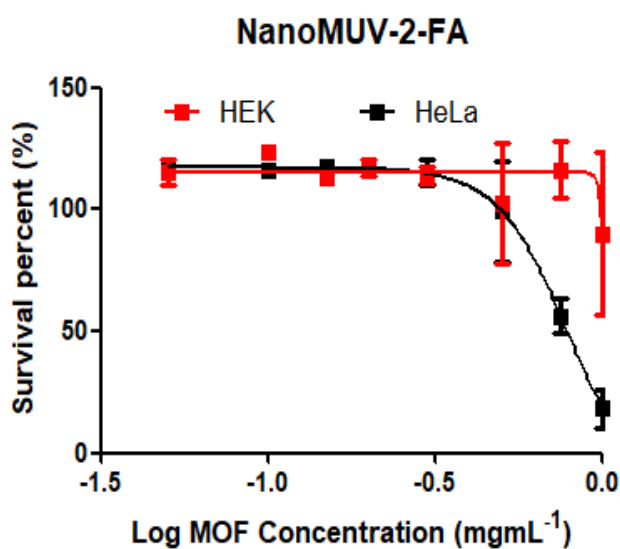


Figure S84: Cell proliferation assays (MTS) carried out on HeLa and HEK cells after 72 h incubation with NanoMUV-2-FA in growth media. Each experiment has been performed 3 independent times, each with n=4. IC₅₀ for HeLa cells $0.785 \pm 0.251 \text{ mg} \cdot \text{mL}^{-1}$, for HEK it cannot be determined with the available data but is $>1 \text{ mg} \cdot \text{mL}^{-1}$

S10.3 Comparison of cytotoxicity from empty samples

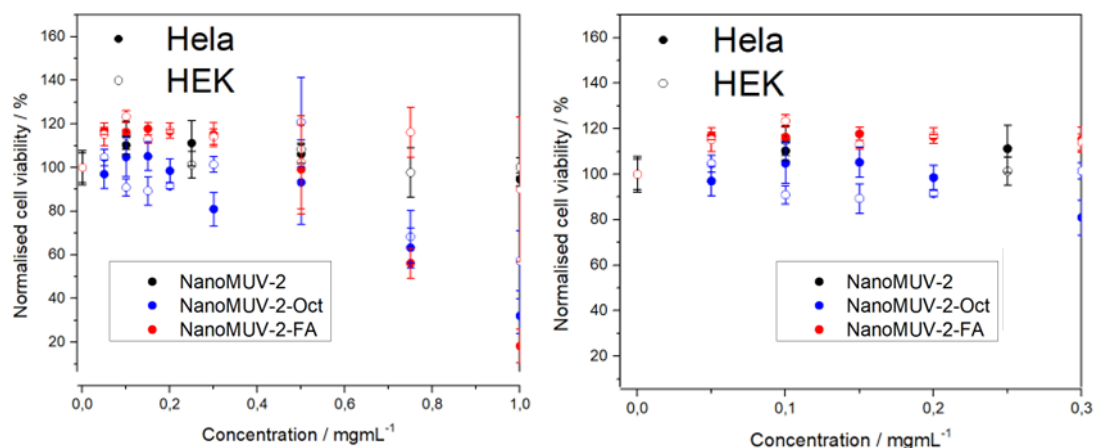


Figure S85: (Left) Comparison of cell proliferation assays (MTS) carried out on HeLa and HEK cells after 72 h incubation with different MOFs in growth media. Each experiment has been performed 3 independent times, each with n=4. (Right) Magnification.

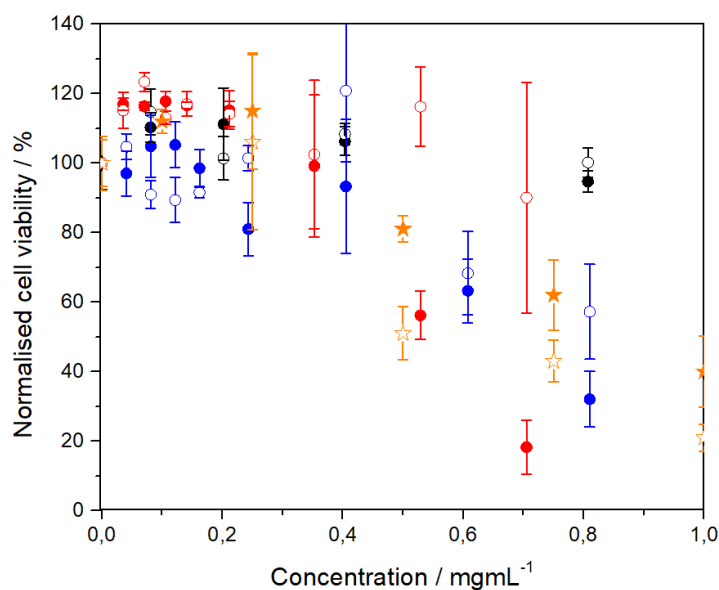


Figure S86: Comparison of cell proliferation assays (MTS) carried out on HeLa and HEK cells after 72 h incubation with different MOFs in growth media, as a function of the maximum ligand concentration, compared with the free ligand salt. Each experiment has been performed 3 independent times, each with n=4. (Legend from **Fig S85** applies, orange represents free ligand salt)

S11. Characterisation of calcein-loaded surface-functionalised MUV-2

S11.1 Characterisation of Cal@NanoMUV-2-Oct

Calcein determination: as no leaching was observed during the surface functionalization process, the calcein loading (*ca.* 12 w/w %) was calculated based on the calcein loading of the precursor and the extra weight from the surface functionalization (calculated by EDX).

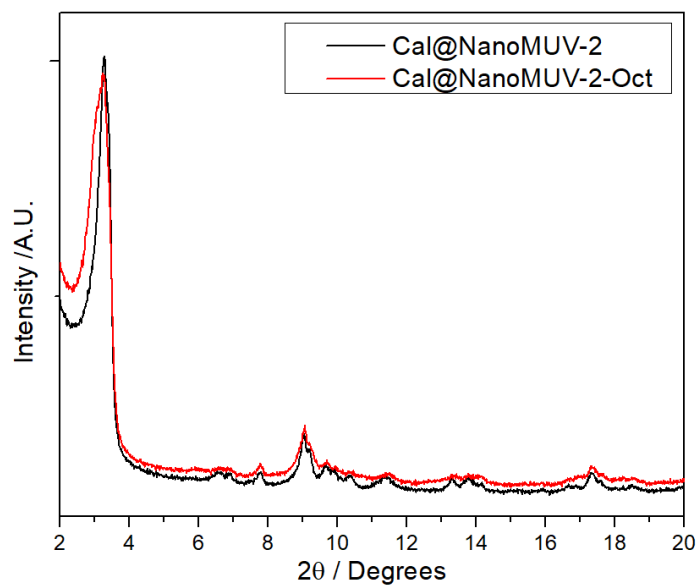


Figure S87: Comparison of experimental PXRD pattern of Cal@NanoMUV-2 and Cal@NanoMUV-2-Oct, showing retained crystallinity after surface functionalization.

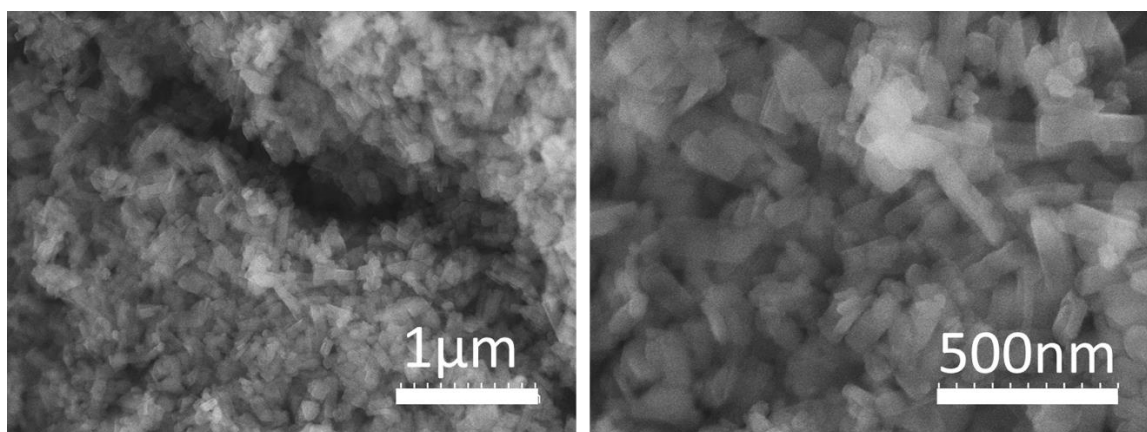


Figure S88: Scanning electron microscope images of Cal@NanoMUV-2-Oct, showing maintained morphology.

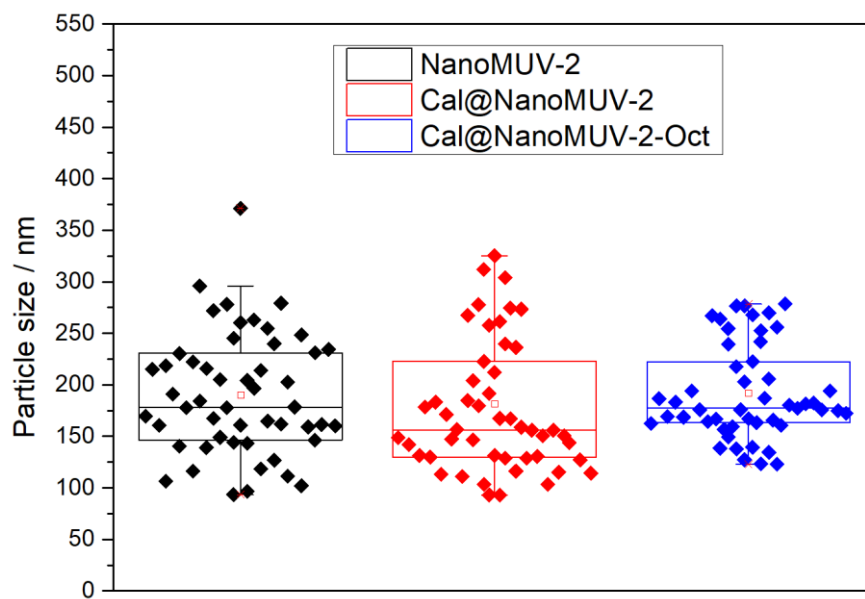


Figure S89: Comparison of particle size analysis of NanoMUV-2 and Cal@NanoMUV-2 and Cal@NanoMUV-2-Oct, showing no statistical difference between the samples.

Table S15: Data extracted from EDX analysis. The EDX profile of Cal@NanoMUV-2-Oct shows 2.29 S per Fe according to the theoretical molecular formula $(\text{Fe}_3\text{O})_2(\text{L})_3$. The presence of Br in 8-Bromo octanoic acid allows for the calculation of its molecular ratios in comparison to S and Fe, which can be converted into a mass fraction within the estimated structure $\text{Cal} @ (\text{Fe}_3\text{O})_2(\text{L})_3(\text{Oct})_{1.68}$ structure, in which Br-Oct correspond to ca. 12 w/w%, taking into account the determined calcein loading in weight.

Br-Fe	Br/L	S/Fe	L/Fe
0.279	0.486	2.293	0.573

Table S16: Molar and mass fractions extracted from EDX analysis.

Molar fraction Br Vs Fe	0.220
Mass fraction Oct	0.123

$$\text{Mass fraction Oct} = \frac{1.68 * \text{Mw oct}}{\text{Mw Cal} * \text{mass fraction cal (cal@MUV-2)} + \text{Mw MUV-2} + 1.68 * \text{Mw Oct}}$$

$$\text{Mass fraction Cal} = \frac{\text{Mw Cal} * \text{mass fraction Cal in Cal@MUV-2}}{\text{Mw Cal} * \text{mass fraction cal (cal@MUV-2)} + \text{Mw MUV-2} + 1.68 * \text{Mw Oct}}$$

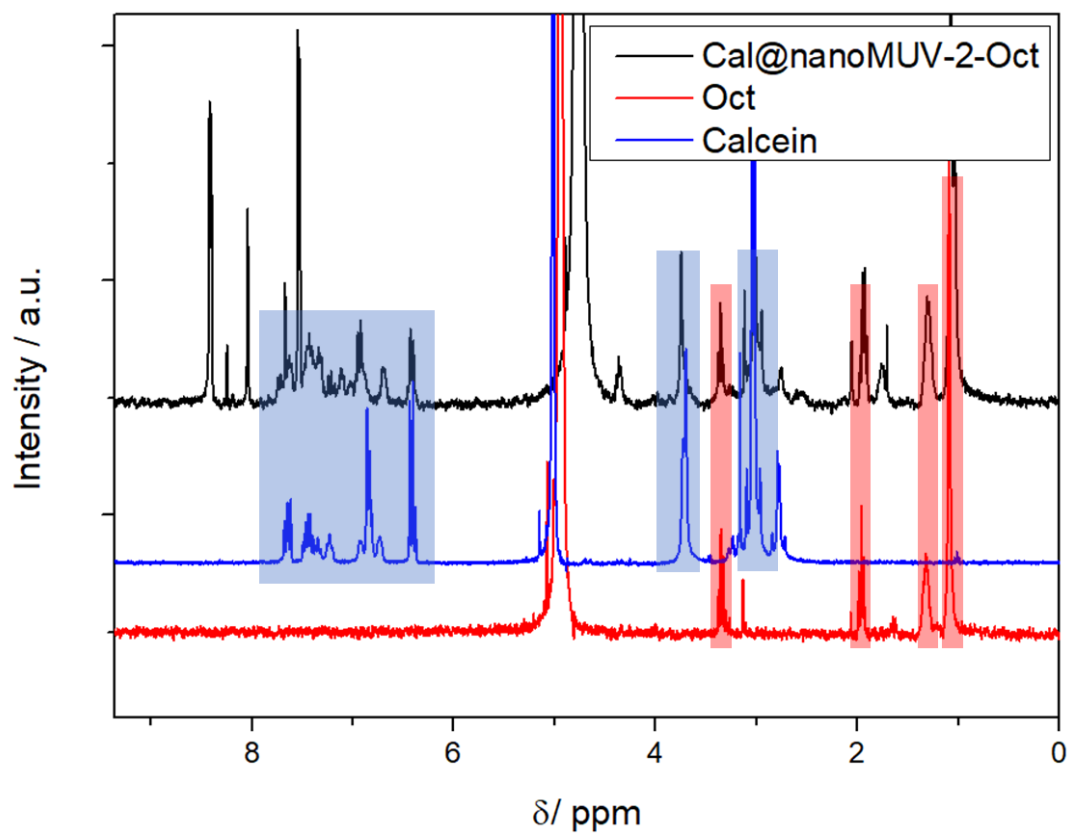


Figure S90: Base-digested ¹H NMR profile of Cal@NanoMUV-2-Oct in D₂O, compared to free Oct and Calcein, showing successful Oct functionalization after Calcein loading.

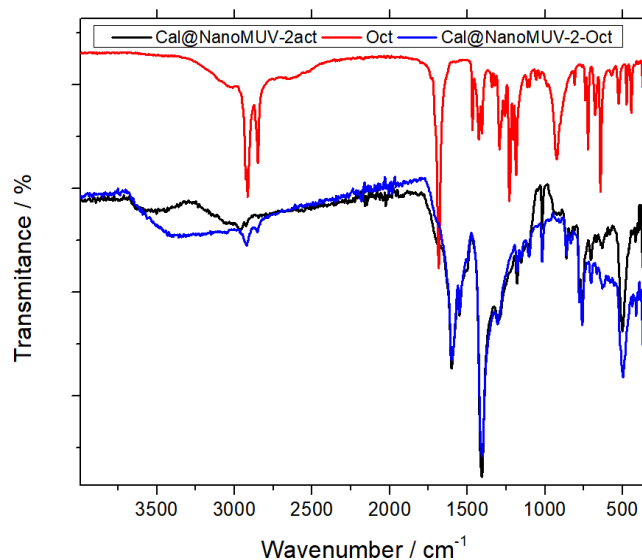


Figure S91: FT-IR profiles of Cal@NanoMUV-2, free oct and Cal@NanoMUV-2-Oct, showing vibration bands corresponding to oct functionalisation.

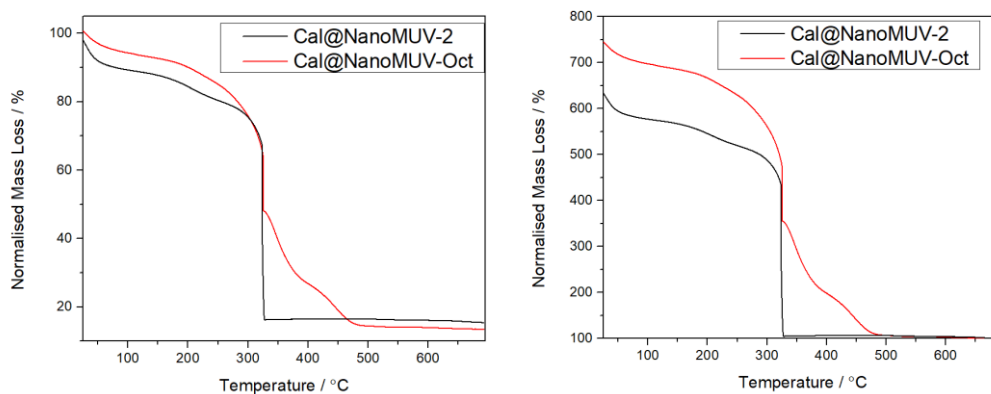


Figure S92: TGA profiles of Cal@NanoMUV-2-Oct with the start (left) or the end (right) of the decomposition profile normalized to 100% compared to Cal@NanoMUV-2, showing an increase in the organic content and changes in the decomposition profile that corresponds to Oct functionalization, from which calculation in Section S10.1 are applied.

Table S17: mass fractions of Oct within the Samples extracted by different techniques.

EDX	TGA	Average \pm SD
12.3	11.1	11.7 \pm 0.6

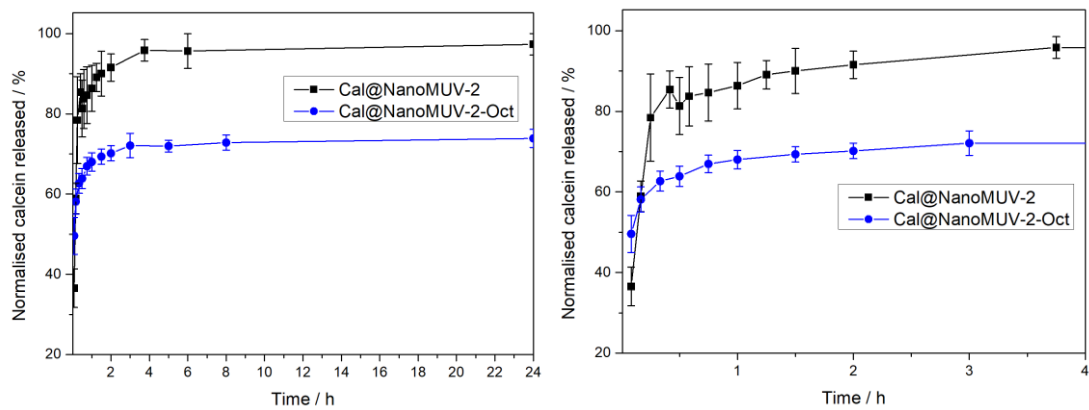


Figure S93: (Left) Calcein release profile of Cal@NanoMUV-2-Oct in PBS 10X compared with pristine Cal@NanoMUV-2. The incomplete release could be a consequence of the formation of a phosphate corona due to partial pore blockage, in great agreement with degradation studies. (Right) Magnification.

S11.2. Characterisation of Cal@MUV-2-FA

Calcein determination: The calcein loading (*ca.* 10 w/w %) was calculated based on the calcein loading of the precursor, the calcein released during the surface functionalisation (calculated by UV-Vis) and the extra weight from the surface functionalisation (calculated by a combination of NMR, EDX and TGA).

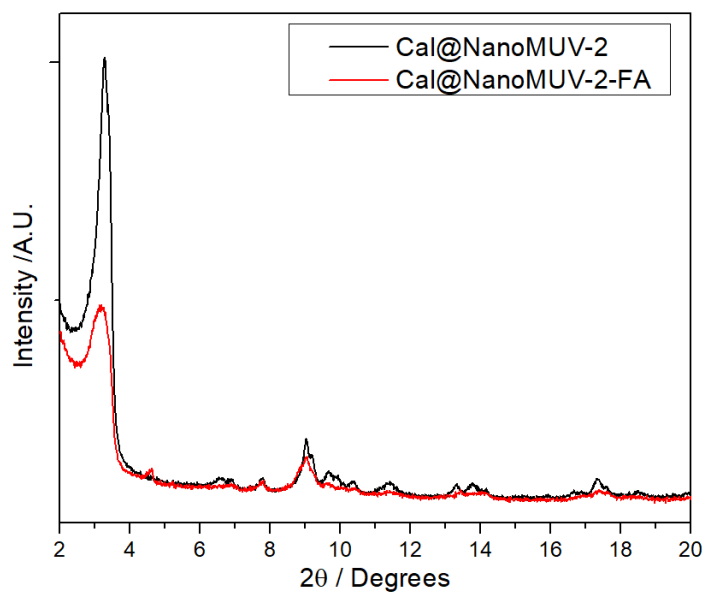


Figure S94: Comparison of experimental PXRD pattern of Cal@NanoMUV-2 and Cal@NanoMUV-2-FA, showing retained crystallinity after surface functionalization.

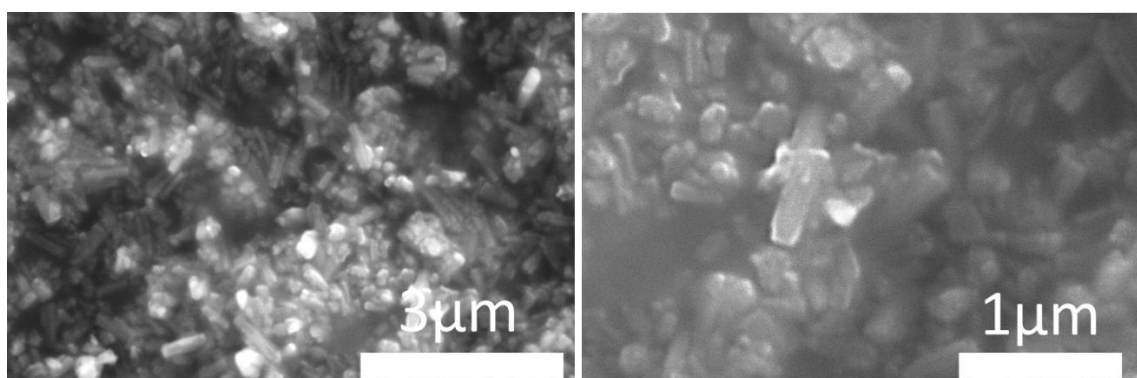


Figure S95: Scanning electron microscope images of Cal@NanoMUV-2-FA showing maintained morphology.

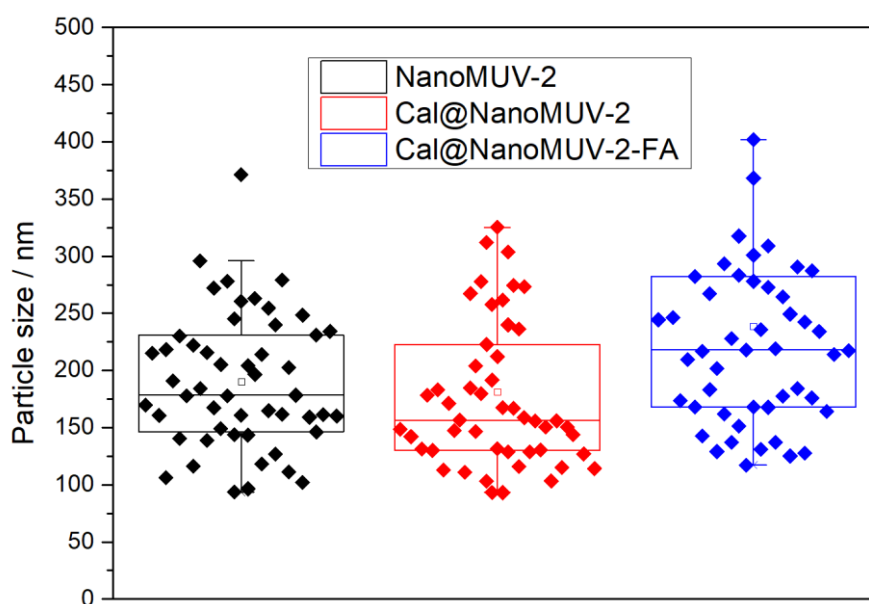


Figure S96: Comparison of particle size analysis of NanoMUV-2, Cal@NanoMUV-2 and Cal@NanoMUV-2-FA, showing no statistical difference between the samples.

Table S18: Data extracted from EDX analysis. The EDX profile of Cal@NanoMUV-2-FA shows 1.65 S per Fe which is significantly lower than the expected ($S/Fe = 2$) for the theoretical molecular formula $(Fe_3O)_2(L)_3$. The experimental ratio corresponds to a structure with the approximated linker to metal ratio of $Cal@(Fe_3O)_2(L)_{2.468}(FA)_x$

S/Fe	L/Fe
1.65	0.411

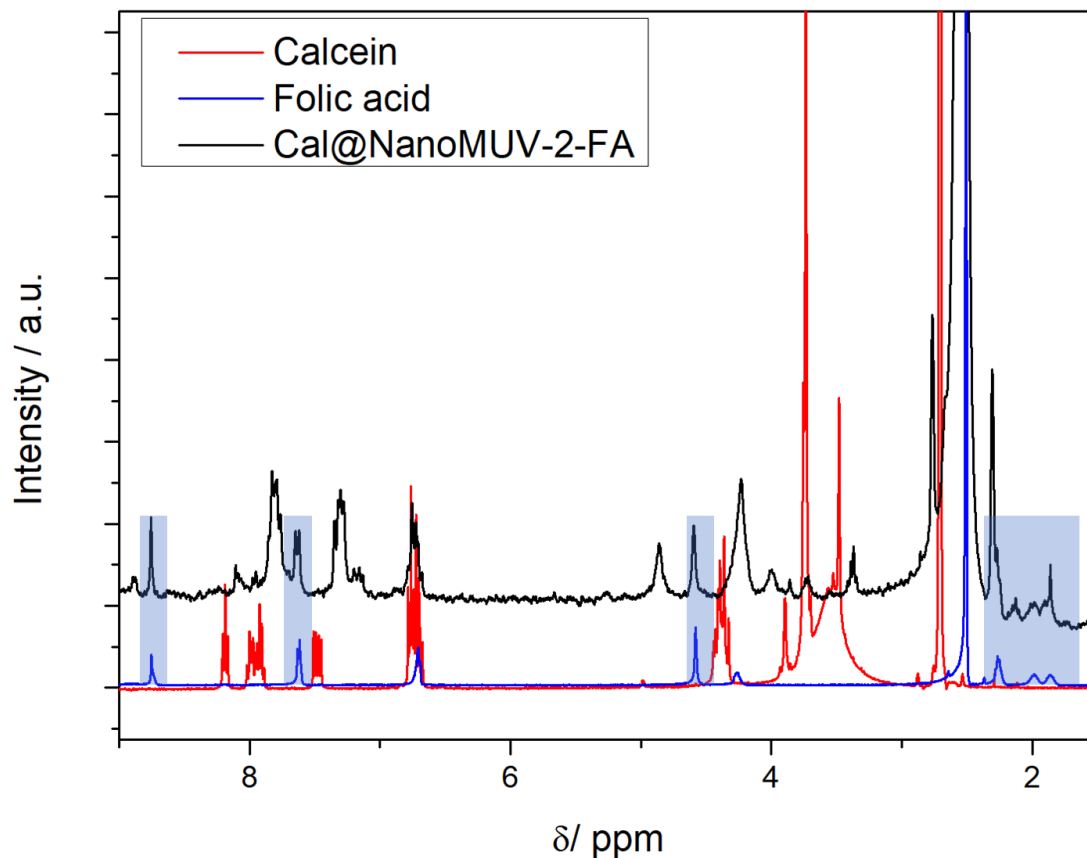


Figure S97: Acid-digested ^1H NMR profile of Cal@NanoMUV-2-FA in DMSO, compared to free Oct and Calcein, showing successful FA functionalization after Calcein loading. Analysis results in ca. 0.20 FA per Ligand. Merging this with EDX data and the calcein leaching determined by UV-Vis during the surface modification results in the theoretical molecular formula of $\text{Ca}_{0.54} @ (\text{Fe}_3\text{O})_2 (\text{L})_{2.47} (\text{FA})_{0.494}$, with a ca. 8.01 w/w% of FA and ca. 13.74 w/w% of calcein. However, since the linker signals are masked by Calcein signals, this data will not be taken into account.

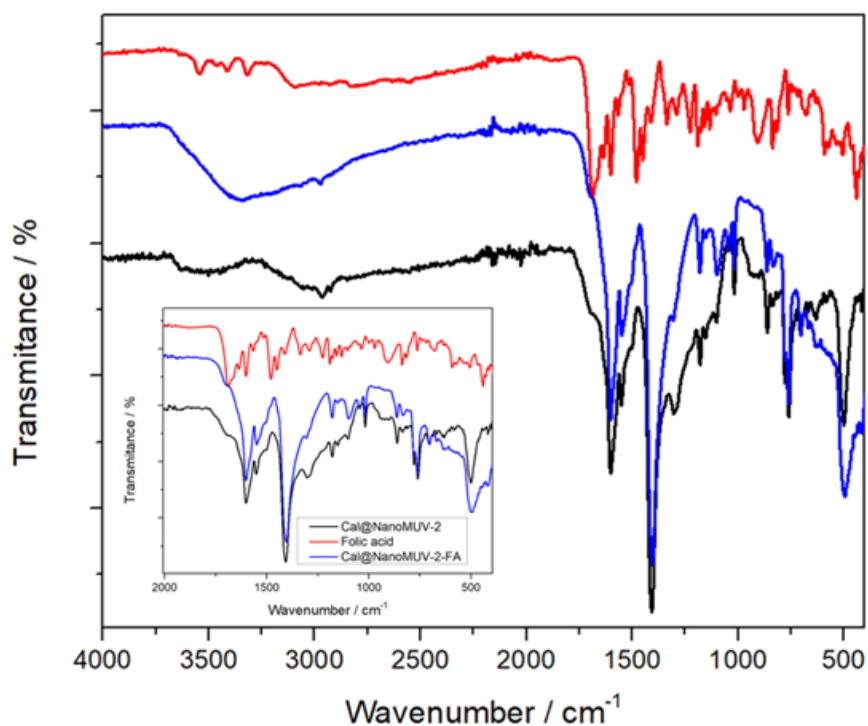


Figure S98: FT-IR profiles of Cal@NanoMUV-2-FA, Free folic acid and Cal@NanoMUV-2, showing vibration bands corresponding to folic acid functionalization.

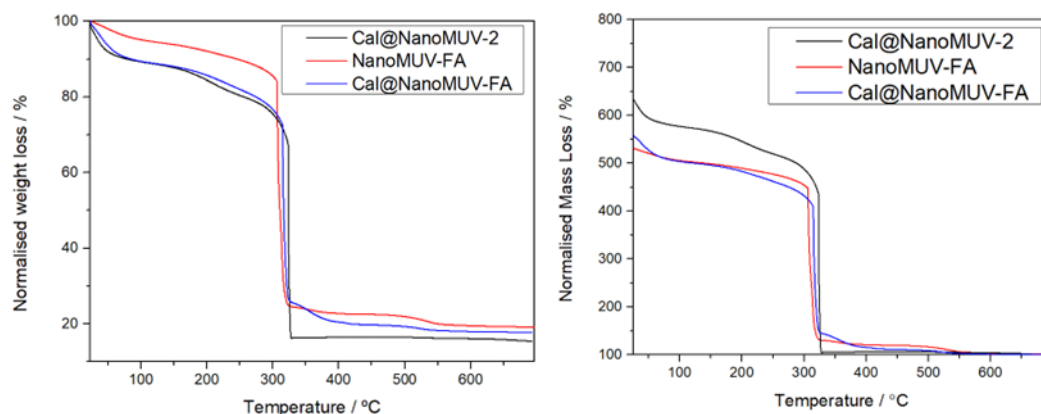


Figure S99: TGA profiles of Cal@NanoMUV-2-FA with the start (left) or the end (right) of the decomposition profile normalized to 100% compared to Cal@NanoMUV-2 and NanoMUV-2-FA.

Analysis as in NanoMUV-2-FA considering the calcein leaching determined during the surface modification by UV-Vis, results in the theoretical formula $\text{Ca}_{0.54} @ (\text{Fe}_3\text{O})_2(\text{L})_{2.103}(\text{FA})_{0.407}$, with a *ca.* 10.05 w/w% of calcein and *ca.* 8.83 w/w % of FA, applying the formulas from Section S10.2.

Table S19: mass fractions of FA within the samples extracted by different techniques.

EDX + NMR	TGA	Average \pm SD
8.01	8.83	8.42 \pm 0.41

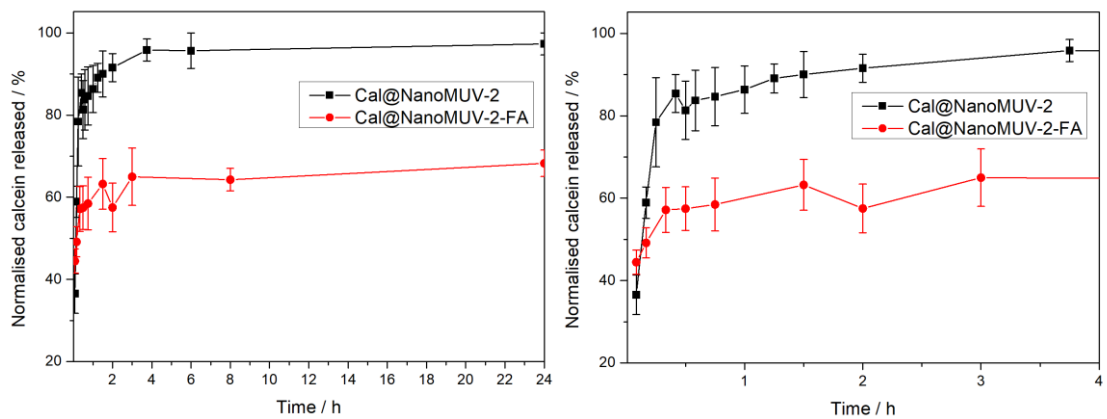


Figure S100: (Left) Calcein release profile of Cal@NanoMUV-2-FA in PBS 10X compared with pristine Cal@NanoMUV-2, The incomplete release could be a consequence of the formation of a phosphate corona due to partial pore blockage, in great agreement with degradation studies. (Right) Magnification.

S12. Cellular internalization of functionalized MOFs

S12.1 Flow Assisted cell sorting.

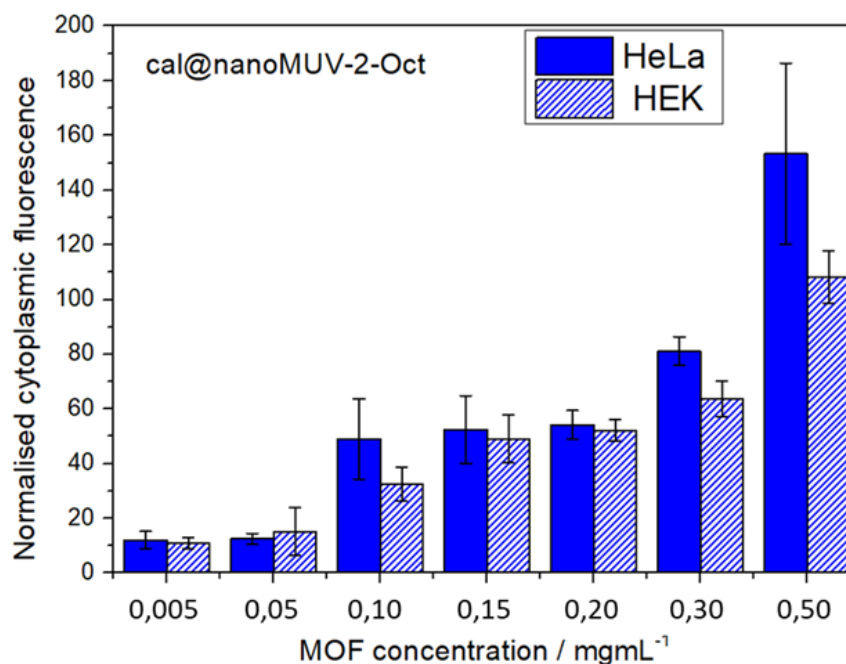


Figure S101: Normalised cytoplasmic fluorescence of HeLa and HEK cells upon incubation with different concentrations of Cal@NanoMUV-2-Oct. Normalisation was performed at the highest value for HeLa cells functionalization of Cal@NanoMUV-2 (100%) taking into account the different calcein loadings. Error bars represent the standard deviation of 3 independent experiments.

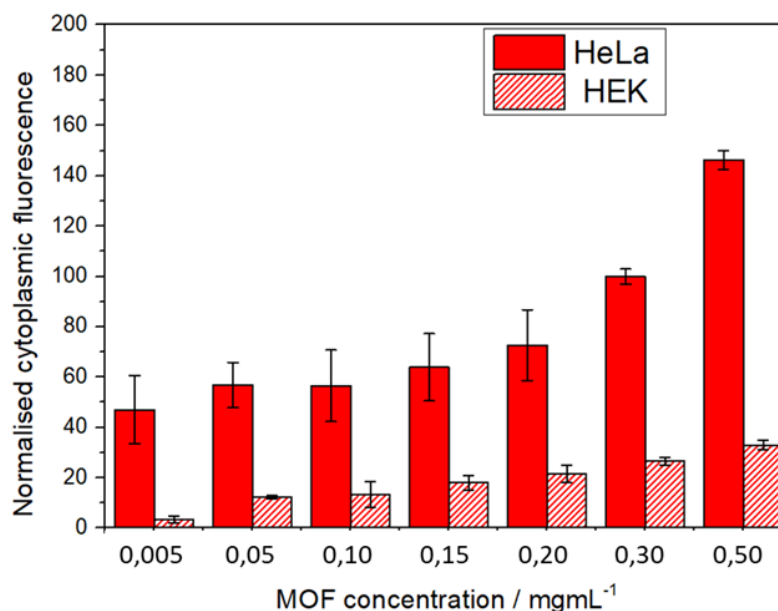


Figure S102: Normalised cytoplasmic fluorescence of HeLa and HEK cells upon incubation with different concentrations of Cal@NanoMUV-2-FA. Normalisation was performed at the highest value for HeLa cells functionalization of Cal@NanoMUV-2 (100%) taking into account the different calcein loadings. Error bars represent the standard deviation of 3 independent experiments.

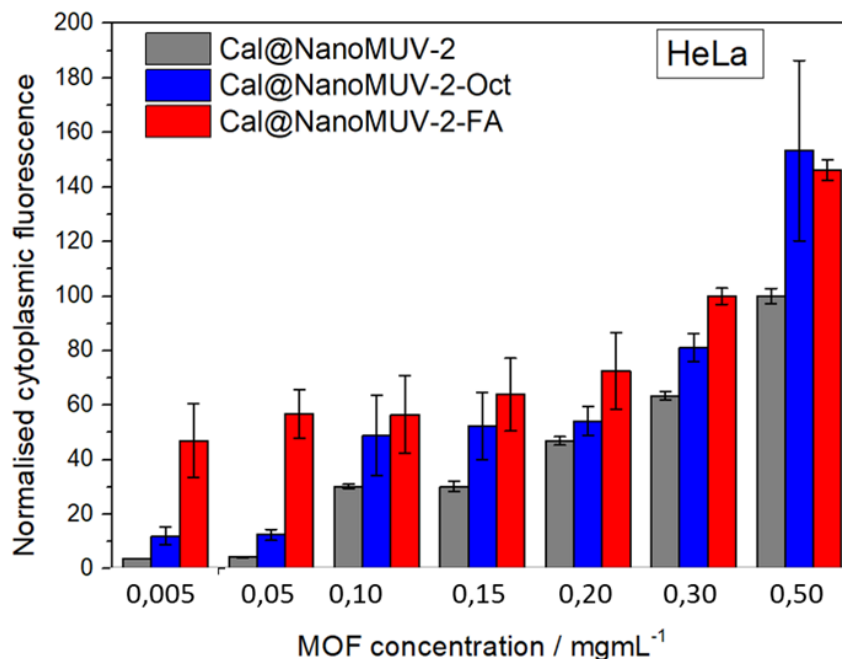


Figure S103: Comparison of normalized cytoplasmic fluorescence of HeLa cells upon incubation with different concentrations of calcein-loaded MOFs. Normalisation was performed at the highest value for HeLa cells functionalization of Cal@NanoMUV-2 (100%) taking into account the different calcein loadings. Error bars represent the standard deviation of 3 independent experiments.

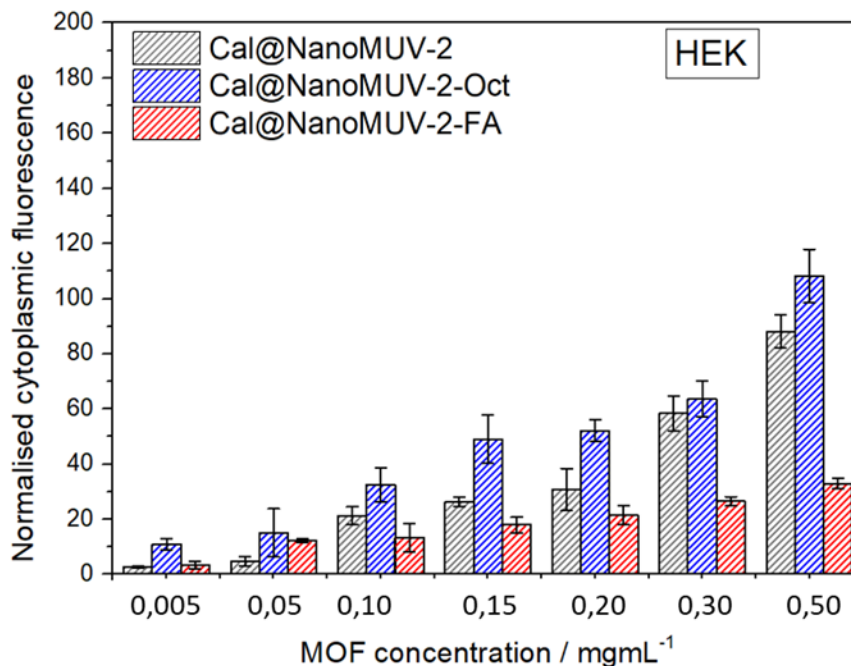


Figure S104: Comparison of normalized cytoplasmic fluorescence of HEK cells upon incubation with different concentrations of calcein-loaded MOFs. Normalisation was performed at the highest value for HeLa cells functionalization of Cal@NanoMUV-2 (100%) taking into account the different calcein loadings. Error bars represent the standard deviation of 3 independent experiments.

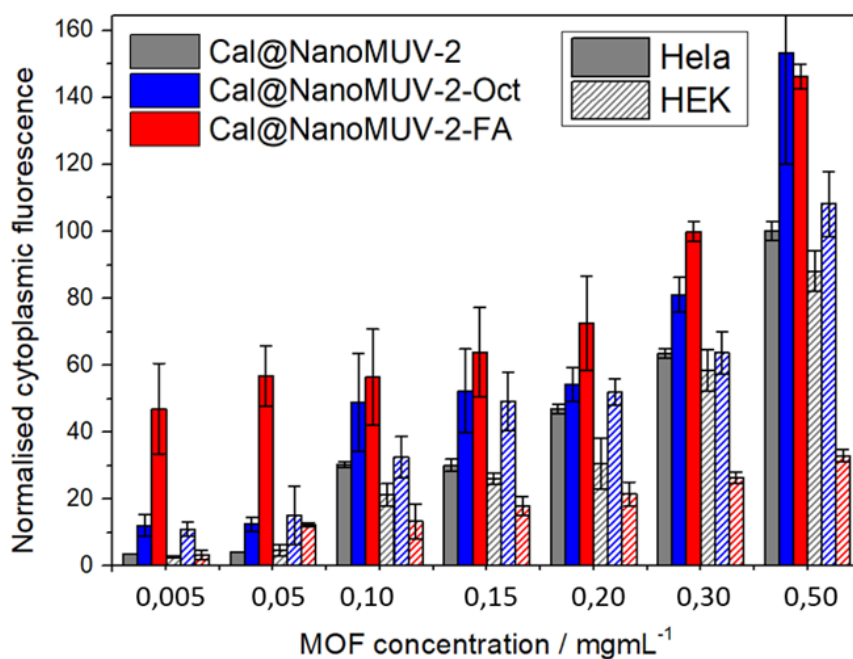


Figure S105: Comparison of normalised cytoplasmic fluorescence of HeLa and HEK cells upon incubation with different concentrations of calcein-loaded MOFs. Normalisation was performed at the highest value for HeLa cells functionalization of Cal@NanoMUV-2 (100%) taking into account the different calcein loadings. Error bars represent the standard deviation of 3 independent experiments.

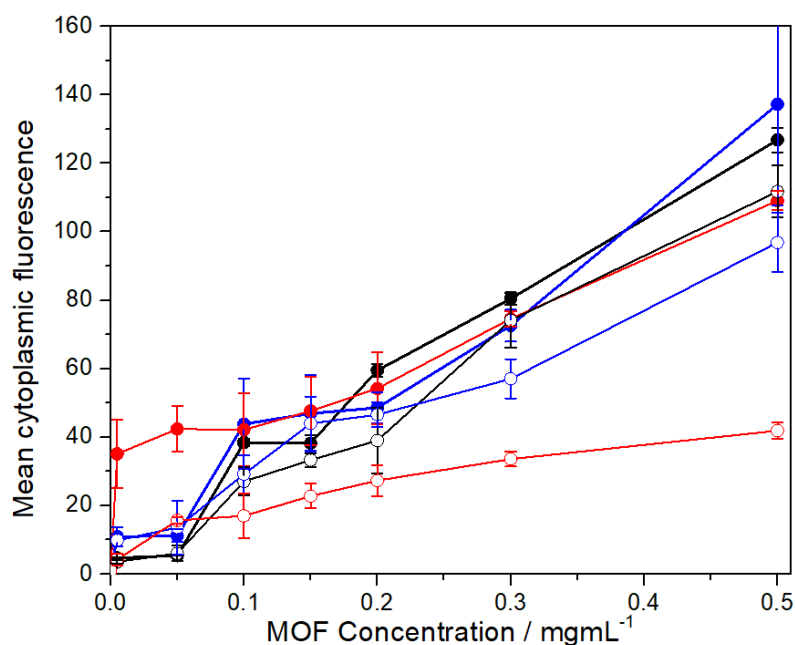


Figure S106: Comparison of normalised cytoplasmic fluorescence of HEK cells upon incubation with different concentrations of calcein-loaded MOFs. Normalisation was performed toward the cytoplasmic fluorescence of the untreated controls (as a fold increase). Error bars represent the standard deviation of 3 independent experiments.

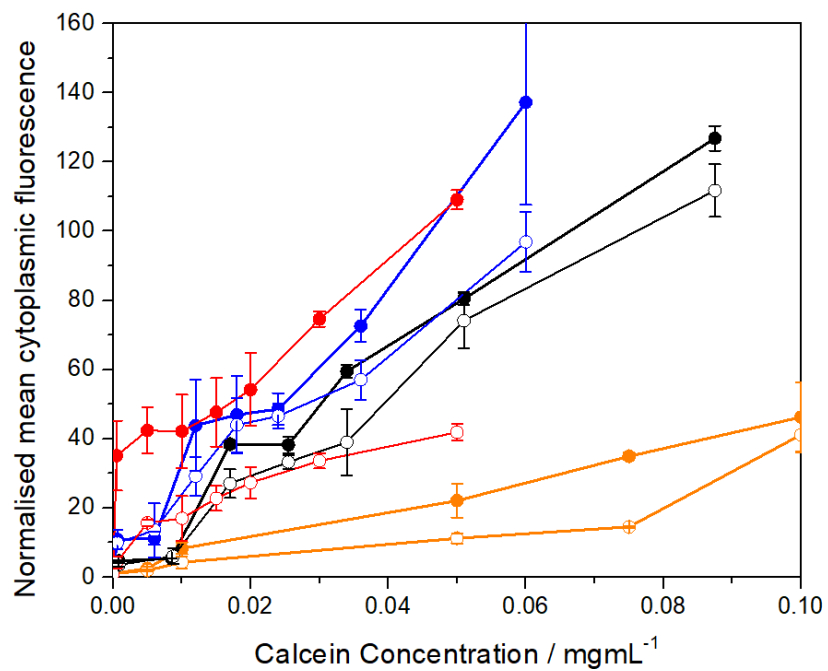


Figure S107: Comparison of normalised cytoplasmic fluorescence of HEK cells upon incubation with different concentrations of calcein-loaded MOFs. Normalisation was performed towards the cytoplasmic fluorescence of the untreated controls (as a fold increase). Error bars represent the standard deviation of 3 independent experiments.

S12.2 Confocal microscopy

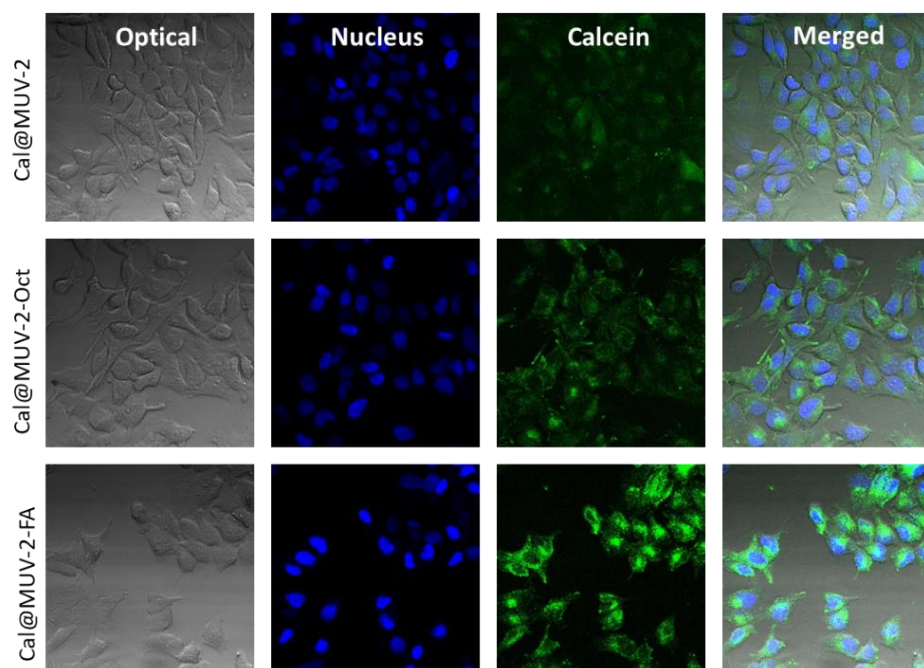


Figure S108: Confocal microscopy images of HeLa cells upon incubation with $0.2 \text{ mg}\cdot\text{mL}^{-1}$ of Cal@NanoMUV-2 and the equivalent free calcein concentration.

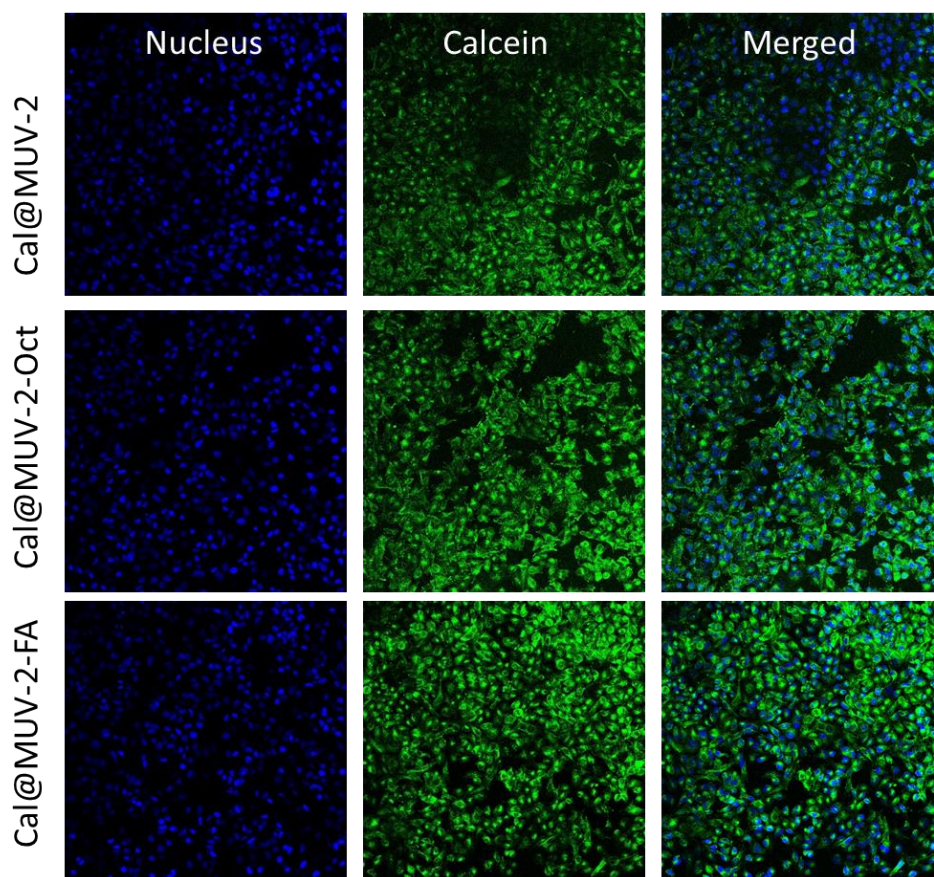


Figure S109: Confocal microscopy images of HeLa cells upon incubation with $0.2 \text{ mg}\cdot\text{mL}^{-1}$ of Cal@NanoMUV-2 and the equivalent free calcein concentration. 10X amplification.

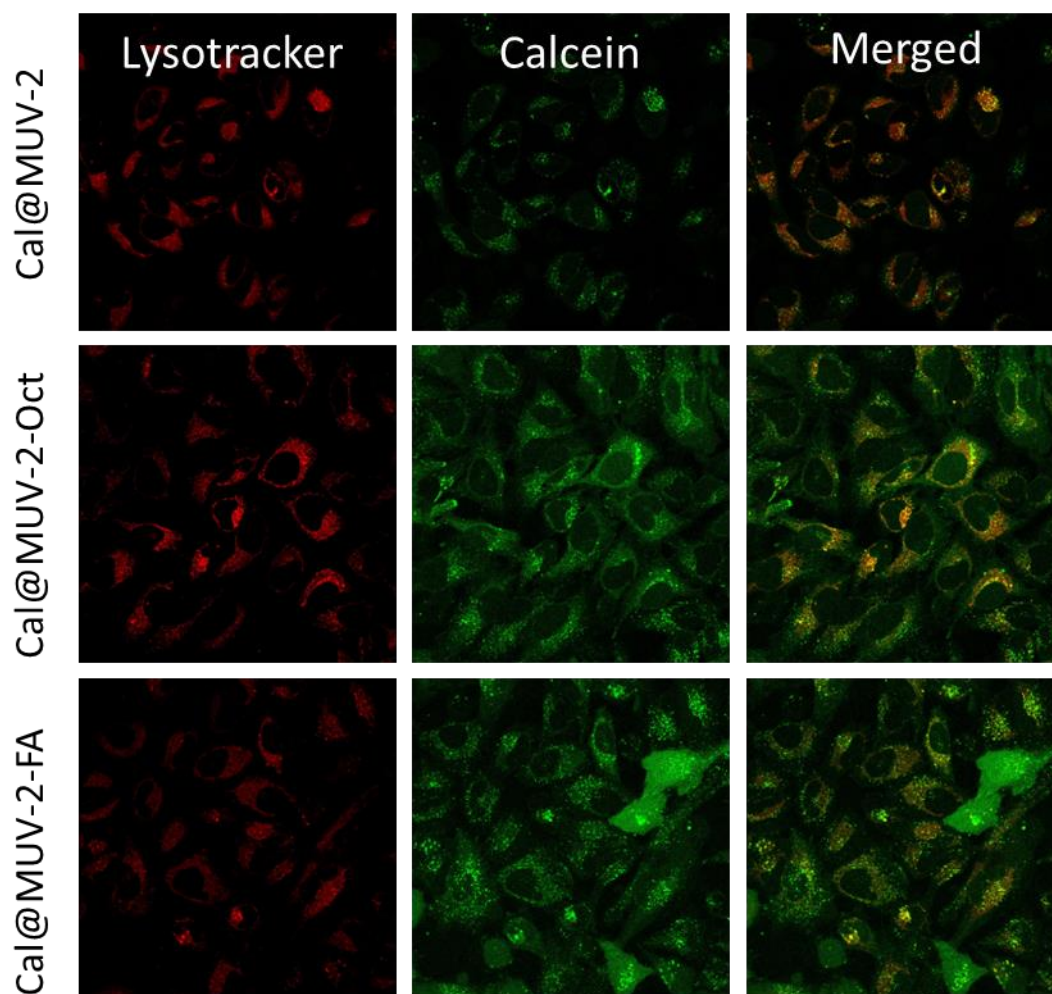


Figure S110: Confocal microscopy images of HeLa live cells upon incubation with $0.2 \text{ mg}\cdot\text{mL}^{-1}$ of Calcein-loaded MOFs.

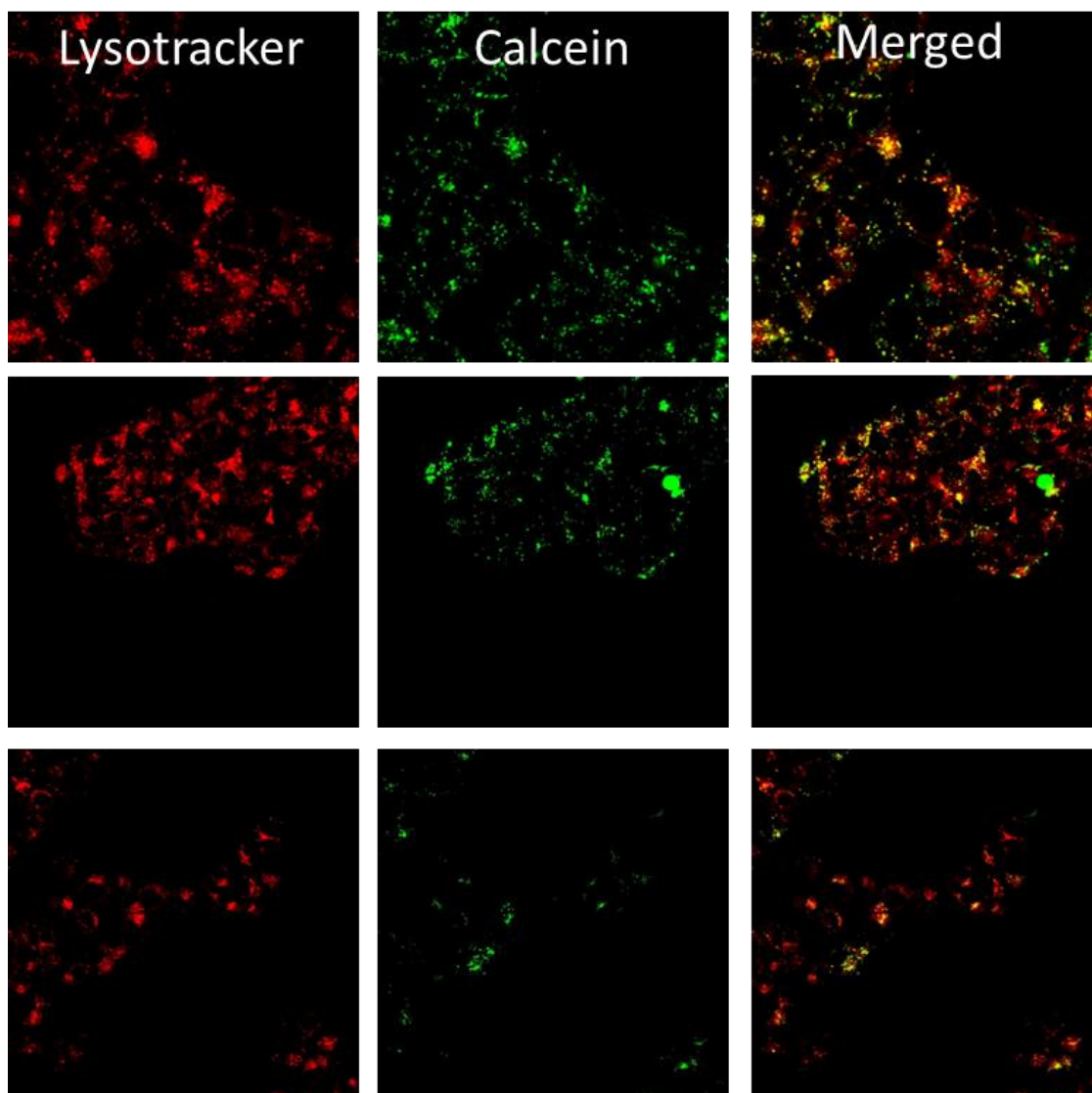


Figure S111: Confocal microscopy images of HEK live cells upon incubation with 0.2 mg·mL⁻¹ of Calcein-loaded MOFs.

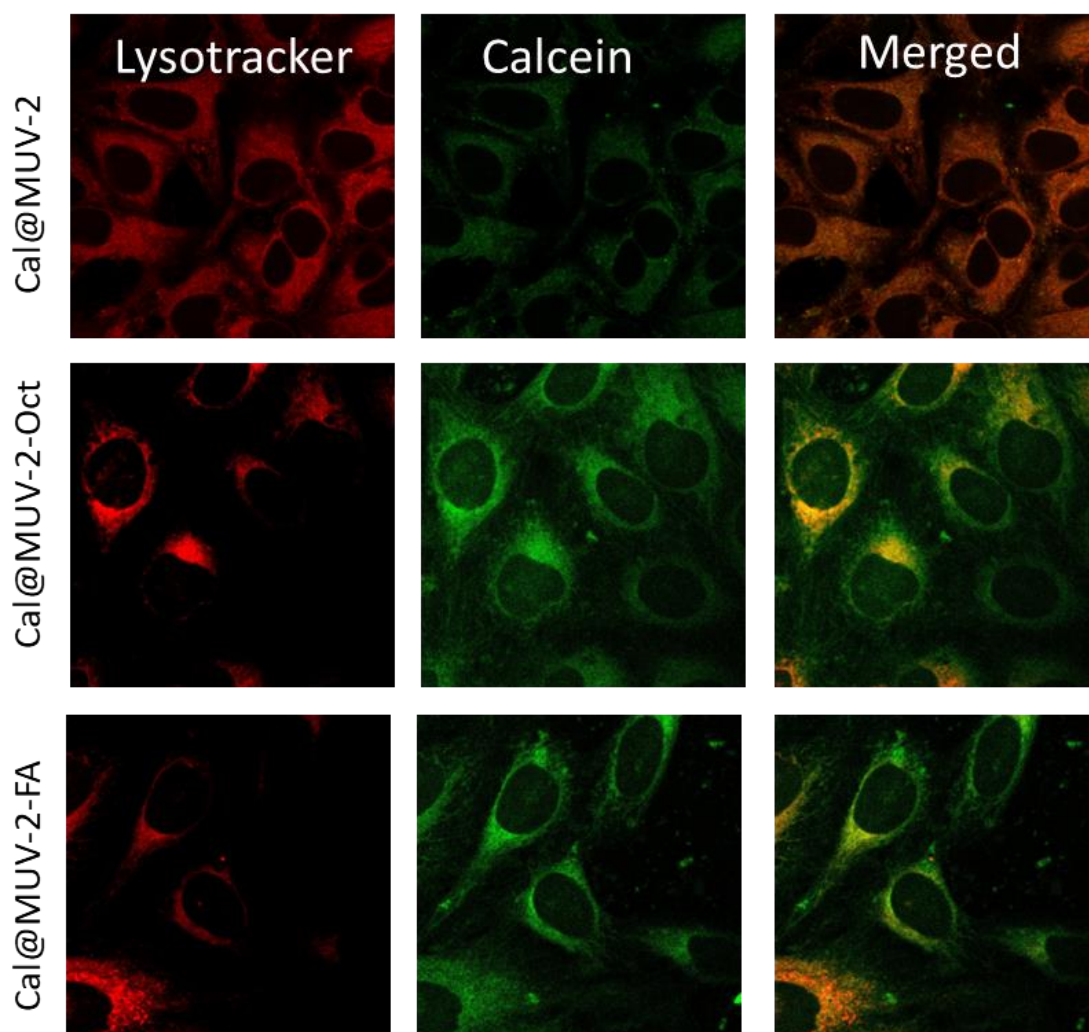


Figure S112: Confocal microscopy images of HeLa fixed cells upon incubation with $0.05 \text{ mg}\cdot\text{mL}^{-1}$ of Calcein-loaded MOFs.

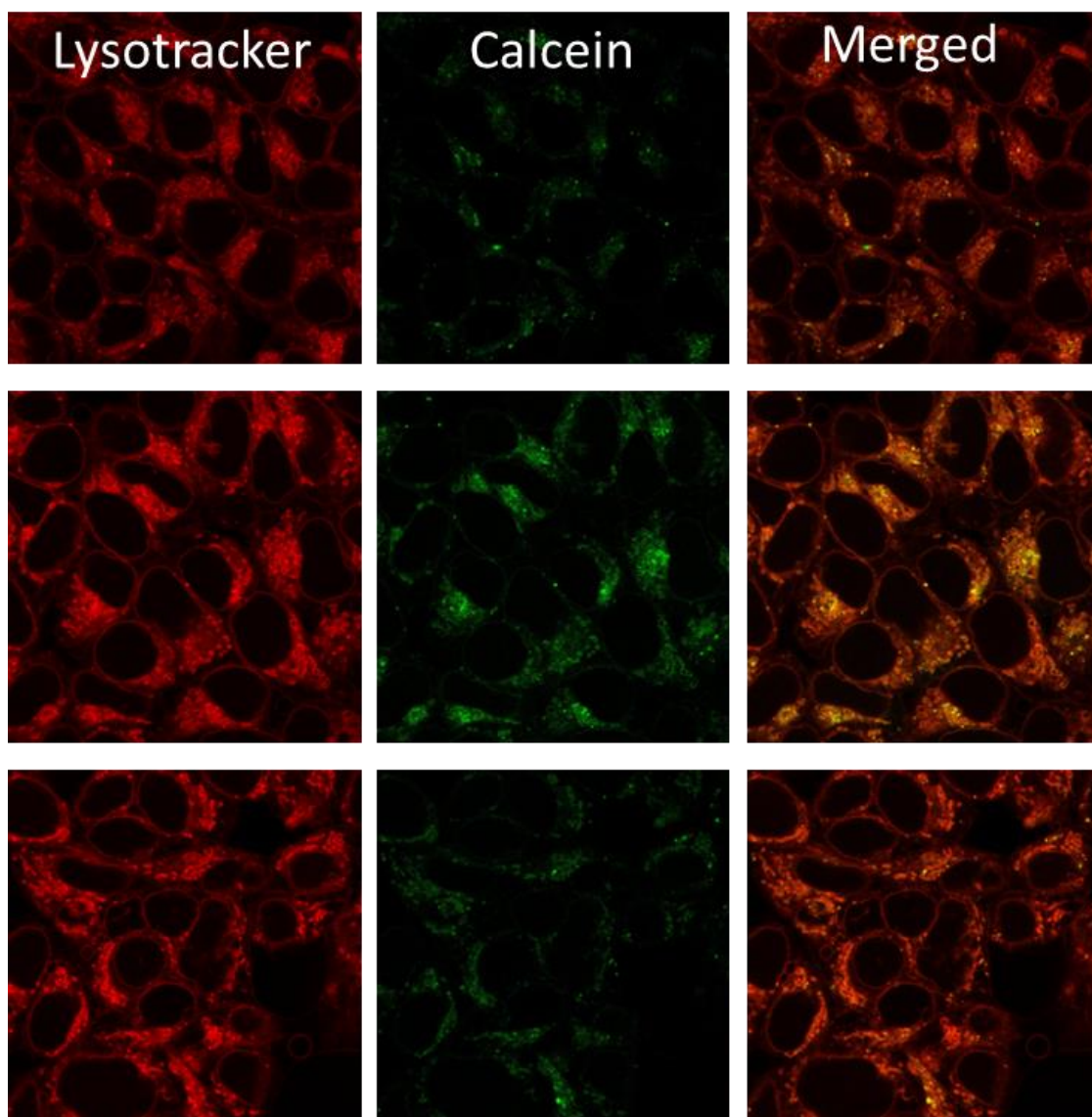


Figure S113: Confocal microscopy images of HEK fixed cells upon incubation with $0.05 \text{ mg}\cdot\text{mL}^{-1}$ of Calcein-loaded MOFs.

S13. Characterisation of Paclitaxel-loaded surface-functionalised MUV-2

S13.1 PTX@NanoMUV-2-Oct

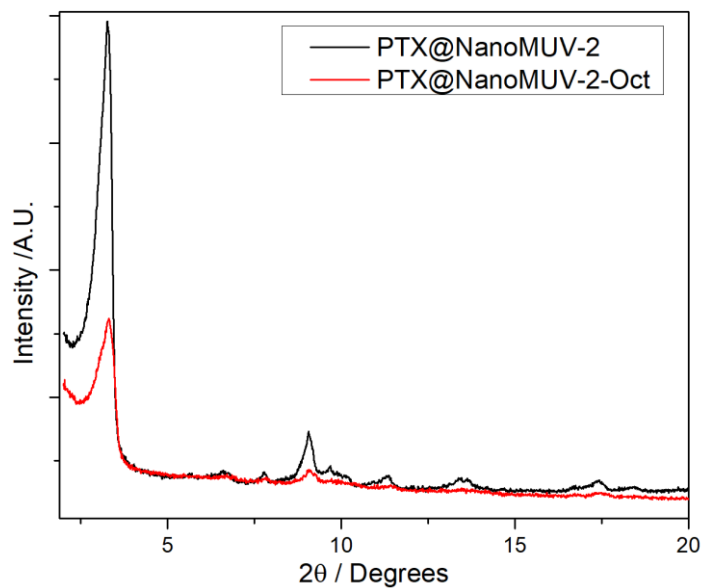


Figure S114: Comparison of PXR D patterns of PTX@NanoMUV-2 before and after 8-Br Octanoic acid functionalization.

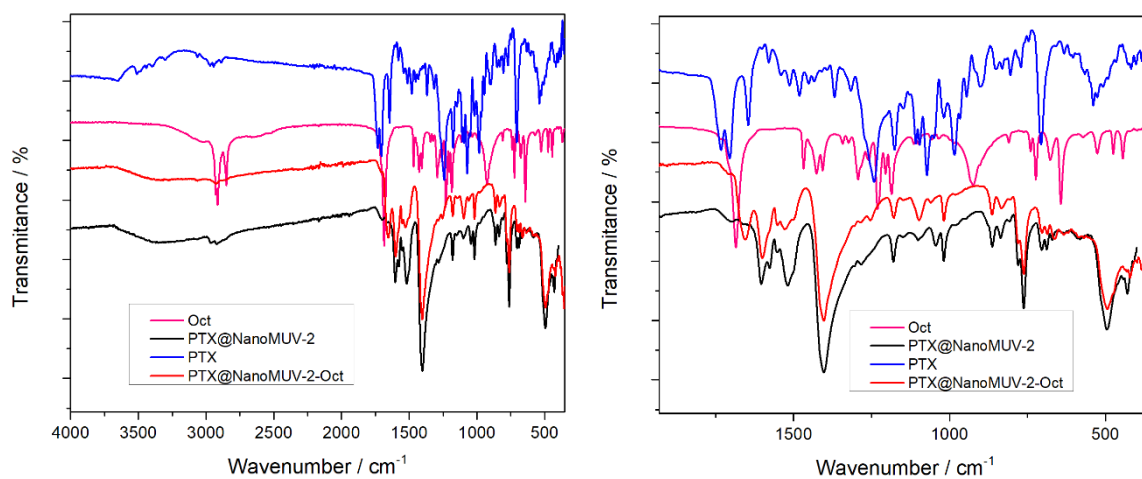


Figure S115: FT-IR profiles of PTX@NanoMUV-2, 8-Br Octanoic acid and PTX@NanoMUV-2-Oct.

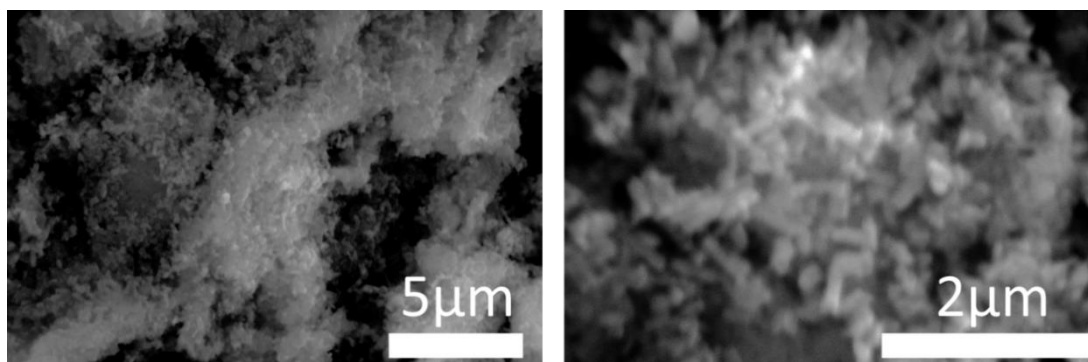


Figure S116: Scanning electron microscope images of PTX@NanoMUV-2-Oct.

Table S20: Data extracted from EDX analysis. The molar ratios extracted from EDX result in the theoretical formula $(\text{Fe}_3\text{O})_2(\text{L})_{2.928}(\text{Oct})_{1.182}(\text{PTX})_{0.77}$.

Br/Fe	Br/L	S/Fe	L/Fe
0.111	0.227	1.951	0.488

Table S21: Molar and mass fractions extracted from EDX analysis, taking into account the mw of the MOF.

Molar fraction Br vs Fe	0.100
Mass fraction oct	0.045
Mass fraction PTX	0.2012

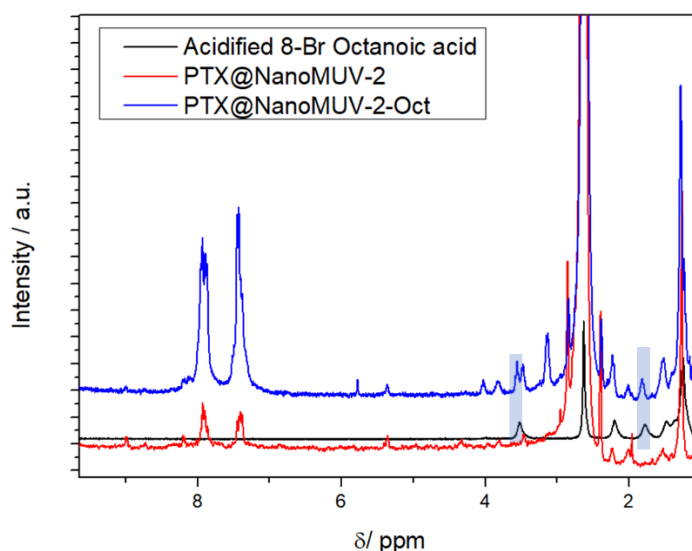


Figure S117: Acid-digested ^1H NMR profiles of PTX@NanoMUV-2-Oct, compared to acidified PTX@NanoMUV-2-Oct and acidified Br-Octanoic acid, showing the characteristic band of PTX. Unfortunately, PTX signals mask Oct signals and do not allow for determination based on the most intense signal, but the presence of some Oct signals can be observed and lead to ca. 0.49 Oct per Ligand for the theoretical molecular formula $(\text{Fe}_3\text{O})_2(\text{L})_3(\text{Oct})_{1.47}(\text{PTX})_{0.77}$, although this is only an approximation given the previously determined missing linker defects and the masking of signals.

Taking into account the linker deficiency characterized by EDX for PTX@NanoMUV-2-Oct results in ca. 17.9 w/w% PTX and ca. 8.6 w/w% oct in the theoretical formula $(\text{Fe}_3\text{O})_2(\text{L})_{2.93}(\text{Oct})_{1.436}(\text{PTX})_{0.77}$.

However, as the ^1H NMR spectra signals are masked by PTX signals and thus could lead to a higher Oct determination, we will not take into account this data for statistical analysis.

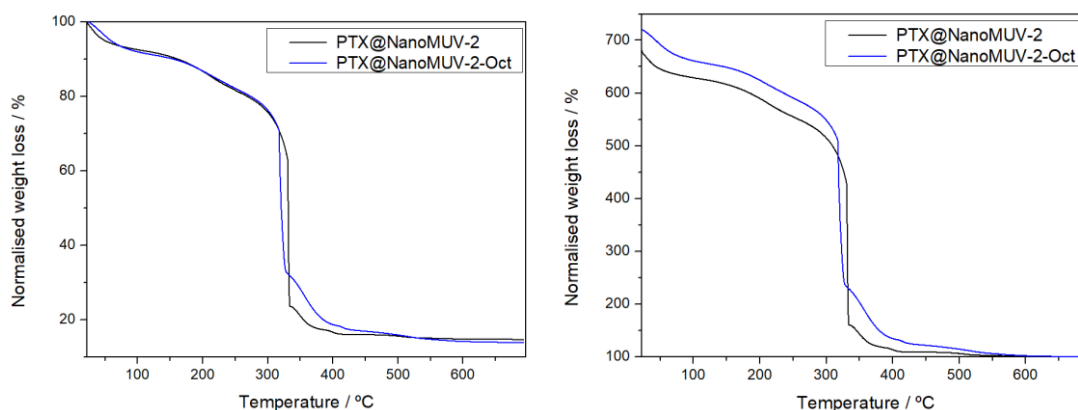


Figure S118: TGA profiles of PTX@NanoMUV-2-Oct with the start (left) or the end (right) of the decomposition profile normalized to 100% compared to PTX@NanoMUV-2.

Analysis performed as for NanoMUV-2-Oct corresponds ca. 0.198 Oct per ligand leading to the theoretical molecular formula $(\text{Fe}_3\text{O})_2(\text{L})_{2.149}(\text{Oct})_{1.18}(\text{PTX})_{0.77}$ (ca. 7.6 w/w % Oct and ca. 20.40 w/w% PTX).

Table S22: mass fractions of Oct within the Samples extracted by different techniques.

EDX	TGA	Average \pm SD
4.5	7.6	6.5 \pm 1.1

Table S23: mass fractions of PTX within the Samples extracted by different techniques.

EDX	TGA	Average \pm SD
20.12	20.40	20.26 \pm 0.14

S13.2 PTX@NanoMUV-2-FA

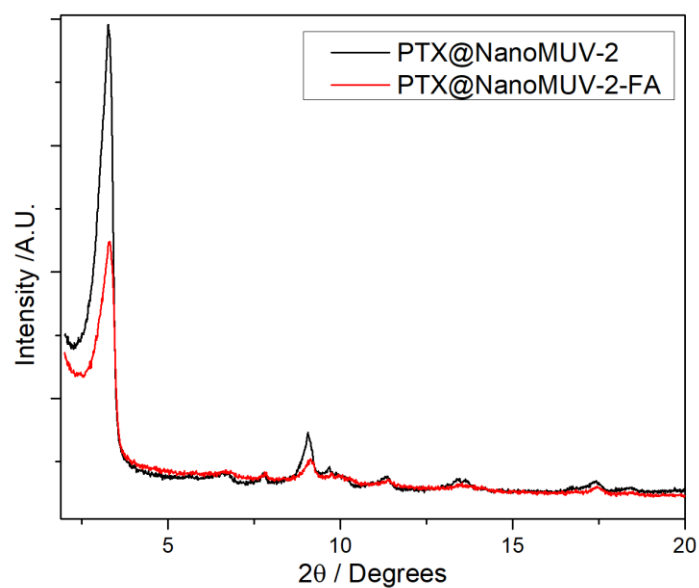


Figure S119: Comparison of PXRD patterns of PTX@NanoMUV-2 before and after Folic acid functionalisation.

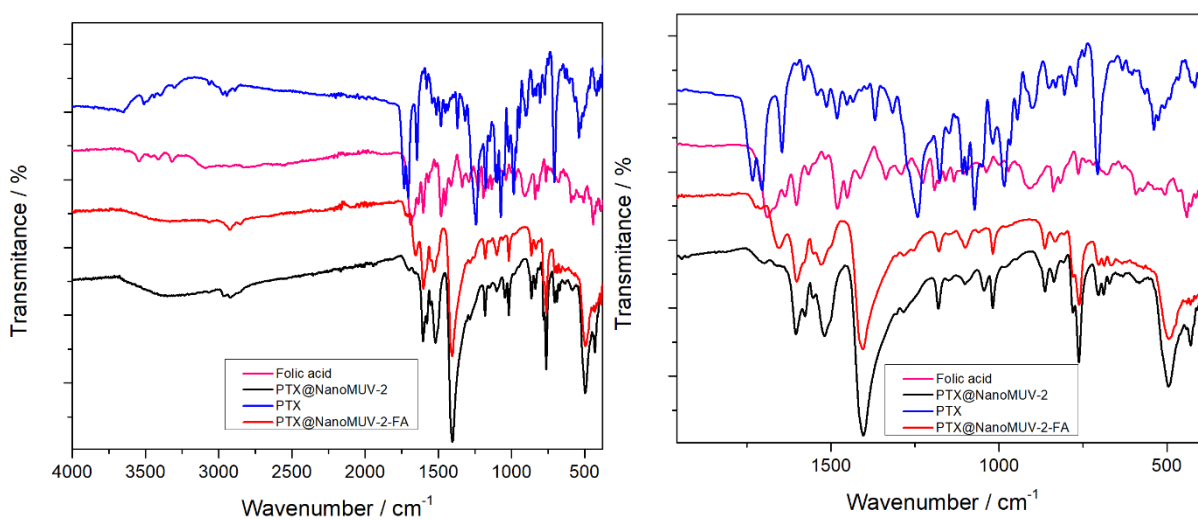


Figure S120: (Left) FT-IR profiles of PTX@NanoMUV-2, folic acid and PTX@NanoMUV-2-FA. (Right) Magnification.

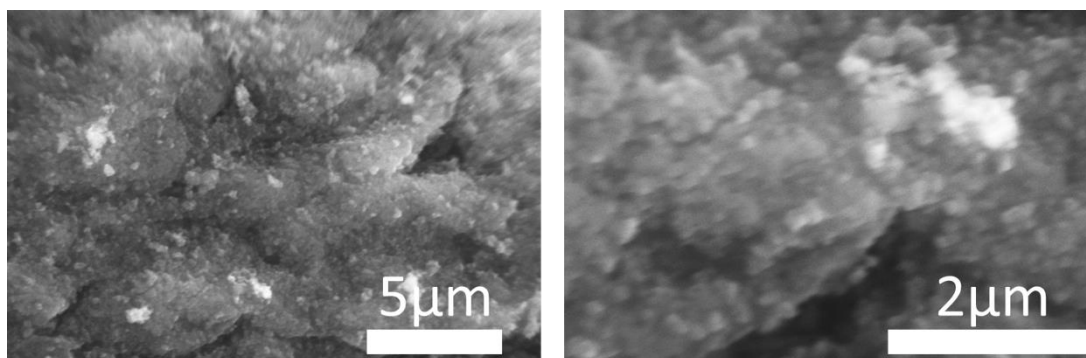


Figure S121: Scanning electron microscope images of PTX@NanoMUV-2-FA.

Table S24: Data extracted from EDX analysis, resulting in the theoretical formula $(\text{Fe}_3\text{O})_2(\text{L})_{2.92}(\text{FA})_y(\text{PTX})_x$.

S/Fe	L/Fe
1.946	0.487

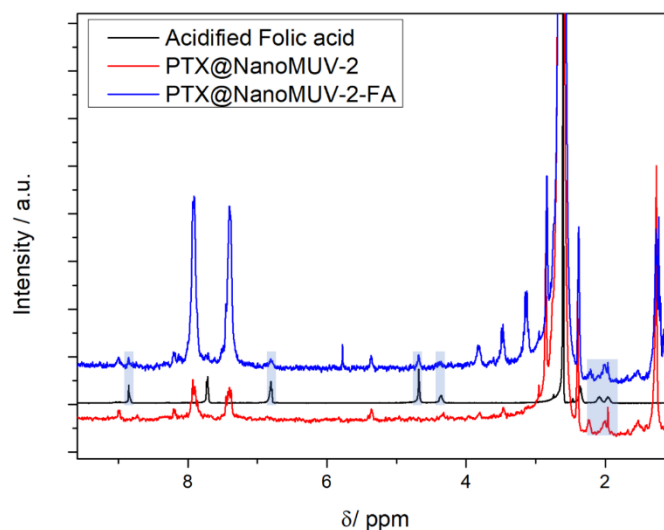


Figure S122: Acid-digested ^1H NMR profiles of PTX@NanoMUV-2-FA, compared to acidified PTX@NanoMUV-2 and acidified folic acid, showing the characteristic band of PTX and FA functionalisation. The analysis based on the molar ratio between unmasked FA and ligand signals results in ca. 0.39 FA per ligand.

Taking into account the linker deficiency characterized by EDX for PTX@NanoMUV-2-FA results in ca. 18.16 w/w% PTX and ca. 13.8 w/w% FA in the theoretical formula $(\text{Fe}_3\text{O})_2(\text{L})_{2.92}(\text{FA})_{1.13}(\text{PTX})_{0.77}$.

Note that although the FA content is quite high, the functionalisation is performed using a water solution of FA, where PTX shall not be soluble, and the extensive washing of PTX@NanoMUV-2 shall have left the surface highly available.

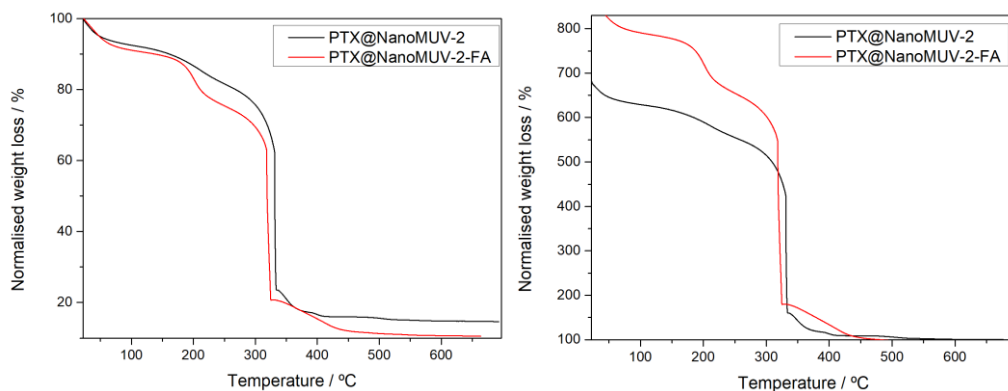


Figure S123: TGA profiles of PTX@NanoMUV-2-FA with the start (left) or end (right) of the decomposition profile normalized to 100% compared to PTX@NanoMUV-2.

TGA of PTX@NanoMUV-2-FA as in NanoMUV-2-FA results in the molecular formula $(\text{Fe}_3\text{O})_2(\text{L})_{2.96}(\text{FA})_{1.16}(\text{PTX})_{0.77}$, corresponding to a ca. 16.4 w/w % of folic acid and ca. 18.03 w/w % PTX.

Table S25: mass fractions of FA within the Samples extracted by different techniques.

EDX + ¹ HNMR	TGA	Average ±SD
13.8	16.4	15.1±1.3

Table S26 mass fractions of PTX within the Samples extracted by different techniques.

EDX + ¹ HNMR	TGA	Average ±SD
18.2	18.03	18.1±0.1

S14. Cytotoxicity Paclitaxel-functionalised samples

S14.1 Cytotoxicity of PTX@NanoMUV-2-Oct

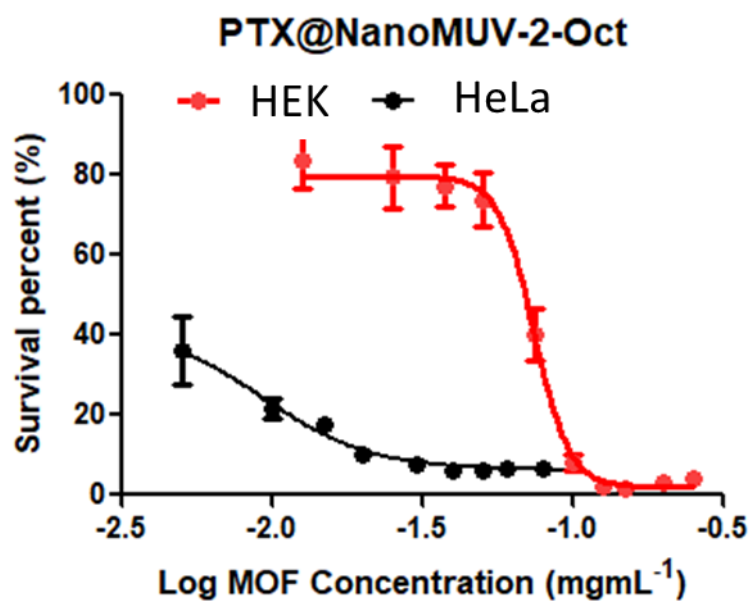


Figure S124: Cell proliferation assays (MTS) carried out on HeLa and HEK cells after 72 h incubation with PTX@NanoMUV-2-Oct in growth media. Each experiment has been performed 3 independent times, each with n=4.

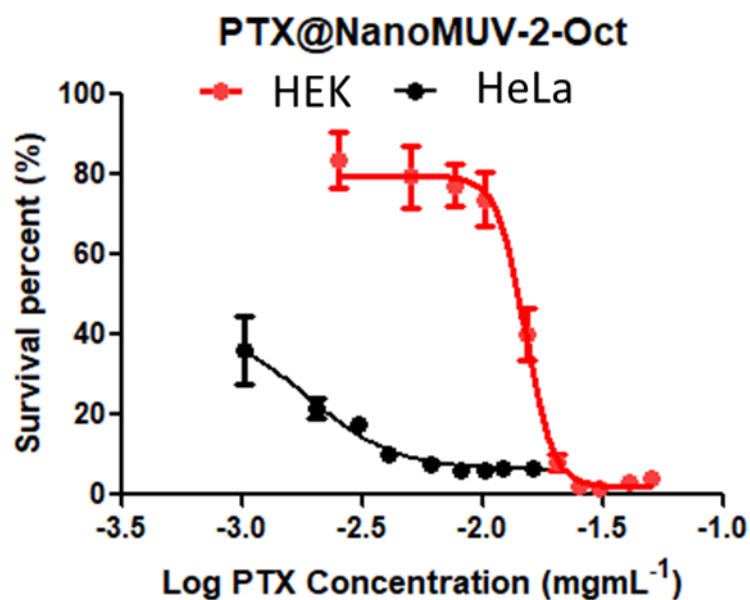


Figure S125: Cell proliferation assays (MTS) carried out on HeLa and HEK cells after 72 h incubation with PTX@NanoMUV-2-Oct in growth media. Each experiment has been performed 3 independent times, each with n=4.

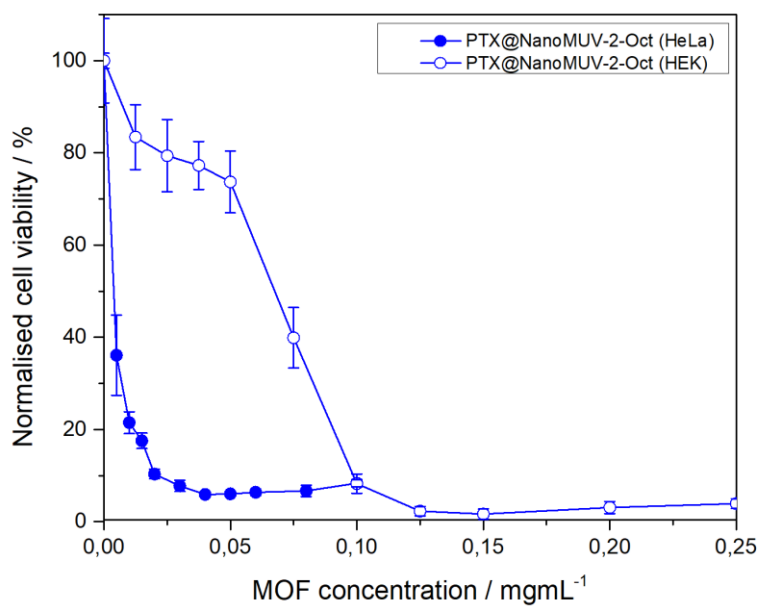


Figure S126: Comparison of cell proliferation assays (MTS) carried out on HeLa and HEK cells after 72 h incubation with PTX@NanoMUV-2-Oct in growth media. Each experiment has been performed 3 independent times, each with n=4.

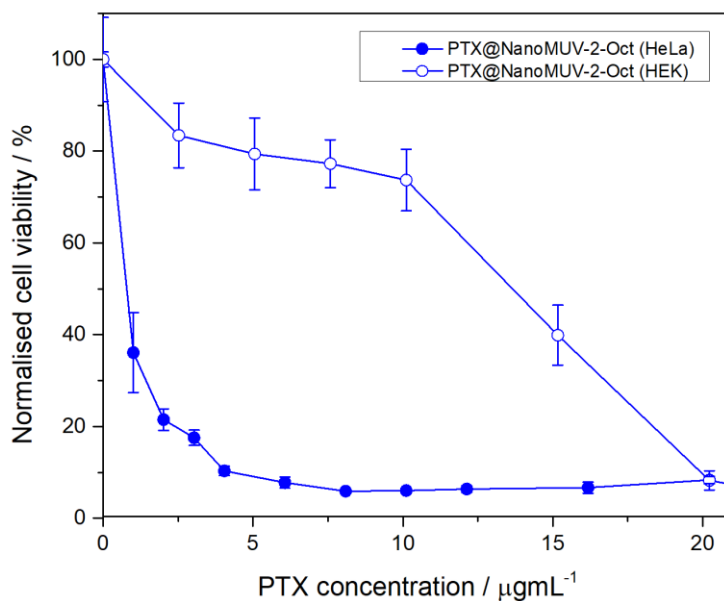


Figure S127: Comparison of cell proliferation assays (MTS) carried out on HeLa and HEK cells after 72 h incubation with PTX@NanoMUV-2-Oct in growth media. Each experiment has been performed 3 independent times, each with n=4.

S14.2 Cytotoxicity of PTX@NanoMUV-2-FA

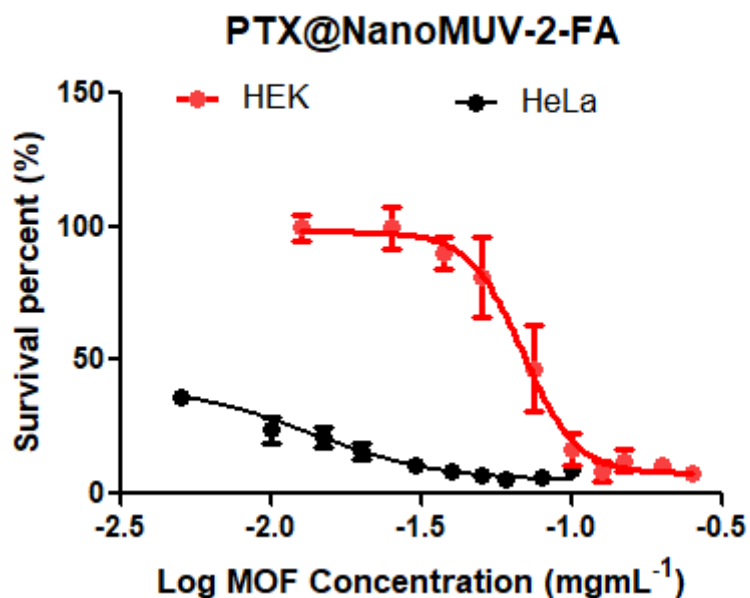


Figure S128: Cell proliferation assays (MTS) carried out on HeLa and HEK cells after 72 h incubation with PTX@NanoMUV-2-FA in growth media. Each experiment has been performed 3 independent times, each with n=4.

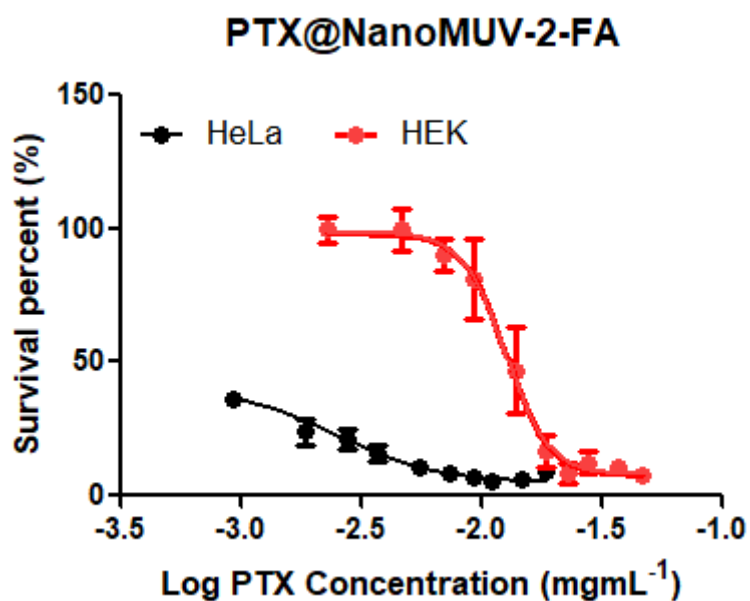


Figure S129: Cell proliferation assays (MTS) carried out on HeLa and HEK cells after 72 h incubation with PTX@NanoMUV-2-FA in growth media. Each experiment has been performed 3 independent times, each with n=4.

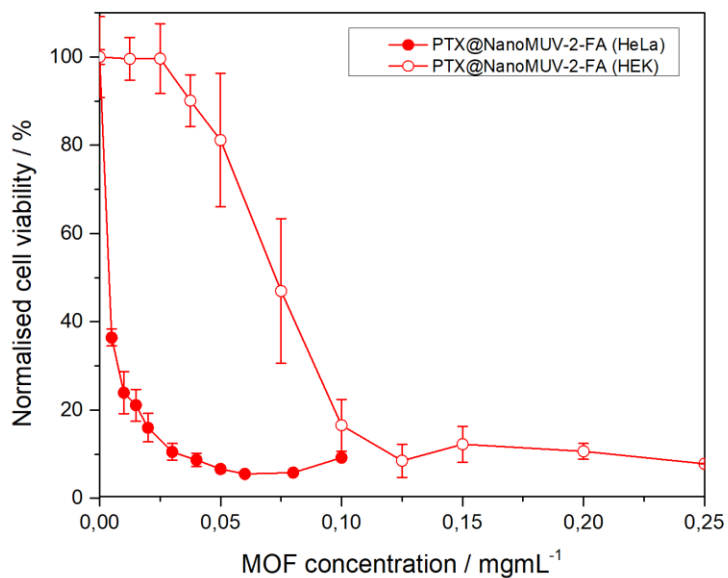


Figure S130: Comparison of cell proliferation assays (MTS) carried out on HeLa and HEK cells after 72 h incubation with PTX@NanoMUV-2-FA in growth media. Each experiment has been performed 3 independent times, each with n=4.

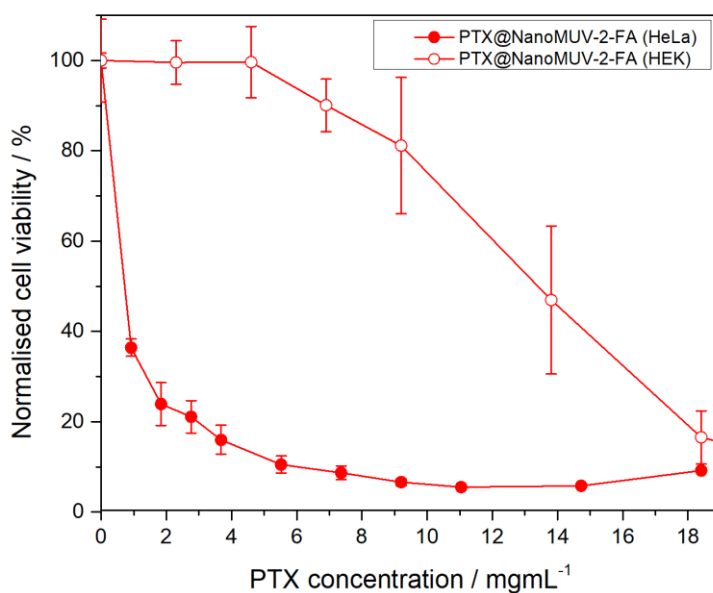


Figure S131: Comparison of cell proliferation assays (MTS) carried out on HeLa and HEK cells after 72 h incubation with PTX@NanoMUV-2-FA in growth media. Each experiment has been performed 3 independent times, each with n=4.

S14.3 Comparison of Cytotoxicity Paclitaxel-functionalised samples

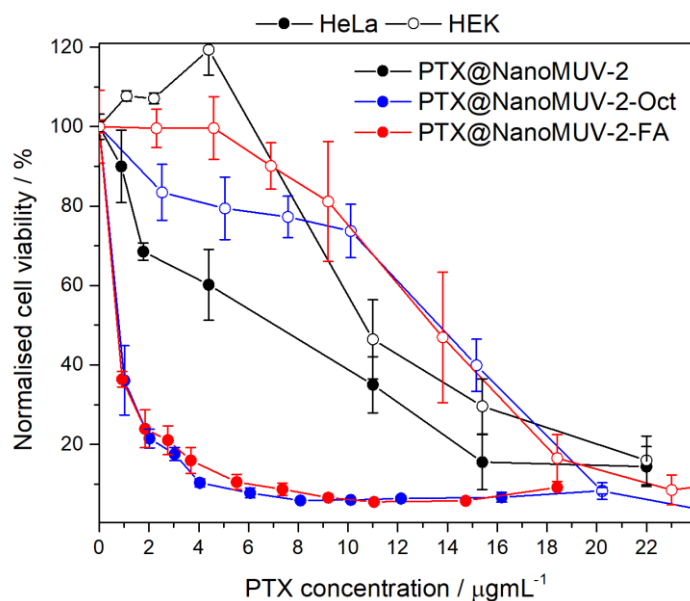


Figure S132: Comparison of cell proliferation assays (MTS) carried out on HeLa and HEK cells after 72 h incubation with different MOFs in growth media. Each experiment has been performed 3 independent times, each with n=4.

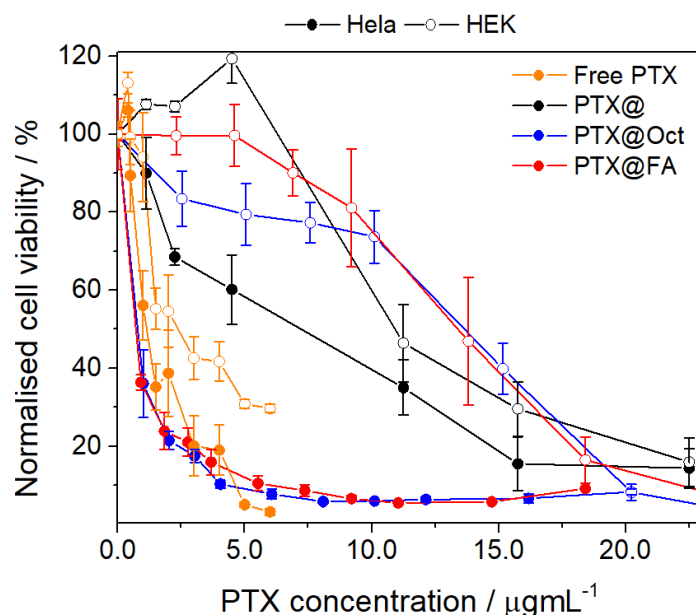


Figure S133: Comparison of cell proliferation assays (MTS) carried out on HeLa and HEK cells after 72 h incubation with different MOFs in growth media, compared with free PTX. Each experiment has been performed 3 independent times, each with n=4.

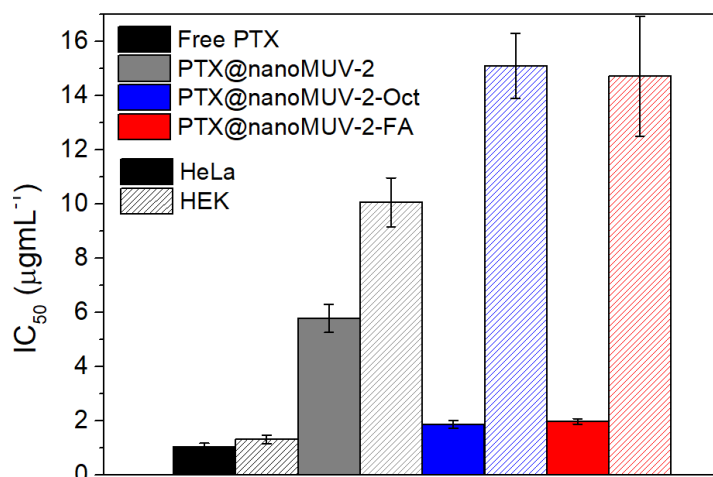


Figure S134: Comparison of IC₅₀ doses obtained for the different PTX-loaded MOFs and free PTX.

Table S27: Comparison of the extracted IC₅₀ values of the samples of this study.

MOF	IC ₅₀ MOF concentration mg mL ⁻¹		IC ₅₀ Maximum delivered drug concentration µg·mL ⁻¹		Selectivity index
	HeLa	HEK	Hela	HEK	
MUV-2	1.92 ± 0.31	2.02 ± 0.32	N/A	N/A	1.00
Free Paclitaxel	n/a	n/a	1.05 ± 0.12	1.32 ± 0.16	1.26
PTX@MUV-2	0.024 ± 0.002	0.044 ± 0.004	5.77 ± 0.52	10.06 ± 0.90	1.76
MUV-2-Oct	0.733 ± 0.110	0.830 ± 0.102	N/A	N/A	1.13
MUV-2-FA	0.785 ± 0.118	>1	N/A	N/A	1.56
PTX@MUV-2-Oct	0.0092 ± 0.0007	0.074 ± 0.006	1.87 ± 0.15	15.10 ± 1.21	8.07
PTX@MUV-2-FA	0.0107 ± 0.0006	0.080 ± 0.012	1.97 ± 0.10	14.72 ± 2.21	7.47

S15. References

1. M. Souto, A. Santiago-Portillo, M. Palomino, I. J. Vitórica-Yrezábal, B. J. C. Vieira, J. C. Waerenborgh, S. Valencia, S. Navalón, F. Rey, H. García and G. M. Espallargas, *Chem. Sci.*, 2018, **9**, 2413–2418.
2. I. A. Lázaro, E. C. Mazarakioti, E. Andres-Garcia, B. J. C. Vieira, J. C. Waerenborgh, I. J. Vitórica-Yrezábal, M. Giménez-Marqués and G. M. Espallargas, *J. Mater. Chem. A*, 2023, **11**, 5320–5327.
3. I. A. Lázaro, S. Haddad, J. M. Rodrigo-Muñoz, C. Orellana-Tavra, V. del Pozo, D. Fairen-Jimenez and R. S. Forgan, *ACS Appl. Mater. Interfaces*, 2018, **10**, 5255–5268.
4. A. G. Márquez, A. Demessence, A. E. Platero-Prats, D. Heurtaux, P. Horcajada, C. Serre, J. Chang, G. Férey, V. A. de la Peña-O’Shea, C. Boissière, D. Grosso and C. Sanchez, *Eur. J. Inorg. Chem.*, 2012, **2012**, 5165–5174.
5. I. A. Lázaro, *Eur. J. Inorg. Chem.*, 2020, **2020**, 4284-4294.